# Targeting Cellular and Molecular Mediators of Pathologic Biomechanical Remodeling in Pulmonary Arterial Hypertension

By

Nathaniel Craig Bloodworth

Dissertation

Submitted to the Faculty of the

Graduate School of Vanderbilt University

in partial fulfillment of the requirements

for the degree of

DOCTOR OF PHILOSOPHY

in

Biomedical Engineering

June 30, 2017

Nashville, Tennessee

Approved:

W. David Merryman, Ph.D.

James West, Ph.D.

Susan Majka, Ph.D.

Todd Giorgio, Ph.D.

Craig Duvall, Ph.D.

# DEDICATION

This work is dedicated to my father, who taught me to think with my head;

To my mother, who taught me to love with my heart;

To my brother, who taught me to laugh with my soul.

To my wife, life partner, and best friend, Melissa Harintho Bloodworth, to our daughter, Penelope Tresna Bloodworth, and to all of our children yet unborn. You lift my head to the heights of heaven and plant my feet firmly in the earth.

" 'Be comforted, small one, in your smallness. He lays no merit on you. Receive and be glad. Have no fear, lest your shoulders be bearing this world. Look! It is beneath your head and carries you.' "

– C.S. Lewis, Peralandra

# ACKNOWLEDGEMENTS

“No man is an Iland, intire of itselfe; every man
is a peece of the Continent, a part of the maine;
if a Clod bee washed away by the Sea, Europe
is the lesse, as well as if a Promontorie were, as
well as if a Manor of thy friends or of thine
owne were; any mans death diminishes me,
because I am involved in Mankinde”

– John Donne, Meditation XVII, Devotions Upon Emergent Occasions

I would first acknowledge my colleagues and co-authors for their invaluable experimental and intellectual contributions to the presented work: Larisa Rhyzhova for teaching me the finer points of molecular biology, Cyndi Clark for sharing her expertise with mouse models of disease, and Sheila Shay, Santhi Gladson, Michelle Clifton, Tom Blackwell, Christy Moore, Christa Gaskill, Harikrishna Tanjore, and all members of the West, Majka, and Blackwell laboratories.

I would like to extend a special thanks to my fellow lab members, both past and present. Joe Chen, Josh Hutcheson, M.K. Sewell-Loftin, Steve Boronyak, Alison Schroer, Meghan Bowler, Mark Vander Roest, Cami Johnson, Caleb Snider, Natalie Noll, and Ethan Joll. You are the reason that each day is a great day to be in the Merryman Lab.

I would like to acknowledge the support and dedication of my thesis mentors: James West, Sue Majka, Craig Duvall, and Todd Giorgio. You have each played a special role in guiding me both scientifically and professionally. And last, but certainly not least, my advisor David Merryman, who taught me that time invested in people is time well spent.

Lastly I would like to thank the National Institutes of Health and American Heart Association for the funding of this work.

TABLE OF CONTENTS

LIST OF TABLES

Page

LIST OF FIGURES

Page

GLOSSARY OF TERMS AND ABBREVIATIONS

| | |
|---|---|
| 5-HT | Serotonin |
| $5\text{-HT}_{1B}$ | Serotonin Receptor 1B |
| $5\text{-HT}_{2B}$ | Serotonin Receptor 2B |
| AFM | Atomic Force Microscopy |
| Alk1 | Activin Receptor-Like Kinase 1 |
| BM | Bone Marrow |
| BMP | Bone Morphogenetic Protein |
| BM-PAC | Bone Marrow-Derived Pro-Angiogenic Cells |
| Bmpr1a | Bone Morphogenetic Protein Receptor 1a |
| Bmpr2 | Bone Morphogenetic Protein Receptor 2 |
| CAS | Crk-Associated Substrate, also known as p130 |
| CAV1 | Caveolin-1 |
| Cdc42 | Cell Division Control Protein 42 Homolog |
| cKit | Tyrosine-Protein Kinase Kit, also known as CD117 |
| DMEM | Dulbecco's Modification of Eagle's Medium |
| DMSO | Dimethylsulfoxide |
| DTa | Diphtheria Toxin |
| ECM | Extracellular Matrix |
| EGF | Epidermal Growth Factor |
| EGFR | Epidermal Growth Factor Receptor |
| EndMT | Endothelial to Mesenchymal Transition |
| eNOS | Endothelial Nitric Oxide Synthase |
| ET-1 | Endothelin-1 |
| FA | Focal Adhesion |
| FAK | Focal Adhesion Kinase |
| FGF | Fibroblast Growth Factor |
| Fhl-1 | Four and a Half LIM Domains-1 |
| GO | Gene Ontology |
| HIV | Human Immunodeficiency Virus |
| IL-1β | Interleukin-1 Beta |
| IL-6 | Interleukin-6 |

| | |
|---|---|
| kPa | Kilopascals |
| LIMK1 | LIM Domain Kinase 1 |
| MMP | Matrix Metalloproteinase |
| mPAP | Mean Pulmonary Arterial Pressure |
| NFκB | Nuclear Factor Kappa-Light-Chain-Enhancer of Activated B Cells |
| NO | Nitric Oxide |
| PAC | Pulmonary Arterial Compliance |
| PAEC | Pulmonary Artery Endothelial Cell |
| PAH | Pulmonary Arterial Hypertension |
| PASMC | Pulmonary Artery Smooth Muscle Cell |
| PBMC | Peripheral Blood Mononucleocyte |
| PBS | Phosphate Buffered Saline |
| PVR | Pulmonary Vascular Resistance |
| Rac1 | Rho-family GTPase |
| RhoA | Ras homolog gene family, member A |
| RV | Right Ventricle |
| RVSP | Right Ventricular Systolic Pressure |
| S100A4 | S100 Calcium Binding Protein A4 |
| SB204741 | Serotonin Receptor 2B Antagonist |
| SCL | Stem-Cell Leukemia |
| SERT/5-HTT | Serotonin Transporter |
| SMAD | Intracellular mediators of Bmpr2 signaling |
| Src | Proto-oncogene (“Sarcoma”) Tyrosine Protein Kinase |
| Talin-1 | Cytoskeletal adapter protein |
| TCTEX | Dynein Light Chain TCTEX-type 1 |
| TG-2 | Transglutaminase 2 |
| TGF-β1 | Transforming Growth Factor Beta 1 |
| TIMP | Tissue Inhibitor of Matrix Metalloproteinase |
| TMLC | Transformed Mink Lung Cells |
| VEGFR2 | Vascular Endothelial Growth Factor Receptor 2 |
| YFP | Yellow Fluorescent Protein |

# CHAPTER 1: PROJECT MOTIVATION

## *A Brief Introduction to Pulmonary Arterial Hypertension*

Each year in the United States alone, over 200,000 people are hospitalized with some form of pulmonary hypertension as either a primary or secondary diagnosis. For these patients, and estimated 15,000 will succumb to their illness.[1] The remainder will undergo medical management with modest success in improving their symptoms and quality of life, but little to no chance of reversing the disease's course or improving their chances of survival.[2] There thus exists an urgent need for new drugs and therapies designed specifically to treat this insidious and mortal illness.

Pulmonary hypertension is defined clinically as a mean pulmonary arterial pressure (mPAP) above 25 mm Hg, as measured by right ventricle catheterization.[3] The World Health Organization further refines this definition by categorizing the various clinical presentations based on underlying conditions in addition to their hemodynamic presentation (Table 1).[4] Group 1 pulmonary hypertension, or pulmonary arterial hypertension (PAH), is pulmonary hypertension that presents without a primary underlying pulmonary condition and characterized hemodynamically by a pulmonary capillary wedge pressure of less than 15 mm Hg. PAH is one of the least common of the pulmonary hypertension subtypes and considered a rare disease, with an incidence of 1.1 to 2.4 new cases per million per year and a prevalence of 6.6 to 15 cases per million per year.[5,6] Despite advances in both categorization and treatment, the mortality rate for PAH remains high: merely 67% of patients survive 3 years after diagnosis, only a modest improvement compared to the 47% 3-year survival rate over a decade prior.[6–8] Even this estimate may be overly optimistic; as this data comes from clinical trial patients, the majority tends to have less severe disease at the time they are enrolled.[9] These estimates are also strongly influenced by survival bias, introduced by pulling data from a registry of existing patients who may have survived due to intrinsic variations in disease lethality or treatment

| Disease Subtype | Disease Eitiology |
|---|---|
| 1 Pulmonary Arterial Hypertension | Hereditary (Familial)<br>Idiopathic<br>Drug- and toxin- induced<br>Associated with other diseases (HIV, Scleroderma, etc)<br>Persistent pulmonary hypertension of the newborn<br><br>Pulmonary veno-occlusive disease |
| 2 Pulmonary Hypertension due to left ventricle dysfunction | Systolic<br>Diastolic<br>Valvular |
| 3 Pulmonary Hypertension due to lung diseases or hypoxia | Chronic obstructive pulmonary disease<br>Interstitial lung disease<br>Other pulmonary diseases<br>Sleep disorders<br>Alveolar hypoventilation disorders<br>Chronic high altitude exposures<br>Developmental Abnormalities |
| 4 Chronic Thromboembolic Pulmonary Hypertension | |
| 5 Miscellaneous | Hematologic disorders<br>Systemic disorders<br>Metabolic disorders<br>Other |

**Table 1.1: The Dana Point classification of pulmonary hypertension.**
Pulmonary hypertension is grouped into five functional classes and further stratified by etiology in order to aid in clinical management. Pulmonary arterial hypertension (shown in red) is formally classified as group 1 pulmonary hypertension.

efficacy.[10] In addition to a high mortality and morbidity, PAH exacts a tremendous economic impact. The cost of treatment alone can exceed $200,000 annually per patient, and this cost is further compounded by the extreme expense associated with end stage heart and lung transplantation.[11] The disproportionate number of reproductive-age women further compounds both the economic and societal impact of PAH, with estimates ranging from a 1.7:1 to a 4:1 female to male ratio among those diagnosed.[5,12,13]

PAH is further subdivided into clinically relevant categories by etiology. These categories include hereditary (or familial), idiopathic, drug induced, and PAH associated with other conditions such as HIV and scleroderma.[14] Among these categories idiopathic PAH, or PAH

with no known cause, occurs the most frequently (between 39.2% and 46.5% of PAH cases depending on the registry queried[5,13]). Hereditary or familial PAH is much less common, accounting for 3-4% of all PAH cases.[5,13] Regardless of the subtype, small vessel remodeling resulting in vessel obstruction, stiffening, and luminal narrowing is the characteristic feature of PAH pathophysiology.[15] This proliferative remodeling results in an elevation of mPAP, total pulmonary vascular resistance (PVR), and (importantly) decreased arterial compliance, increasing the workload on the RV until it eventually dilates and fails.[3,16]

Treatment options are limited for PAH. Current therapies include three classes of medications: prostacyclin analogues, phosphodiesterase type 5 inhibitors, and endothelin receptor antagonists.[17] These mediations were originally developed for the treatment of other illnesses and subsequently adopted for PAH. They provide only modest improvements in symptoms through transitory vessel dilation, leaving the underlying pathology of vascular remodeling and vessel stiffening unaddressed.[2] End-stage therapy for PAH is a heart/lung transplant, an exceptionally expensive procedure that adds its own host of complications and difficulties.[18] Since the first successful clinical trial for PAH (intravenous epoprostenol, a biosynthetic prostacyclin analogue) the number of publications on experimental PAH therapies has increased five-fold, and there are currently nearly 600 ongoing registered clinical trials for PAH.[18] Despite this explosion of interest, less than 10% of these trials test new therapies and none of the compounds under investigation were developed specifically for PAH.[18]

*Project Aims*

The currently poor understanding of PAH molecular pathogenesis is the most significant barrier to the development of effective therapies. Until the mechanisms that drive disease progression and small vessel remodeling are better understood, the rational selection of targets for disease-modifying medications will remain an elusive goal. This Doctoral Thesis aims to present novel findings on both the molecular and cellular mechanisms that drive proliferative

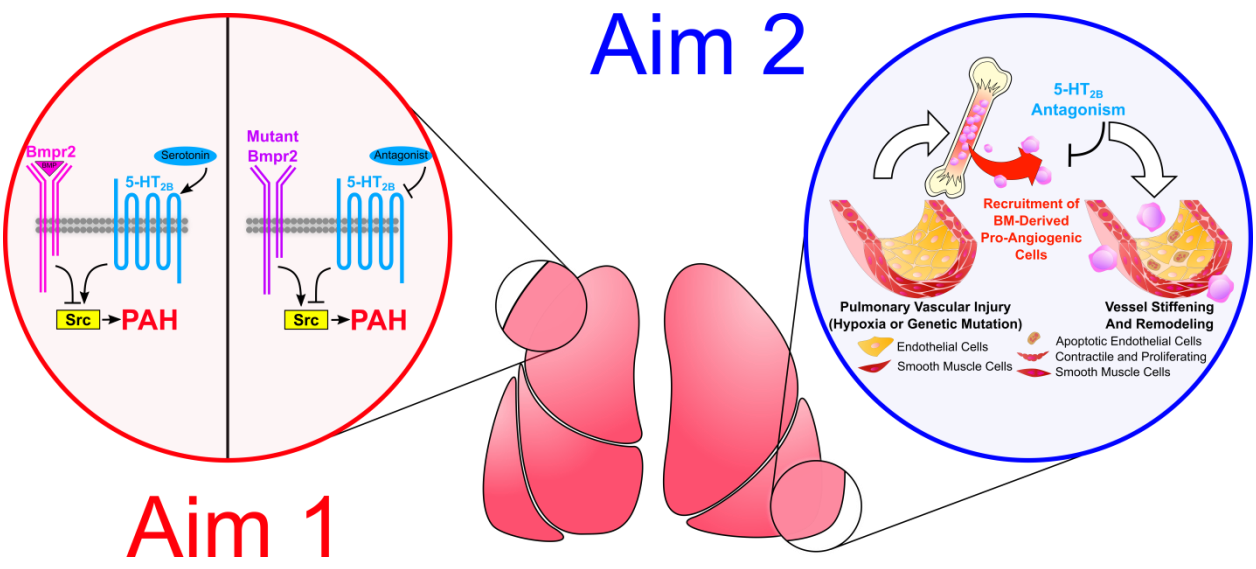


**Figure 1.1: A graphical summary of dissertation aims 1 and 2.**

vascular remodeling during PAH pathogenesis, with an emphasis on mediators of biomechanical changes in the vessel wall. The project is subdivided into two specific aims shown graphically in Figure 1.1 and summarized below:

> **Aim 1:** Test the hypothesis that antagonism of the serotonin 2B receptor inhibits small vessel remodeling and the development of familial PAH through a Src-kinase dependent mechanism.
>
> **Aim 2:** Test the hypothesis that proangiogenic hematopoietic cells mediate pathologic biomechanical remodeling in a manner dependent on serotonin 2B receptor signaling.

To begin, a concise background on vessel biomechanics in pulmonary hypertension, molecular mediators of vessel stiffening in PAH, and hematopoietic cell contributions to vessel remodeling is provided. The findings for each aim are then considered separately along with a focused introduction and set of materials and experimental methods used to interrogate the hypothesis at hand. The dissertation concludes with a discussion on the impact and limitations of the work as well as a far-reaching consideration of potential future directions made possible by these

findings. It is the author's sincere hope that this body of work contributes in some small but meaningful way to the advancement towards an effective therapy for PAH that is so desperately needed by the patients and families suffering from this illness.

# CHAPTER 2: BACKGROUND

Text and figures adapted in part from:

Bloodworth N.C., West J.D., Merryman W.D. *Microvessel Mechanobiology in Pulmonary Arterial Hypertension: Cause and Effect*. Hypertension. 2015; 65(3): 483-9.[19]

## *Pulmonary Arterial Hypertension Biomechanics: A Disease of Vessel Compliance*

Small vessel remodeling resulting in vessel obstruction and luminal narrowing is the characteristic feature of PAH pathophysiology.[15] This proliferative remodeling results in an elevation of mean pulmonary arterial pressure (mPAP) and total pulmonary vascular resistance (PVR), increasing the workload on the RV until it eventually fails.[3,16] While these hemodynamic parameters are useful for clinical diagnosis, alone they have limited prognostic value; furthermore, vasodilator therapy aimed at reduction of PVR has achieved only modest success, and increases in patient survival are attributed primarily to earlier diagnosis and intervention.[2,7,8,17,18] The increasingly clear limitations of using PVR to characterize and manage PAH has motivated research focused on identifying measurable physiologic parameters that could both predict mortality and serve as measures for therapeutic efficacy.

A growing body of recent work implicates decreased pulmonary arteriolar compliance (or capacitance, PAC) as a major factor contributing to the increased RV workload and subsequent RV failure in PAH. Arteriolar compliance measures a vessel's ability to deform under loading and is inversely proportional to stiffness: as a blood vessel stiffens its compliance decreases, and vise-versa. Total vessel compliance is typically estimated as stroke volume divided by pulse pressure (PP). This estimation alone is a strong positive predictor of survival in idiopathic PAH[20,21] as well as familial PAH.[22] Further attention to proximal pulmonary artery stiffness changes in other forms of pulmonary hypertension suggest a complex crosstalk occurs between the distal and proximal vasculature, advancing disease progression and further vessel stiffening

in a positive feedback cycle.[23–27] While proximal artery stiffness is undoubtedly important in increasing RV workload, changes in vessel compliance affect the entire pulmonary vasculature with the largest portion of that change occurring in vessels distal to the lung hilum.[28] Furthermore, the vascular remodeling that drives PAH disease progression is restricted to these smaller and more distal muscular arteries.[29]

RV overload and failure is the ultimate cause of death in PAH. Classically, RV failure is attributed to the RV's inability to adapt to an increased workload caused by elevated PVR. However, PVR alone provides little predictive value in determining PAH survival.[7] Moreover, vasodilators – intended to decrease PVR by widening the vessel lumen and restoring flow rates – provide only transitory relief with minimal impact on mortality (with a majority of PAH patients altogether unresponsive to vasodilatory therapy).[2,17] PVR is a measure for the intrinsic resistance to steady state flow. However, because of the steady state flow assumption, measurements of PVR fail to capture the oscillatory pumping action of the RV[30]. Oscillatory work accounts for up to one-third of the RV workload fraction under normal conditions[30,31]. This fraction is significantly more than in systemic circulation, and remains constant in diseased states such as PAH.[32,33] A more complete representation of pulmonary hemodynamics takes into account both PVR, primarily localized to the microvasculature and modulated by vessel diameter, PAC, a mechanical property inversely related to the intrinsic stiffness of the vessel wall and distributed throughout the entire vasculature[34–36].

Vessel stiffness is increasingly recognized as an important determinant of RV workload in PAH. The stiffness of the large conduit pulmonary arteries[20,37] as well as the overall compliance of the entire vascular bed[21,22] has been shown to predict mortality in PAH patients. The stiffness of large pulmonary vessels also directly impacts oscillatory work by the RV. The normally high compliance of conduit and large elastic vessels allows them to accommodate and store pulse wave energy from the cyclic contractions of the heart. This property allows for dissipation of pulse wave energy and decreased PP and RV afterload, a phenomenon captured

by measures of pulmonary vascular impedance.[38–41] Research using animal models of chronic hypoxic pulmonary hypertension illustrates that increases in proximal pulmonary artery stiffness and corresponding decreases in PAC contribute significantly to the RV workload by elevating PP.[42–44] Stiffening of the large arteries also increases pulse reflections in the vasculature, further augmenting total PP.[39,40,45,46]

While this suggests that the increased stiffness (and decreased PAC) of the conduit arteries contributes to disease progression in PAH, proximal large artery compliance comprises only 15-25% of the total PAC; the remainder is distributed across the entirety of the arterial bed.[28] Compliance of the distal vasculature is important in normal physiology for regulating pulmonary flow rates, especially during exercise.[47] Direct information of distal artery compliance is difficult to obtain due to the small size and limited accessibility of the vessels. Efforts to develop methods from a combination of pressure-diameter curves, echocardiography, and non-linear regression analysis have yielded reasonable estimates of distal compliance.[48–50] Models explaining the pressure-flow relationship in the pulmonary circulation as a function of PAC (rather than PVR) also provide more accurate representations of pulmonary hemodynamics. For a typical flow-pressure curve, pressure increases linearly with flow and gradually tapers to a constant for higher flow rates. According to the PVR model (or ohm-Starling resistor model), as the flow increases this gradual tapering of pressure is explained by the recruitment of new vessels in parallel, decreasing resistance to flow. The vessel distensibility model by contrast explains this tapering as pulmonary vessels distending to accommodate increased flow rates. Both models fit well to experimental data in normal and PAH affected animals, but, while mathematically simpler, the PVR model fails to account for how changes in blood viscosity (as in cases of increased red blood cell content, or hematorcrit) alter the pressure-flow relationship.[50,51]

Distal PAC estimations in PAH patients employing models for estimating small vessel compliance have found a strong correlation between elevated pulse pressure and distal artery

stiffness[52]. Furthermore, studies correlating PVR with PAC have shown that the product of the two values remains constant – as one parameter increases the other decreases, and vise-versa[28,34]. This relationship is maintained in idiopathic PAH patients as well.[38] The inverse hyperbolic association suggests that small initial changes in PVR result in large changes in vessel compliance and comparably large changes in PP and RV oscillatory workload, and these initial large changes in PAC are evident early in the disease[34,35,53]. Together, these results suggest that PAC plays a vital role in modulating RV afterload in the distal as well as the proximal vasculature, and compliance changes in distal arteries influence the progression of abnormal hemodynamics that characterize PAH.

While the biomechanical changes that lead to PAH begin in the distal vasculature, the distal and proximal arteries communicate with one another through PP transmission and wave reflections likely contributing to a cycle of positive feedback that detrimentally influences disease progression[24,27,43,54] (Figure 2.1). Initially, chronic vasoconstriction and vessel remodeling causes decreased PAC in the distal vasculature.[29] Proximal artery walls thicken in response to elevated mPAP and also stiffen, increasing impedence and RV workload further.[55,56,53] Decreased proximal PAC amplifies pulse wave transmission to the distal vasculature, resulting in an inflammatory response that drives further distal vascular remodeling and loss of PAC.[24,25,27] Understanding the molecular mechanisms that drive initial alterations in distal arterial compliance will allow for new drug targets capable of preventing disease progression in the early stages of development.

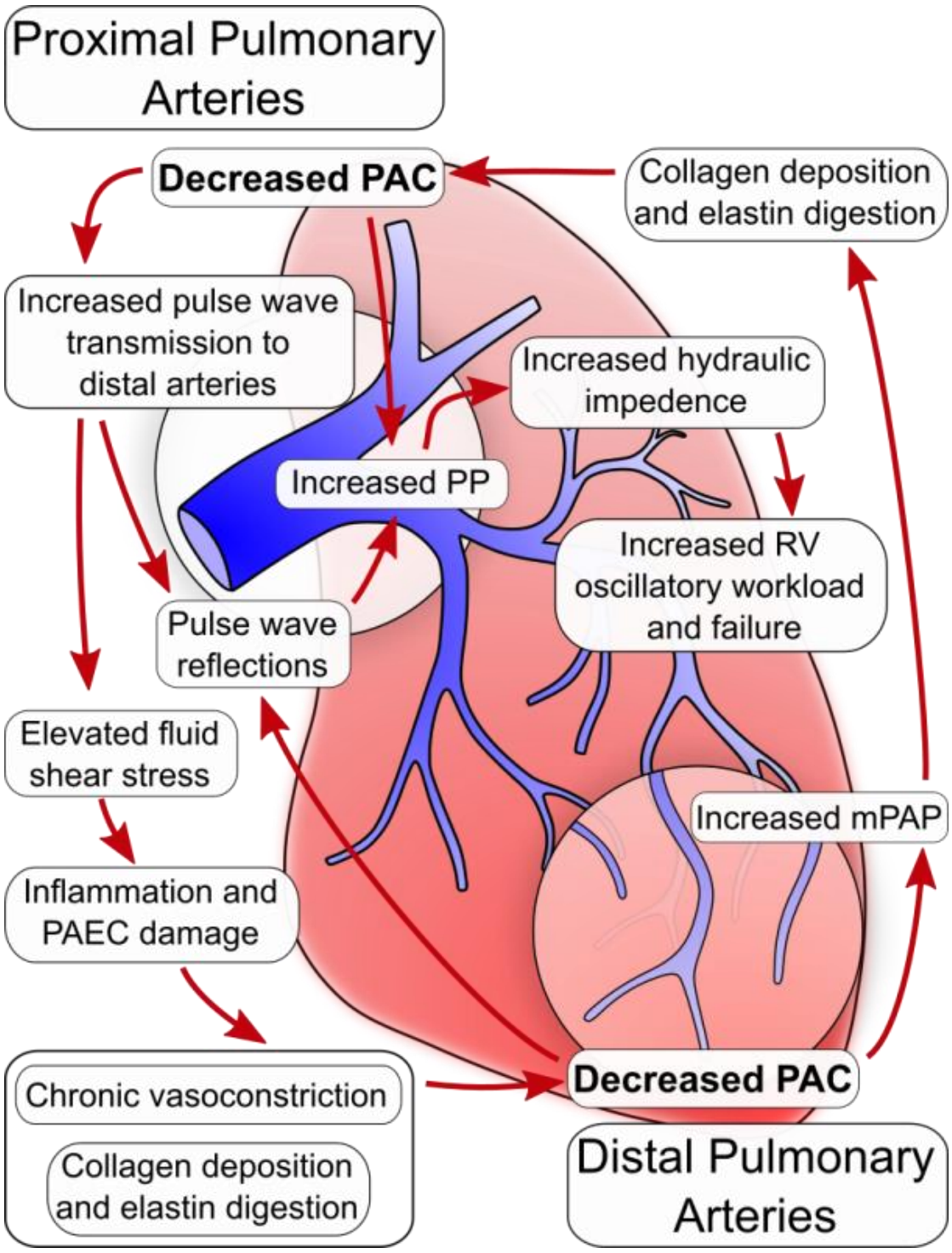


**Figure 2.1: Positive feedback of biomechanical remodeling in PAH.**
Decreases in distal vessel PAC begin a positive feedback cycle advancing the progression of PAH leading to RV failure and death secondary to increased oscillatory workload. PAC = pulmonary arterial compliance, PP = pulse pressure, PAEC = pulmonary arterial endothelial cells, mPAP = mean pulmonary arterial pressures, RV = right ventricle. Figure reproduced from Bloodworth et.al., ref. 19.

Recent studies in both small animal models and with human tissue suggest that alterations in distal arteriole compliance occur much earlier than previously believed, preceding many of the other aspects of proliferative vascular remodeling including pulmonary arterial endothelial and smooth muscle cell (PAEC and PASMC) proliferation and migration. In both mice and rat models of PAH pulmonary arterioles stiffness was observed to dramatically increase prior to the development of elevated pressures.[57] Evidence suggests that the mechanosensing protein YAP/TAZ mediates these early changes in compliance, and pharmacologic targeting of proteins promoting extracellular matrix stiffening effectively prevents vessel stiffening and PAH *in vivo*.[58,59] PAECs cultured on stiff substrates *in vitro* also exhibit alterations in metabolism that promote proliferation by these same mechanisms.[60] Taken together, these data emphasize how early changes in PAC precede and catalyze the progression of PAH.

Multiple aspects of vascular remodeling are responsible for inducing distal vascular stiffening and accelerating RV failure. Stimulation of matrix metalloproteinase activity, elastase activity, and transition of PASMCs from a mature contractile phenotype to a synthetic phenotype results in a change in composition and amount of extracellular matrix (ECM) that alters vessel wall mechanics[61–64]. The molecular mechanisms for these changes rage from the consequences of mutations in the transforming growth factor β (TGF-β) superfamily of receptors (predominately the bone morphogenetic protein receptor 2, or Bmpr2), altered serotonin signaling dynamics, and inflammation[29,65–68]. A more detailed understanding of these mechanisms and how they contribute to altered pulmonary compliance is essential to developing effective PAH therapy. Numerous interactions within these pathways may offer many promising novel drug targets for PAH that address the fundamental mechanical changes ultimately responsible for disease morbidity and mortality.

*Extracellular Matrix Remodeling and Cell Stiffening: Contributions to Vessel Compliance*

Decreased PAC is caused by certain aspects of proliferative vascular remodeling and represents a change in the mechanical properties of the vessel itself distinct from transitory vasoconstriction. Traditionally, increased vascular stiffness have been attributed to alterations in ECM content, especially collagen accumulation. However, recent evidence suggests that a number of other mechanisms may be responsible as well and include altered ECM organization, dysregulation of cell-ECM and cell-cell force transduction, and an intrinsic stiffening of PASMCs themselves. The molecular pathways that drive changes during PAH development include the downstream effects of mutations in the TGF-β superfamily of receptors (most notably Bmpr2), mutations in and abnormal responses to serotonin signaling, and the recruitment and activation of inflammatory cells.

The ECM is an important regulator of the elastic and viscous properties of blood vessels. ECM accumulation on its own does not necessitate a decrease in elasticity; rather, the mechanical properties and arrangement of the ECM is critical to determining how it alters the mechanics of the blood vessel wall. Collagen is widely regarded as the primary component of the ECM responsible for increased vascular stiffness in PAH. Collagen engagement occurs gradually as stress is applied to the vessel wall, progressively heightening the vessel's resistance to further deformation until a maximum strain is reached. Studies of systemic arteries suggest that collagen in the media of the vessel is engaged throughout the duration of the vessel expansion, while adventitial collagen begins to resist further strain after about 20% deformation.[69] Due to its inherent non-compliance, as collagen accumulates in the vessel wall the elasticity of that wall decreases.[70] Vascular remodeling and stiffening in the proximal conduit pulmonary arteries is primarily a phenomenon of collagen accumulation in hypoxic pulmonary hypertension models.[44,70–72] Collagen accumulation may also be responsible for the loss of small artery compliance in PAH: in the vascular endothelial growth factor receptor 2 (VEGFR2) inhibitor model of PAH, collagen accumulates in both the media and adventitia of the small

arteries and is actively synthesized in the small muscular arteries of patients with idiopathic PAH.[73–76] PASMCs with a synthetic phenotype and fibroblasts in the vessel adventitia are generally identified as the cellular source for collagen accumulation[77]. Recent studies also implicate the trans-differentiation of PAECs into myofibroblasts and PASMC-like cells in the progression of PAH vessel remodeling (endothelial to mesenchymal transition, or EndMT); these trans-differentiated cells could also serve as a source for increased collagen production (given their expression of collagen type-1 markers).[78–80]

In addition to collagen accumulation, increased collagen turnover and altered organization may also contribute to vessel stiffness changes. Matrix metalloproteinases (MMP) are responsible for collagen breakdown and turnover. MMPs are negatively regulated by tissue inhibitors of MMPs (TIMPs), which also control cell proliferation. There are many types of MMPs that play various roles in PAH pathogenesis. Ample evidence from several animal models of PAH suggest both MMPs and TIMP-1 are abnormally regulated during disease; however, the roles that the various MMPs and TIMPs play differs depending on the type of animal model used.[63,81–83] In cultured PASMCs from human idiopathic PAH patients, MMP-2 expression and activity is elevated while MMP-3 is decreased and MMP-1 is unchanged[84]. MMP-9 is elevated in the plasma and urine of PAH patients, as are circulating biomarkers of collagen metabolism and TIMP-1.[85,86] Transgenic expression of MMP-9 also augments vascular remodeling in the monocrotaline mouse model of PAH.[87] Proper alignment of collagen is an important determinate of its mechanical properties[69,88]; in systemic arteries, proper collagen fiber alignment controls vessel wall stiffness.[89] Continual degradation and re-synthesis of collagen, a process stimulated by MMPs, compromises collagen fiber organization. MMP-2 also promotes production of tenascin-C, a glycoprotein that amplifies the response of PASMCs to various growth factors.[90] MMP-induced PASMC proliferation and transition to a synthetic phenotype provides a possible explanation for how simultaneously increased collagen breakdown and synthesis can result in

net increased collagen deposition. This deposition, coupled with disordered alignment, likely contributes to decreased PAC.

Both collagen and elastin contribute to the nonlinear deformation of vessel walls. Where collagen imparts rigidity, engaging and resisting further stress after an initial distention, elastin imparts compliance at lower PPs. Elastin is normally found in an organized alignment in the internal and external elastic lamina of large pulmonary arteries and in the media of small arteries. Loss or disruption of elastin organization has been hypothesized to contribute decreased PAC.[75,91] In the carotid arteries, elastin degradation results in significantly increased vessel stiffness.[92,93] Mice with graded vascular elastin expression exhibit gradually increasing mPAP that inversely correlates to the amount of elastin expressed.[94] However, other studies have demonstrated concomitant increases in elastin and collagen content as well as arterial stiffness for both large arteries and small muscular arteries.[43,95] Thus, elastin disorganization and fragmentation, rather than amount, is likely the more important contributor to PAC.[96] Serine elastase activity is elevated in the monocrotaline model of PAH, and inhibition of serine elastase reverses disease progression.[97] As organization of elastin is critical for proper mechanical response to stress, it is possible that serine elastase-mediated disruption of this organization contributes to elevated PAC.[98,99] In porcine aortas, the gradual degradation of elastin induces collagen fiber alignment with subsequent early collagen engagement and rapid stiffening of the vessel wall.[69,100] Additionally, serine elastase induces growth factor release (such as FGF) and tenascin-c production, which in turn clusters and upregulates growth factor receptors in PASMCs (such as EGFR); therefore, serine elastase inhibition is expected to exert anti-proliferative and pro-apoptotic effects on PASMCs and thereby reverse remodeling of distal arteries.[90,101–104] It is likely that elastin degradation decreases PAC through a combination of the effects discussed here, though the magnitude of each effect to overall PAC remains unclear.

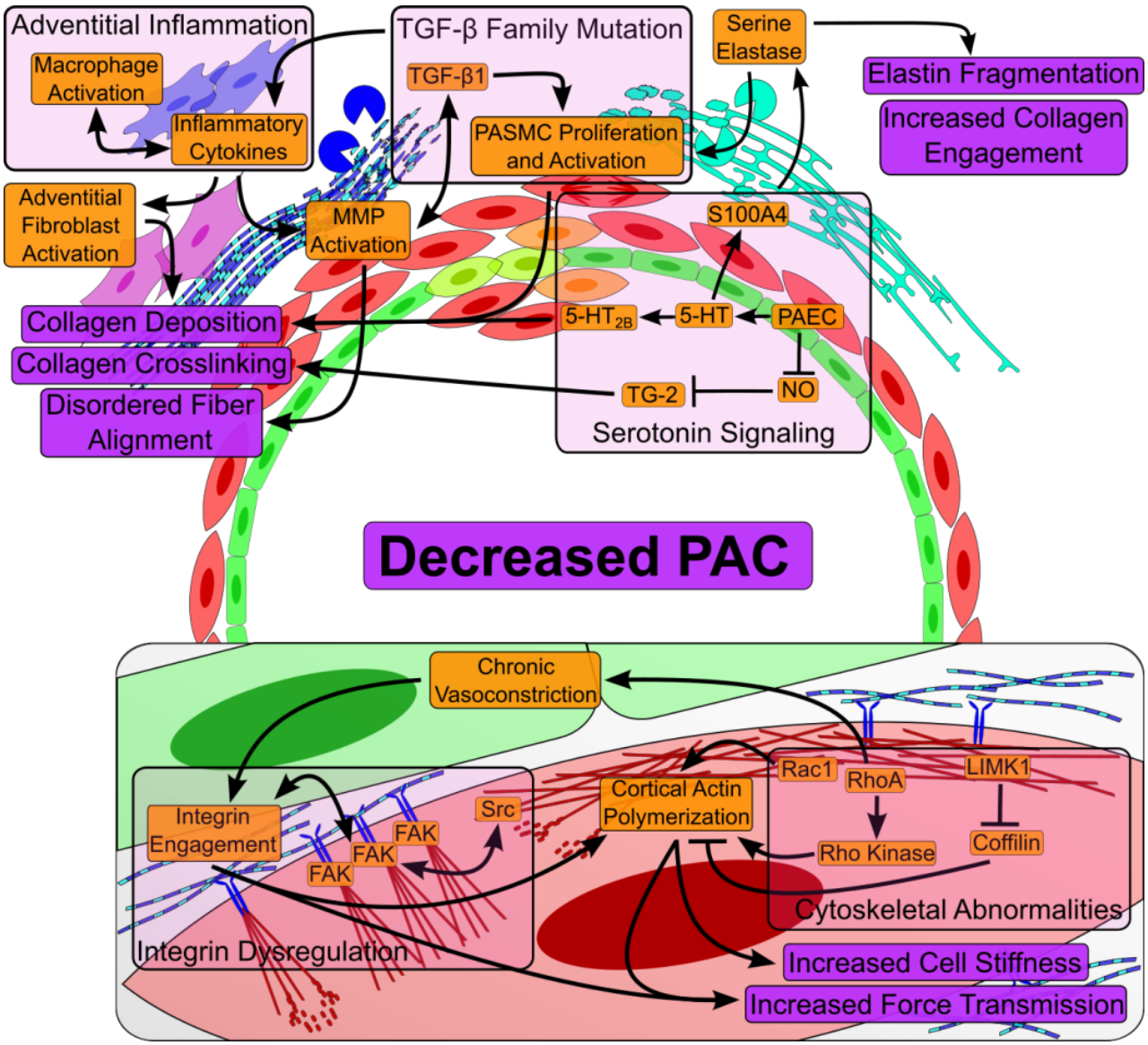


**Figure 2.2: The molecular mechanisms responsible for driving changes in PAC.**
(Top) Changes in ECM organization and content change the mechanical properties of the vessel walls. These changes are driven by a variety of molecular mediators (shown in orange) and involve multiple cell types acting in tandem. (Bottom) Chronic vasoconstriction, integrin engagement, and dysregulation of small GTPase regulators of the actin cytoskeleton cause polymerization of non-contractile F-actin with a consequential increased transmission of force between the cell and ECM and stiffening of PASMCs. MMP = matrix metalloproteinase, NO = nitric oxide, PAEC = pulmonary artery endothelial cell, PASMC = pulmonary artery smooth muscle cell, PAC = pulmonary arterial compliance, TG-2 = transglutaminase-2. Figure reproduced from Bloodworth et.al., ref 19.

Alterations in how cells transmit force between one another and the surrounding ECM may significantly alter vascular stiffness. Increased force transduction between cells and their environment allows for prolonged resistance to deformation in addition to increased transitory contraction, and the resulting increased stiffness in turn may further influence cell behavior. Cells transmit forces to and from their environment through integrins, a class of matrix binding proteins. The cytoplasmic domains of integrins are associated focal adhesions (FAs), which are large protein complexes that directly transmit forces between the ECM and the cytoskeleton. These forces are also translated by the cell into chemical signaling pathways in a process known as mechanotransduction.[105,106] Integrin binding and FA organization help to mediate the stiffening of systemic arteries (as occurs in atherosclerosis and aging), and impaired regulation of FA organization inhibits the integrins' ability to serve as fluid flow shock absorbers.[107] While this method of cell-induced stiffening is partially regulated by vasoconstrictors it is distinct from the stiffening caused by transitory contraction: vasoconstrictor stimulation of vascular smooth muscle cells causes integrin clustering and engagement with the ECM, increasing cell stiffness in a process involving non-contractile cytoskeletal elements.[108] Supporting this concept, when stretched at sites of integrin attachment vascular smooth muscle cells exhibit an increase in cell stiffness dependent on non-contractile and contractile elements, with stretch responses possibly dependent on activation of stretch-sensitive calcium channels.[109]

While the contributions of integrin force transmission and mechanotransduction to the development of systemic hypertension are increasingly well studied, relatively little is known about how integrins contribute to PAC in PAH. Integrin expression is significantly altered in PASMCs localized to the small pulmonary arteries of monocrotaline and hypoxia treated rats. While altered ECM deposition patterns might regulate some integrin subunits, non-specific regulation of other subunits (specifically $\alpha_5$, $\beta_1$, and $\beta_3$) appears to directly contribute to disease progression by advancing PASMC proliferation, vascular remodeling, and contractility.[110] Specific motifs in ECM proteins, including the argentine-glycine-aspartic acid sequence, induce

PASMC contraction through integrin $\beta_3$ subunits.[111] Integrin modulation of intercellular calcium levels also induces contractile responses in PASMCs and other types of smooth muscle cells, and advances small vascular remodeling in systemic hypertension via the $\alpha_5$ subunit.[112–114] Further work with hypoxic rats and idiopathic PAH patients has illustrated that integrin binding may regulate PASMC cytoskeletal dynamics and proliferation in small arteries and arterioles by controlling Fhl-1 signaling (a regulator of cell cycle progression through cyclin D1) through the cytoskeletal adapter protein Talin-1.[115] Reduction of $\beta_1$ integrin in PAH also induces PAEC apoptosis by reducing $\alpha_3\beta_1$ complex formation and signaling through adenomatous poliposis coli.[110,116]

Prolonged integrin engagement may lead to permanent rearrangements in cytoskeletal organization that contribute to a long term decrease in PAC. The transduction of force between the cell and its surrounding ECM largely depends on integrin attachment to the non-contractile cortical cytoskeleton underlying the cell membrane.[117] Chronic vasoconstrictor stimulation of smooth muscle cells causes a reorganization of the non-contractile cytoskeleton favoring net polymerization, a response that facilitates low-energy maintenance of decreased vessel diameter and disengagement of the contractile apparatus.[118,119] Furthermore, changes in cytoskeletal organization – as seen in continuously contractile smooth muscle cells – have the potential to significantly alter PAC by inducing an intrinsic stiffening of PASMCs independent of transient cell contraction.[120] While these changes may initially begin as adaptive by enabling the cell to withstand increased force transmission, dysregulation of the underlying molecular mediators could pathologically alter cytoskeletal organization and consequently induce maladaptive changes in cell stiffness.[121]

*Molecular Mediators of Vessel Compliance: Bmpr2, 5-HT$_{2B}$, and Src*

Research at Vanderbilt University beginning in 1980 eventually revealed Bmpr2 as the causative mutation responsible for hereditary PAH.[122–125] Subsequently, Bmpr2 mutations were

discovered in a cohort of patients with idiopathic PAH, and decreased Bmpr2 expression found in patients with PAH associated with other conditions.[29,126] The consequences of a mutation in the Bmpr2 receptor are thought to be a result of decreased Bmpr2 expression or function, either as a result of functional haploinsufficiency or dominant-negative effects, respectively.[127] Normally the BMP ligand binding to Bmpr2 causes a signaling cascade mediated by the SMAD family of signaling proteins and transcription factors. BMP signaling in this manner serves to inhibit the cellular response to injury and subsequent upregulation of genes associated with tissue regeneration and repair, bringing a resolution to the process of wound healing. When Bmpr2 signaling is decreased, either as a consequence of decreased receptor expression or impaired function, the cellular and molecular processes activated in acute injury fail to terminate normally. This results in the proliferative vascular remodeling processes responsible for arteriolar occlusion and stiffening.[127]

Abnormalities in Bmpr signaling axis components that are connected with PAH in humans and animals include mutations and reductions in expression for Bmpr1a (which co-localizes with Bmpr2) and Alk1 receptors as well as their downstream SMAD targets.[29,126,128–130] Mice with a deletion of Bmpr1a from a portion of their PASMCs develop elevated mPAP with exposure to prolonged hypoxia and show evidence of increased adventitial collagen deposition and elastin lamina disruption and deposition in areas of Bmpr1a deletion.[131] Further investigation with this model suggests that while ECM changes induced by Bmpr1a deletion decrease proximal PAC, the deletion is ultimately protective against distal vascular remodeling.[132] TGF-β1 signaling through Alk1 is an important mediator of fibrosis and collagen deposition, and Bmpr2 mutations result in increased TGF-β1 production and an abnormal proliferative response to TGF-β1.[133] In addition to directly stimulating collagen production, TGF-β1 can also activate, and is in turn activated by, MMP-2 and MMP-9, suggesting a feed-forward signaling mechanism that advances vascular remodeling.[134] This initial activation is mediated in part by IL-1β, an inflammatory cytokine secreted by macrophages in response to an IL-6

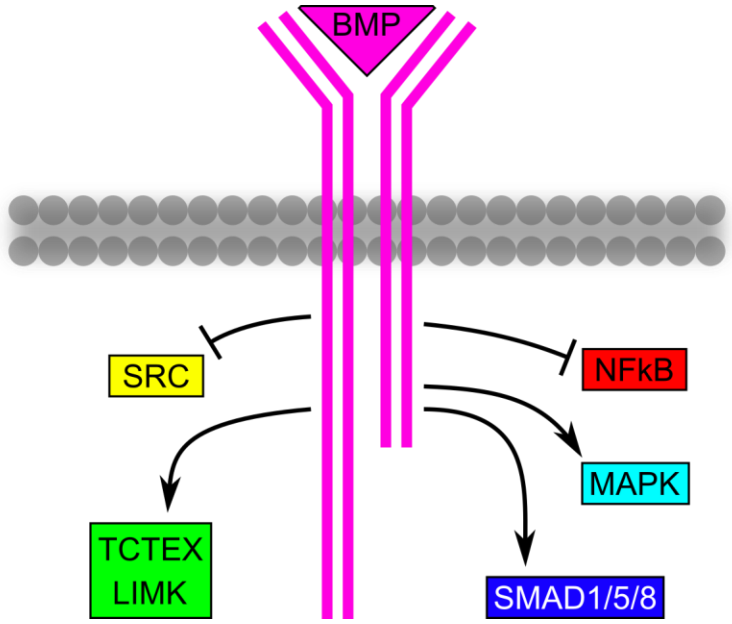


**Figure 2.3: A summary of Bmpr2 signaling pathways disrupted in PAH.**

induced macrophage phenotype transition.[135–137] Both IL-1β and IL-6 are upregulated in PAH; IL-6 is upregulated as a direct consequence of Bmpr2 loss of function (possibly through a p38 MAP kinase-mediated negative feedback loop in PASMCs), and IL-6 can further reduce Bmpr2 expression through STAT3 mediated microRNA regulation.[138,139]

Bmpr2 signaling also controls cell stiffening and force transduction through cytoskeletal protein regulation. Chronic vasoconstriction, caused in part by excessive production vasoconstrictors such as endothelin-1 (ET-1), is a hallmark of PAH. This environment is especially conducive to the development of cytoskeletal changes which lead to cell stiffening.[140] In this process, polymerized F-actin is primarily responsible for force transmission, and the actin toxin cytochalasin D prevents the ability of smooth muscle cells to maintain a prolonged contractile state (likely by preventing actin polymerization).[141,142] Small molecule mediators of actin organization and polymerization including the Rho GTPases RhoA, Rac1, Cdc42, and the protein kinase LIMK1 are also known to be abnormally regulated in PAH, and their dysregulation is also a direct consequence of Bmpr2 mutation and dysfunction (Figure 2.3).[143–147] Specifically, upregulation of Rac1 causes a decrease in actin fiber stability and induces actin reorganization and polymerization, though the mechanism of Rac1 activation by the Bmpr2 mutation is unclear.[145] In addition, a large body of work demonstrates Rho kinase activity (the downstream effector of RhoA) is increased in PAH, and inhibition of Rho Kinase alleviates PAH

development in hypoxic, monocrotaline, and genetic mouse models, though the extent of this improvement is limited.[148–151] In addition to mediating PASMC contractility, RhoA and Rho kinase signaling induces F-actin polymerization and inward vascular remodeling.[143] LIMK1 phosphorylates cofilin, preventing cofilin from inhibiting actin polymerization. Normally, the cytoplasmic tail domain of Bmpr2 directly inhibits LIMK1 activity, and mutations in this domain lead to increased LIMK1 activity and consequently increased potential for actin polymerization.[146] LIMK1 is also regulated by the same Rho GTPases that are dysregulated in hereditary PAH, suggesting that Bmpr2 mutations contribute to cytoskeletal disruption via multiple mechanisms.[152–154]

While Bmpr2 family mutations may be necessary for PAH, they are not always sufficient. The penetrance of PAH is much lower among those heterozygous for Bmpr2 mutations than homozygotes.[29] This variable penetrance, combined with the variable expressivity common to PAH, has led to the hypothesis that the disease phenotype requires that either remaining functional Bmpr2 levels drop below a certain threshold, or secondary processes tip the balance into disarray.[127] Examples of such secondary processes are altered estrogen signaling or metabolism (helping to explain the nearly 2 to 1 female to male ratio among mutation carriers,[155] though this antagonistic relationship is not preserved in other forms of pulmonary hypertension[12]), inhibited function or expression of voltage gated potassium channels[156], exaggerated responses to inflammation,[157] and serotonin signaling.[65]

Among the secondary molecular processes associated with PAH, serotonin signaling is especially important and ubiquitous. The “serotonin hypothesis” of PAH first emerged in following the PAH outbreak among users of the serotonergic anorexigens aminorex and fenfluramine in the 1960’s and 1990’s.[65] Subsequent studies in patients with idiopathic PAH found significant elevations of serotonin in patient serum, likely due to increased synthesis by pulmonary vascular endothelial cells, and serotonin has since been implicated in abnormal smooth muscle cell proliferation and chronic vasoconstriction, elastase degradation, fibrosis,

and vessel stiffening, and mediating thrombosis and perivascular inflammatory cell infiltration.[65,158–162] The mechanisms for these phenomenon are diverse and include alterations in intracellular serotonin transport via SERT or 5HTT, post-translational modification of proteins in a process known as serotonylation, and signaling through the serotonin cell-surface receptors.[158,163] In systemic sclerosis, a disease often associated with PAH, serotonin induces collagen synthesis and ECM production by interstitial fibroblasts by TGF-β1 dependent signaling through the 5-$HT_{2B}$ receptor.[160] In addition to regulating collagen production, serotonin can be utilized to cross-link matrix proteins by the enzyme transglutaminase-2 (TG-2) through a process known as serotonylation, increasing vascular stiffness.[163,164] TG-2 is regulated by nitric oxide (NO), a vasodilator produced by PAECs and known to be significantly downregulated in PAH.[165,166]

Serotonin signaling also regulates elastase activity in PAH through the calcium binding protein S100A4. S100A4 is overexpressed in the PASMCs of the remodeled small muscular arteries in pediatric PAH patients, and consistent with these findings in humans, mice overexpressing S100A4 develop pulmonary hypertension and small vessel remodeling.[159] In addition to promoting PASMC proliferation, S100A4 induces production of serine elastase by PASMCs.[167,168] While the mechanism whereby S100A4 induces PASMC elastase production is poorly defined, S100A4 expression is induced partly by serotonin signaling through the 5-$HT_{1B}$ receptor and activity of the serotonin transporter SERT.[158]

Bmpr2 haploinsufficient mice, which themselves are phenotypically normal, spontaneously develop PAH after infusion with serotonin.[169] Additionally, small pulmonary resistance arteries in Bmpr2 haploinsufficient animals exhibit exaggerated contractile responses to serotonin.[169] Exactly how serotonin contributes to disease progression in Bmpr2-associated PAH is unclear, though some studies suggest RhoA and both serotonin type 1 and 2 receptor signaling may be important.[65,170]

One receptor in particular, the 2B receptor (5-$HT_{2B}$), has attracted attention from PAH researchers since the discovery that the active metabolite of dexfenfluramine (responsible for the PAH outbreak of the 1990's) is a selective agonist for 5-$HT_{2B}$.[171] Subsequent work has demonstrated that 5-$HT_{2B}$ expression is elevated in different PAH animal models, and that antagonism or ablation of the 5-$HT_{2B}$ receptor can prevent disease development in these models.[172–176] 5-$HT_{2B}$ expression is also significantly elevated in the small arteries of patients with idiopathic PAH.[173] In systemic sclerosis, a disease often associated with PAH, serotonin induces fibroblast collagen synthesis by TGF-β1 dependent signaling through 5-$HT_{2B}$, contributing to a loss of vessel compliance[160]. Despite this evidence of 5-$HT_{2B}$'s necessity in the pathogenesis of PAH, there is little data describing the molecular mechanisms downstream of 5-$HT_{2B}$ that mediate these deleterious changes.

The protein kinase Src is a ubiquitous, intracellular signaling molecule that regulates a wide variety of cellular functions. Elevated Src activity is characteristic of PAH: markers of Src activity are elevated in idiopathic PAH[177], and increased Src activity is also correlated with PAH penetrance and severity[178–181] with reductions in cell proliferation and vascular remodeling dependent on Src activity[182]. Src also regulates force transduction from vascular smooth muscle cells to the ECM by controlling levels FAK, and ultimately its associated integrin-cytoskeletal attachments, at the cell surface.[183,184] When Src signaling is elevated, FAK levels at the cell surface increase and lead to greater transmission of force between the cell and ECM.[184] Src activity is also regulated itself by integrin engagement and FAK activation: inhibition of FAK has recently been shown to prevent pulmonary hypertension in monocrotaline treated rats by decreasing Src activity and reversing the migratory phenotype of diseased PASMCs[181]. While the benefit of Src inhibition for PAH treatment has traditionally been associated with reductions in cell proliferation, it is also possible that reducing Src activity could alter abnormal patterns of integrin engagement and signaling and thereby contribute to increased vascular stiffness.[182,185]

Mutations in the cytoplasmic tail domain of the Bmpr2 receptor can cause a loss of Src functional inhibition leading to elevated signaling[186]. In Bmpr2 receptor deficient mice elevated Src signaling is observed in endothelial cells, with pharmacologic inhibition of Src restoring endothelial barrier function.[187] Furthermore, mice with patient-derived mutations in the cytoplasmic tail domain of Bmpr2 spontaneously develop PAH.[145,188] Src also interacts with the serotonin signaling pathways through the 5-$HT_{2B}$ receptor. 5-$HT_{2B}$ mediates its mitogenic effects through Src and acts in concert with the platelet-derived growth factor receptor (PDGFR, also implicated in PAH pathogenesis) to initiate cell cycle progression.[189] [173] 5-$HT_{2B}$ antagonism also arrests TGF-β1-stimulated Src activation and signaling, preventing the development of calcified nodules in an *in vitro* model of calcific aortic valve disease.[190] Thus, Src activation and signaling is represents a likely mechanism in which both Bmpr2 and 5-$HT_{2B}$ signaling converge to mediate PAH pathogenesis.

*Intrinsic Myeloid Abnormalities: Hematopoietic Cells and Pulmonary Arterial Hypertension*

While PAECs, PASMCs, and (more recently) fibroblasts of the adventitia are all known to participate contribute to PAH pathogenesis, evidence from the last 10 years strongly suggests that certain subtypes of hematopoietic cells play an indispensable role in vascular remodeling. Myeloproliferative abnormalities have been observed in patients with familial, idiopathic, and associated PAH, and increased deposition of reticulin in the bone marrow of these patients suggests abnormal hematopoietic processes.[191] These changes in bone marrow composition are also present in the unaffected family members of hereditary PAH patients, suggesting that the changes in hematopoiesis precede disease onset. Transplantation of $CD34^+$ progenitor cells isolated from the peripheral blood of patients with idiopathic PAH into nonobese/diabetic severe combined immunodeficient mice results in the mice developing a PAH-like illness, complete with endothelial injury, thrombosis, right ventricular hypertrophy, and vascular remodeling.[192] In mice, restriction of mutant Bmpr2 expression to the bone marrow

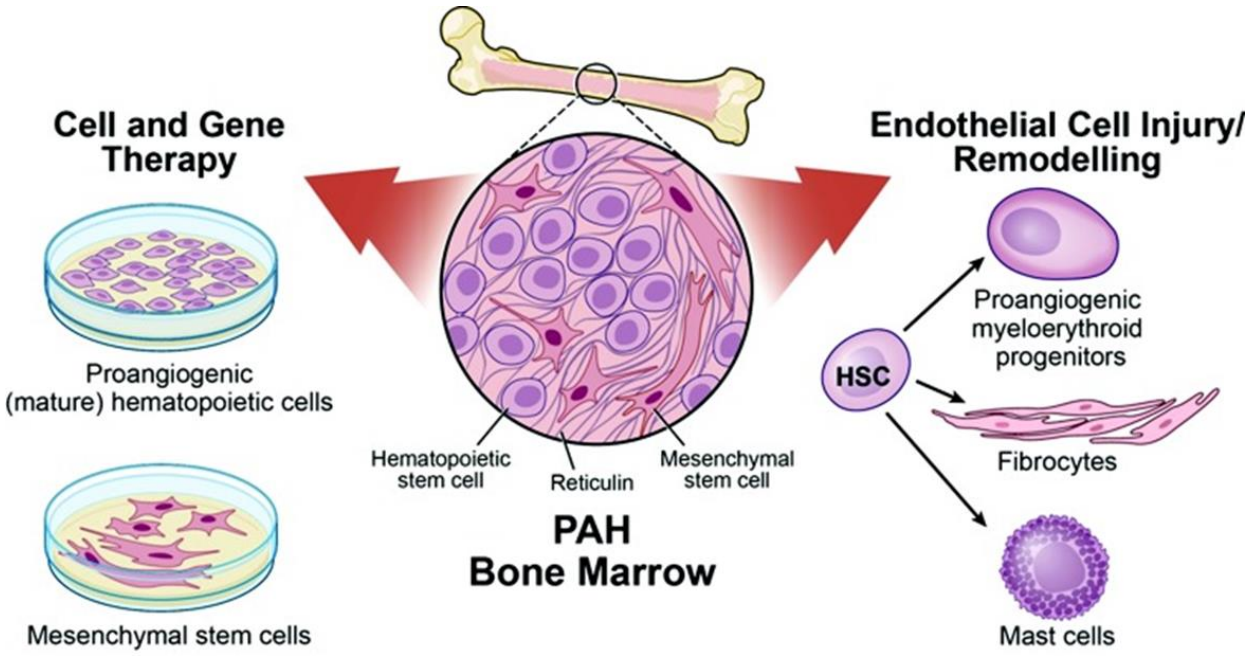


**Figure 2.4: A summary of BM-PAC function in PAH (adapted from Lanzola et.al., 2013)**

alone is sufficient to induce PAH, and conversely restriction of mutant Bmpr2 expression to the periphery (with normal Bmpr2 expressed in the bone marrow alone) significantly improves hemodynamics and metrics of vascular remodeling.[193]

The types of bone marrow derived cells that mediate small vessel remodeling are an active area of ongoing research. Early accumulation and alternative activation of macrophages is observed in mouse models of PAH and production of inflammatory mediators by macrophages directly induces PAEC apoptosis.[194–196] Mice with mutant Bmpr2 receptors also display constitutive activation of tissue macrophages that can directly promote a migratory and proliferative phenotype in co-cultured PASMCs.[197] Lymphoid cell contributions to vascular remodeling are less understood, though suppression of T regulatory cell function may pave the way for sustained peri-vascular inflammation.[198]

Special attention to a subclass of myeloid-derived proangiogenic cells, known alternatively as proangiogenic myeloerythroid progenitors or bone-marrow derived proangiogenic cells (BM-PACs) suggests that these cells may participate directly in small vessel

remodeling. BM-PACs are a heterogenous group of myeloid-derived cells that express a variety of endothelial and/or progenitor cell surface markers.[199] Cells expressing both endothelial and progenitor cell surface markers are also routinely observed to accumulate in the walls of remodeled vessels.[200,201] In humans, these cells are also observed in the perivascular vasa vasorum of pulmonary arteries and concentric and plexiform lesions of the actively remodeling arterioles, suggesting a direct involvement in vascular remodeling.[191,200,202] Pharmacologic antagonism of either chemokine receptors or the progenitor-cell receptor cKit reduces the number of these cells in the peripheral circulation and improves hemodynamic parameters in mouse models of PAH.[200,203] This story is complicated by the fact that the absolute number of BM-PACs can be either elevated, suppressed, or unchanged in the peripheral blood of idiopathic PAH patients.[202–204] Futhermore, *ex vivo* expansion or fresh isolation of BM-PACs followed by re-infusion can actually alleviate PAH in several different small and large animal models.[205–209] In idiopathic PAH, ongoing clinical trials using infusions of *ex vivo* expanded BM-PACs or BM-PACs genetically engineered to express endothelial nitric oxide synthase show small but significant improvements in clinical metrics of disease severity.[210] The inconsistency of these findings can be explained by both lack of a uniform definition of BM-PAC as well as the fact that the function of BM-PACs is likely context-specific. A better understanding of the role BM-PACs and the mechanisms involved in their recruitment and activation in the lung would greatly benefit the rational design of therapeutics for PAH. The varying effects of BM-PACs are summarized in Figure 2.4.

# CHAPTER 3: SEROTONIN 2B RECEPTOR ANTAGONISM PREVENTS HERITABLE PULMONARY ARTERIAL HYPERTENSION

Text and figures adapted in part from:

West JD*, Carrier EJ*, Bloodworth NC*, et al. *Serotonin 2B Receptor Antagonism Prevents Heritable Pulmonary Arterial Hypertension*. PLoS One. 2016;11(2):e0148657.

*Denotes equal contribution

## *Introduction*

PAH is a disease in which a gradual increase in pulmonary vascular resistance eventually leads to right heart failure and death. There are no clinically available disease-modifying therapies for PAH. The strongest epidemiologic risk factor is use of serotonergic anorexigens.[211] There have been two epidemics of serotonergic anorexigen-induced PAH; aminorex in the 1970s and dexfenfluramine in the 1990s.[212,213]

Several mouse models have been developed to examine the role of serotonin signaling in the onset of PAH. Mice with knockout for serotonin transporter (5HTT),[214,215] serotonin receptor 1B ($5\text{-}HT_{1B}$),[216] or $5\text{-}HT_{2B}$ are protected against hypoxic pulmonary hypertension. While excellent work has been done demonstrating that increased serotonin signaling is responsible for the onset of PAH in patients taking anorexigenic drugs, essentially no work has been done previously to mechanistically link signaling at the level of the receptor to physiologic outcomes.

Independent of serotonergic drugs the strongest heritable risk factor for development of PAH is the presence of a mutation in Bmpr2, present in the large majority of familial cases. Mice expressing human-derived Bmpr2 mutations develop PAH within a few weeks.[145,217] In both mice and humans with Bmpr2 mutation, penetrance is incomplete, with lifetime risk of overt disease of about 20-25% in patient families[218], and 30-50% in Bmpr2 mutant mice after 6 weeks of transgene activation.[145] Although serotonin has been shown to increase penetrance in

Bmpr2-deficient mice,[169] the mechanism has never been explored. Anorexigen-associated PAH is clinically indistinguishable from idiopathic or heritable PAH, suggesting that common mechanisms downstream of the cell-surface receptors mediate all forms of the disease.

The mechanism underlying PAH of any kind is unknown; however, heritable and drug-induced PAH share some common features. Both 5-$HT_{2B}$ and Bmpr2 receptors interact directly with the tyrosine kinase, Src. Src binds to the cytoplasmic tail of Bmpr2[186], and Bmpr2 mutation leads to increased Src phosphorylation and downstream activity.[145,180] Likewise, agonism of 5-$HT_{2B}$, by either serotonin or metabolites from anorexigens, does the same.[189,219] Therefore, 5-$HT_{2B}$ and Bmpr2 likely have no effect on one another, but their functionality significantly and independently alters Src activity, which appears to be a key component in the development of PAH. Further, it has been previously published that antagonism of 5-$HT_{2B}$ in heart valve cells inhibits Src translocation after its phosphorylation[190]; this is important since valvular disease often accompanies drug-induced PAH.[171] We thus hypothesized that antagonism of 5-$HT_{2B}$ may be able to prevent heritable PAH through the regulation of Src by preventing its downstream activities, but not its phosphorylation. To test this hypothesis, we examined the ability of a specific small molecule 5-$HT_{2B}$ antagonist, SB204741, to prevent PAH in mice with Bmpr2 mutation.

*Methods*

Bmpr2 Mutant Mice

Rosa26-$Bmpr2^{R899X}$ mice express the patient-derived R899X mutation in Bmpr2 in all tissues when induced with doxycycline. When $Bmpr2^{R899X}$ transgene is induced in adult mice for six weeks of activation, approximately 50% will develop PAH as defined by right ventricular systolic pressures (RVSP) above the normal range.[145] Adult (10-14 weeks of age at start) Bmpr2 mutant mice on an FVB/N strain background were fed doxycycline at 0.2g/kg in western diet (Bioserv) for 6 weeks. After two weeks, osmotic pumps (Alzet 1004) containing either

SB204741 in 50% DMSO/50% water or vehicle with the same DMSO/water formulation were implanted, and delivered SB204741 at 1 mg/kg/day or vehicle for the final four weeks. A similar dose (i.e. 3 mg/kg/day) has been used previously to successfully attenuate liver fibrosis in mice.[220] Mice were then placed under surgical anesthesia (Avertin) and RVSP measured through a catheter introduced into the right heart through the right jugular vein in a closed-chested procedure, as previously described.[221] After sacrifice, tissues were collected for further analysis. All procedures were approved by the Vanderbilt institutional animal care and use committee (IACUC).

Histology & Western Blots

Lungs were flushed with 5 ml PBS introduced through the right ventricle and allowed to flow out through a cut in the left atria to remove blood, then inflated with 0.8% low melt agarose and formalin fixed. Staining for CD45 was with BD Pharmingen # 550286 at 1:100. An observer blinded as to groups counted numbers of CD45 positive cells per field in 10 random 20x fields in each of four mice per group.

Downstream Src targets, p130Cas (CAS) and caveolin-1 (CAV1) were primarily quantified as a measure of Src activity. Antibodies used for Western blots were: Src and pSrc (Cell Signaling, #s 2110 and 2101, 1:1000), CAS and pCAS (Abcam, # ab89459 and Cell Signaling, # 4015, 1:1000), CAV1 and pCAV1 (BD Transduction Laboratories, #s 610684 and 611338, 1:1000 and 1:2000), Smad1 and pSmad1 (Cell Signaling, #s 6944 and 9511, 1:1000). All phosphorylation proteins were normalized to their respective total protein and β-actin (i.e. pSrc/Src/β-actin).

Gene Expression Analysis

Mouse Genome 430 2.0 microarrays (Affymetrix, Foster City, CA) were performed on homogenized whole lung tissue, as previously described.[222] Each array consisted of a pool of 3 mice, and two arrays were used per condition. Array results were submitted to the NCBI gene

expression and hybridization array data repository (GEO, http://www.ncbi.nlm.nih.gov/geo/) accession number (pending).

Preprocessing of all Affymetrix cel files was carried out using the RMA algorithm. Hierarchical clustering of both samples and genes, and principal components analysis, was performed using algorithms within JMP Pro 11.0 (SAS Institute). Statistical analysis of overrepresented gene ontology groups was performed using Webgestalt.[223]

Measurements of pulmonary arteriole wall elastic modulus

Atomic force microscopy (AFM) of whole tissue sections was adapted from previously published techniques for mouse heart valve leaflets.[224] Lungs from mice with or without a doxycycline-inducible mutation in the Bmpr2 receptor were isolated, embedded with Optimal Cutting Temperature compound, and sectioned after the mice were treated for 4 weeks with SB204741 or DMSO vehicle and hemodynamically phenotyped as described. Lung sections were stained with FITC conjugated rat anti-mouse CD31 (BD Biosciences), Cy3 conjugated mouse monoclonal α smooth muscle actin (αSMA, Sigma), and DAPI. Sections were immersed in PBS and CD31 and αSMA positive vessels less than 100 μm in diameter were identified with a Nikon Eclipse Ti microscope. Identified vessels were then scanned using a Bioscope Catalyst AFM at a scanning frequency of 0.25 Hz and a scan window size of 7-10 μm. A total of 5-7 vessels were scanned per animal from two sections of lung, with each vessel scanned in two separate regions.

The data presented are representative of single scans, consisting of 16,384 individual measurements (128x128) spanning an approximately 10-20 $um^2$ area along the vessel wall. The median value for each scan (in kPa) is used as a representative measurement for the entire scan window. This analysis method for AFM data for both tissues and biomaterials has been previously validated[224,225] and the results scale well with bulk modulus measurements.[226]

Bmpr2 mutant Cells

Cells used were derived from Immortomouse X Rosa26-rtTA2 X $TetO_7$-$Bmpr2^{R899X}$ or Immortomouse X Rosa26-rtTA2 X $TetO_7$-$Bmpr2^{delx4+}$ triple transgenic mice. The immortomouse contains a transgenic insertion of the SV40 large T antigen, tsA58, under control of an interferon-inducible promoter. When cells are grown at 33°C and interferon is added, the transgene is activated and the cells are immortalized and proliferate freely; at 37°C, this transgene is inert. The immortomouse therefore produces cells which proliferate as though they were immortalized at 33°C, but revert to a more normal phenotype when cultured at 37°C. Immorto-Bmpr2 mutant pulmonary endothelial and smooth muscle cells were collected from adult mice.

Src and tubulin motility analysis

Immortalized microvascular endothelial and smooth muscle cells, with or without mutant Bmpr2 induced with 300 ng/mL doxycycline, were co-transfected with fluorescently labeled Src and Tubulin and treated with 1 μM SB204741 or DMSO vehicle. Src and Tubulin motion was visualized with a Nikon Eclipse Ti confocal microscope for 15 min in four separate focal planes. Videos were analyzed in MATLAB using a custom Eulerian motion analysis algorithm to determine total motion by assessing differential changes in pixel intensity for each cell as previously described.[190] Src motion was weighted to the perinuclear region of each cell to adjust for anomalies induced by changes in cell edge positioning, and total motion was normalized to total pixel intensity and averaged across the four focal planes visualized for each cell.

Total and active TGF-β1 assay

Total and active TGF-β1 was assayed as described previously.[227] Briefly, immortalized microvascular endothelial and smooth muscle cells with or without a doxycycline inducible Bmpr2 receptor mutation were plated in 6 well plates at 40,000/$cm^2$ and cultured for 24 hours with 300 ng/mL doxycycline to induce expression of the transgene. After 24 hours, media was collected and prepared as follows. For measurements of activated TGF-β1, a 1:1 dilution of

media to serum-free Dulbecco's modification of Eagle's medium (DMEM, Corning CellGro) was prepared, and for measurements of total TGF-β1 media was heated to 100°C for 3 minutes (to activate latent TGF-β1) and diluted 1:10 with serum-free DMEM. The prepared media was added to cultures of transformed mink lung cells (TMLCs) transfected with a luciferase reporter gene with a TGF-β1 specific promoter and incubated for 18 hours. After incubation, cells were lysed and the lysate transferred to a white 96 well plate. Luminescence intensity was measured using a BioTek Synergy HT plate reader after automatically dispensing luciferase substrate from the Promega Luciferase Reporter kit. Luminescence intensity was correlated with TGF-β1 concentration with the aid of a standard curve.

Collagen gel contractility assay

The collagen gel contractility assay was adapted from previously published work.[228] A collagen gel solution consisting of 8:1:1 parts bovine collagen (Advanced BioMatrix PureCol), 10x Dulbecco's phosphate buffered saline (DPBS, Gibco), and 0.1 M NaOH was prepared and the pH adjusted to 7.4. 200 µL of gel solution was dispensed to 1.27 cm diameter Teflon rings (Seastrom Manufacturing Company) and the gel allowed to crosslink for 1.5 hours at 37°C. The top of the gel was seeded with a 200 µL of a cell suspension containing 40,000 immortalized microvascular endothelial and smooth muscle cells with or without a doxycycline inducible Bmpr2 receptor mutation and allowed to settle for 30 minutes. The Teflon rings were removed and media added containing 300 ng/mL of doxycycline and the cells treated with either 1 ng/mL TGF-β1 (porcine, R&D Systems Inc.), 1 µM SB204741 (Tocris), both, or neither. Gels were imaged using a dissection microscope (Olympus) at 30 minutes and 72 hours after seeding, and the treatment media was changed every 24 hours. Gel size was determined using ImageJ (National Institutes of Health).

Statistical methods

Statistics were performed using multiple factor ANOVA (+/- Bmpr2 mutation, +/- SB204741), with Fisher's exact test or Holm-Sidak post hoc test for comparisons between individual groups. Statistics were performed within JMP Pro 11.0 (SAS Institute) or SigmaPlot.

*Results*

5-$HT_{2B}$ Antagonism Prevents PAH in Bmpr2 Mutant Mice

Wild-type and Bmpr2 mutant mice were treated with the 5-$HT_{2B}$ antagonist SB204741 for the last four weeks of a six week transgene activation. While vehicle-treated mice developed elevated RVSP at about 50% penetrance, mice treated with SB204741 have pressures indistinguishable from controls (Figure 3.1 A). This rescue of RVSP was not due to suppressed cardiac output, as cardiac index was maintained (Figure 3.1 B). Note that Bmpr2 mutation in both mice and humans leads to right ventricular dilation under pressure, rather than hypertrophy[229], and so Fulton index was not assessed.

SB204741 did not impact either weight gain or blood glucose in these mice (Figure 3.2 A, B). Lung sections from Bmpr2 mutant mice had increased infiltrating cells, as previously reported[230], with the infiltrating cells being made up in large part of $CD45^+$ inflammatory cells. This increase in infiltrating cells was reduced by SB204741 treatment in Bmpr2 mutant mice, but increased by treatment in control mice (Figures 3.1 C, D, Figure 3.2 C,D), a pattern which will reoccur with many of the following results. 5-$HT_{2B}$ antagonism also reduced both partial and full muscularization of small pulmonary arteries in Bmpr2 mutant mice, without affecting muscularization of vessels in control animals (Figure 3.1 E). Partial muscularization is defined as actin staining surrounding less than 75% of the vessel perimeter, and is usually indicative of muscle spiraling along a vessel rather than completely surrounding it (full muscularization).

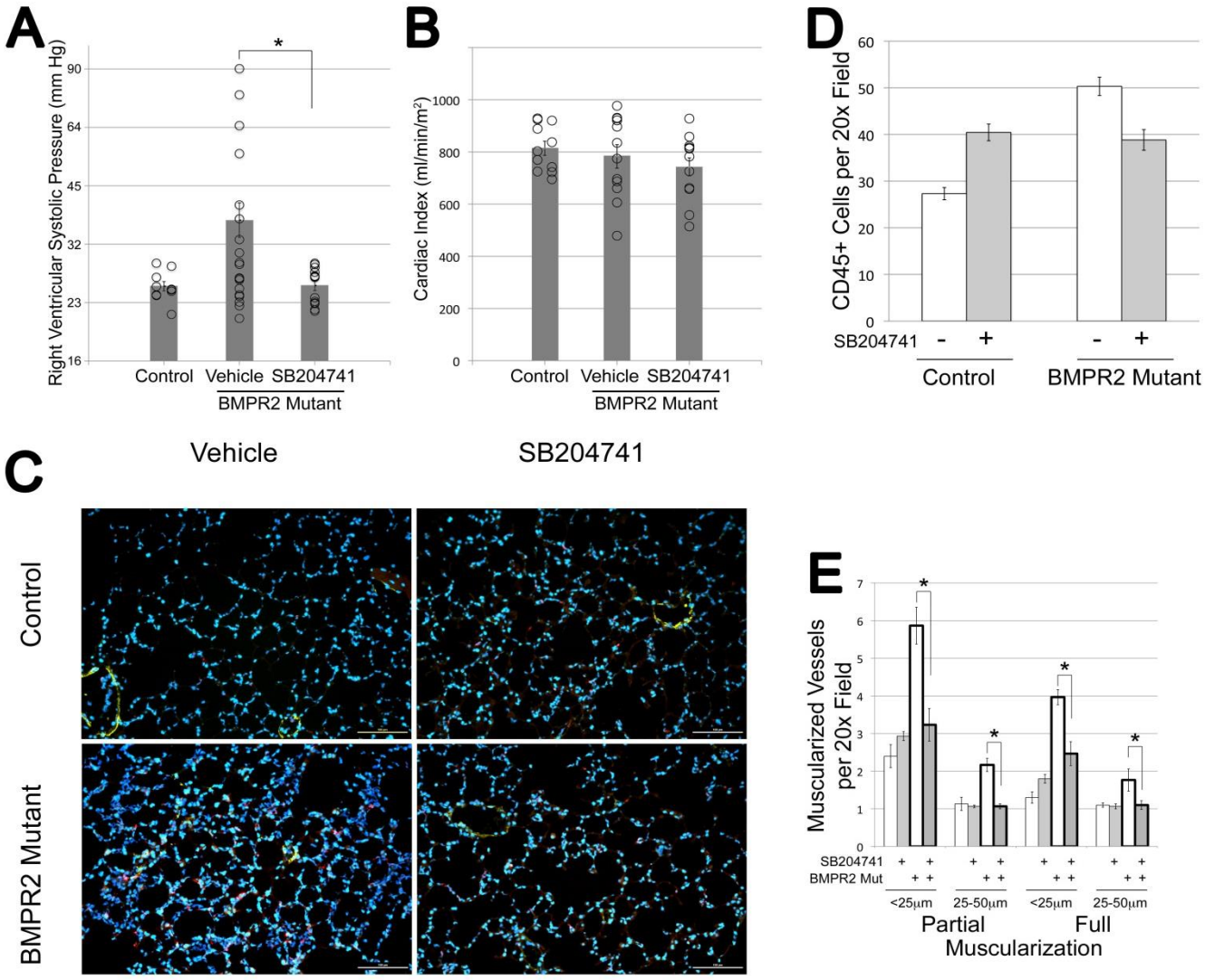


**Figure 3.1: 5-HT$_{2B}$ antagonism improves hemodynamic outcomes in Bmpr2 mutant mice.**
(A) Right ventricular systolic pressures are significantly elevated in Bmpr2 mutant mice with six weeks of transgene activation using doxycycline at 1g/kg in western diet; this elevation was prevented through administration of SB2014741 in pumps for the final four weeks. Circles represent individual mice; columns are averages of $\log_2$-transformed values; error bars are SEM. SB204741 did not affect control mice; both vehicle and treated mice are included in the control column as left and right groups of circles, respectively. (B) Cardiac Index does not change between groups, measured as cardiac output in ml/minute as determined by echocardiography divided by body surface area in square meters. (C) Immunoflourescence staining for CD45 (red), Actin (Green), DAPI (blue) in a 10x field of distal alveoli in agarose-inflated lungs. Individual channels for these images are presented in Supplemental Figure 1D. (D) Bmpr2 mutant mice have ~2x the inflammatory cells per field at baseline, but SB204741 treatment has divergent effects on inflammatory cells in control and Bmpr2 mutant mice, causing significant increases and decreases respectively (*$p<0.05$, $^{§}p<0.01$). (E) Bmpr2 mutant mice have roughly twice the numbers of partially and fully muscularized vessels per field for small and medium sized vessels; this is substantially normalized by SB204741 (*$p<0.01$).

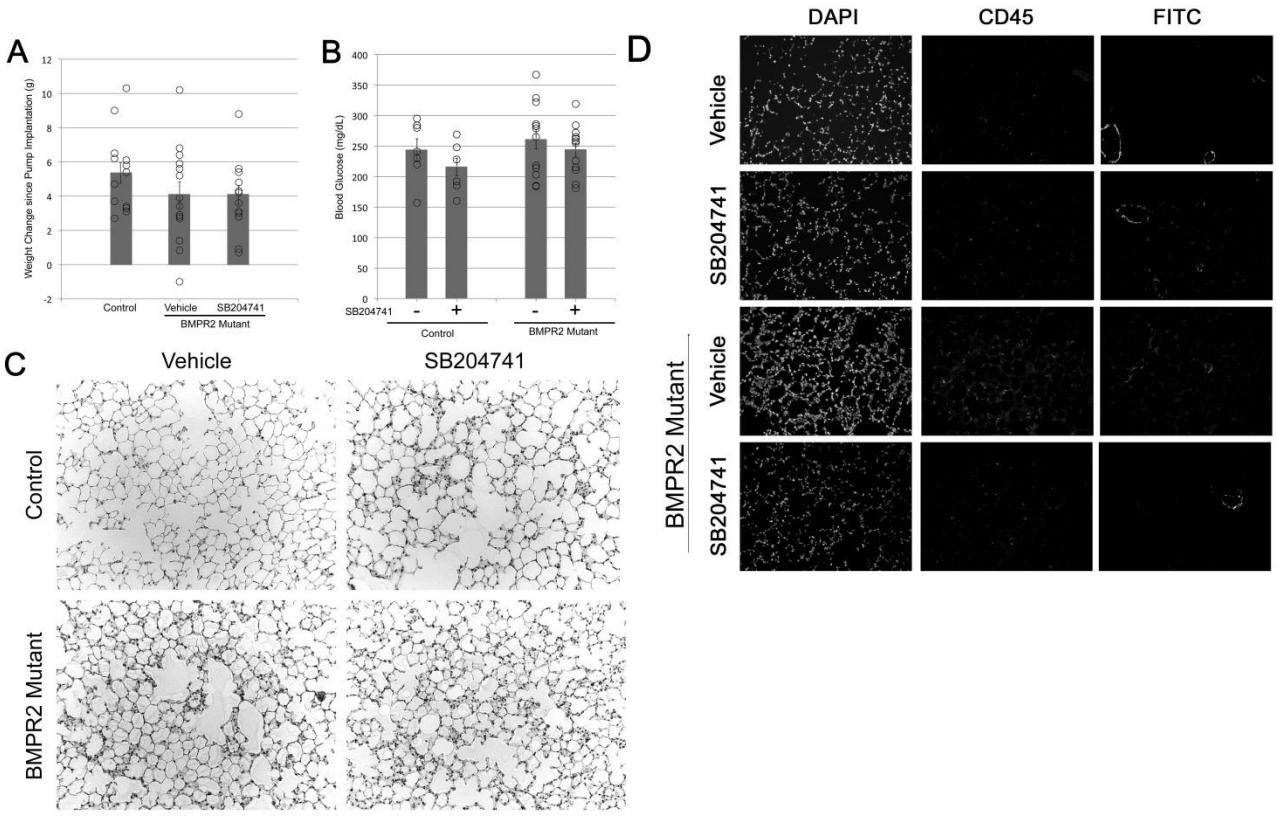


**Figure 3.2: 5-HT$_{2B}$ antagonism does not alter weight gain or blood glucose in Bmpr2 mutant mice.** SB204741 treatment did not significantly alter weight changes (A) or blood glucose measurements (B) in Bmpr2$^{R899X}$ animals. (C) SB204741 did reduce the number of infiltrating cells in Bmpr2 mutant mice. (D) The majority of this cellular infiltrate is composed of CD45$^{+}$ inflammatory cells (DAPI=nuclear staining, FITC = αSMA).

5-$HT_{2B}$ Antagonism Reduces Vascular Stiffness in Bmpr2 Mutant Mice

Although Bmpr2 mutant mice have occlusion of small arteries as determined by microCT[145], particularly at branch points, increase in RVSP in these mice may be driven by increased vascular stiffness. Here, we used atomic force microscopy (AFM) to assess lung sections, and found that small vessels in Bmpr2 mutant mice have twice the stiffness of control animals, with a median elastic modulus of 90 kPa as compared to 45 kPa. This stiffness is significantly normalized when mice are treated with 5-$HT_{2B}$ antagonist (Figure 3.3). The stiffness distribution presented may be bimodal, possibly indicative a heterogeneous deposition of ECM components in the vessel wall. Increased vascular stiffness has been hypothesized to be the pathologic feature of human PAH central to etiology[19,60], and so this prevention has high prognostic significance for translation potential.

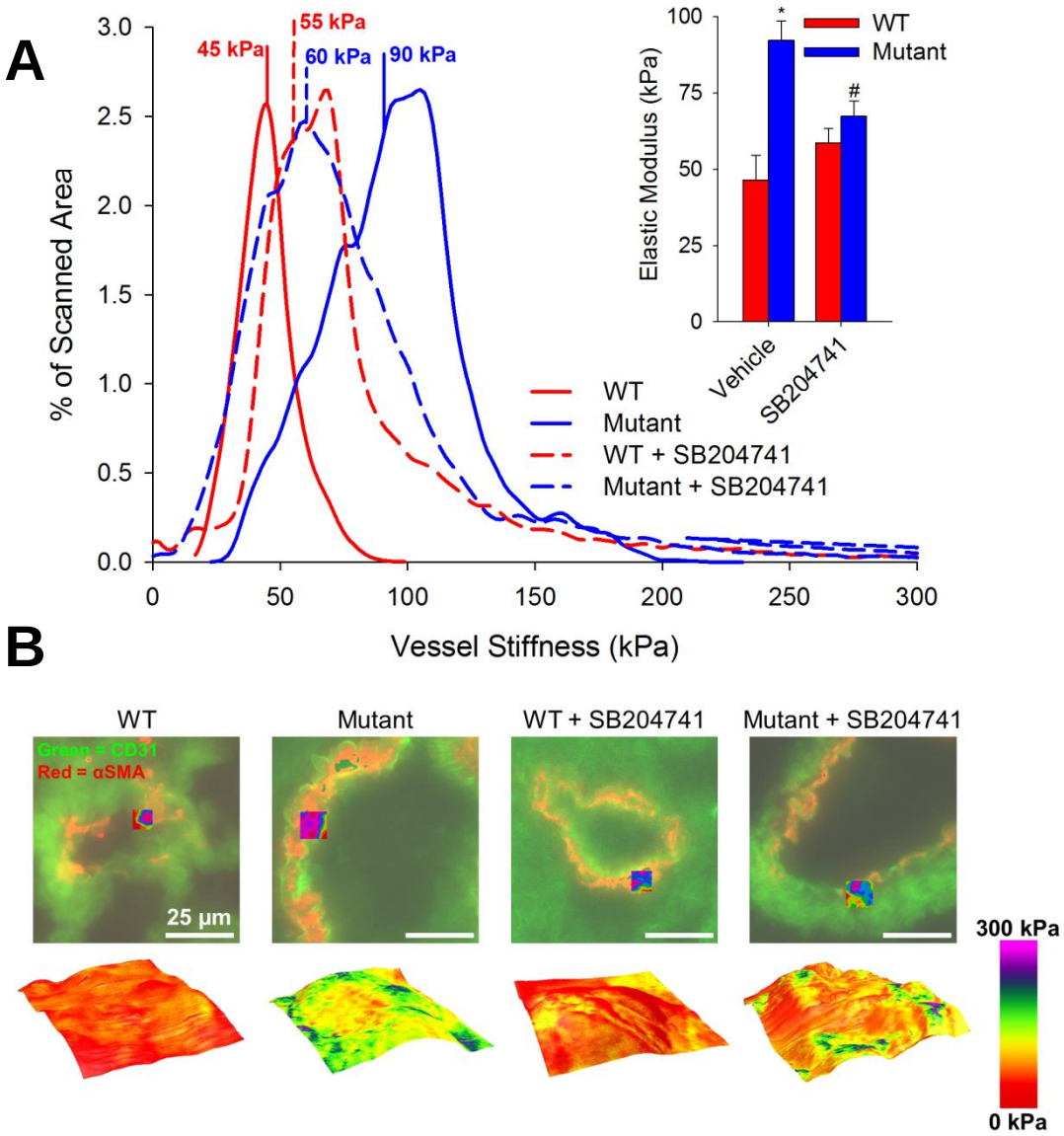


**Figure 3.3: SB204741 prevents arteriole wall stiffening in BMRP2 mutant animals.**
(A) In mutant animals treated for 4 weeks with SB204741, the average elastic modulus is significantly lower than their untreated counterparts. The histogram shows representative vessels with a Gaussian fit of elastic modulus distributions and calculated median values. Inset bar graph shows median stiffness values. (B) Fluorescent images (green = CD31; red = αSMA), with a topographical map of vessel height overlaid with a colorimetric representation of the elastic modulus. Values in the graph in (A) are expressed as mean ± standard error. n=3 per group, *p<0.05 compared to WT, #p<0.05 compared to vehicle treated.

5-$HT_{2B}$ Antagonism Reduces Src Activity and Motion Bmpr2 Mutant Mice and Cells

Antagonism of the 5-$HT_{2B}$ receptor has been shown to reduce Src's downstream activity by restricting its intracellular trafficking without reducing phosphorylation (18) and Bmpr2 mutation has been previously found to increase Src activity (15, 37). Therefore, we sought to determine if SB204741 could reduce Src downstream activity in Bmpr2 mutant mice. By western blot on lungs from mice, we found phosphorylation of Src and its downstream target CAS were increased in Bmpr2 mutants, with Src, CAS, and CAV1 phosphorylation significantly inhibited with chronic SB204741 treatment. Smad1 phosphorylation was not altered due to SB204741 (Figure 3.4 A, B). To determine whether 5-$HT_{2B}$ inhibition affected Src translocation, we motion-tracked fluorescently labeled tubulin and Src in transfected live pulmonary microvascular endothelial cells, cultured from wild-type or Bmpr2 mutant mice, and converted the motion to a heat map. We found that at baseline, Bmpr2 mutant endothelial cells had higher tubulin and Src motion than did wild-type cells, but these were normalized with SB204741 treatment. Conversely, wild-type cells had these motions increased (but not significantly) with SB204741 treatment (Figure 3.5 A,B). Once again, this contrast between drug effect in Bmpr2 mutant and wild-type cells suggests that the drug is impacting a pathway fundamentally altered by Bmpr2 mutation. Important to note, this effect was not observed in smooth muscle cells with a different Bmpr2 mutation – a complete deletion in the tail domain resulting from the insertion of a thymine base and consequential premature stop codon[231] (Figure 3.6). This effect is likely reflective of the different mechanistic effects that various Bmpr2 mutations have on receptor function.

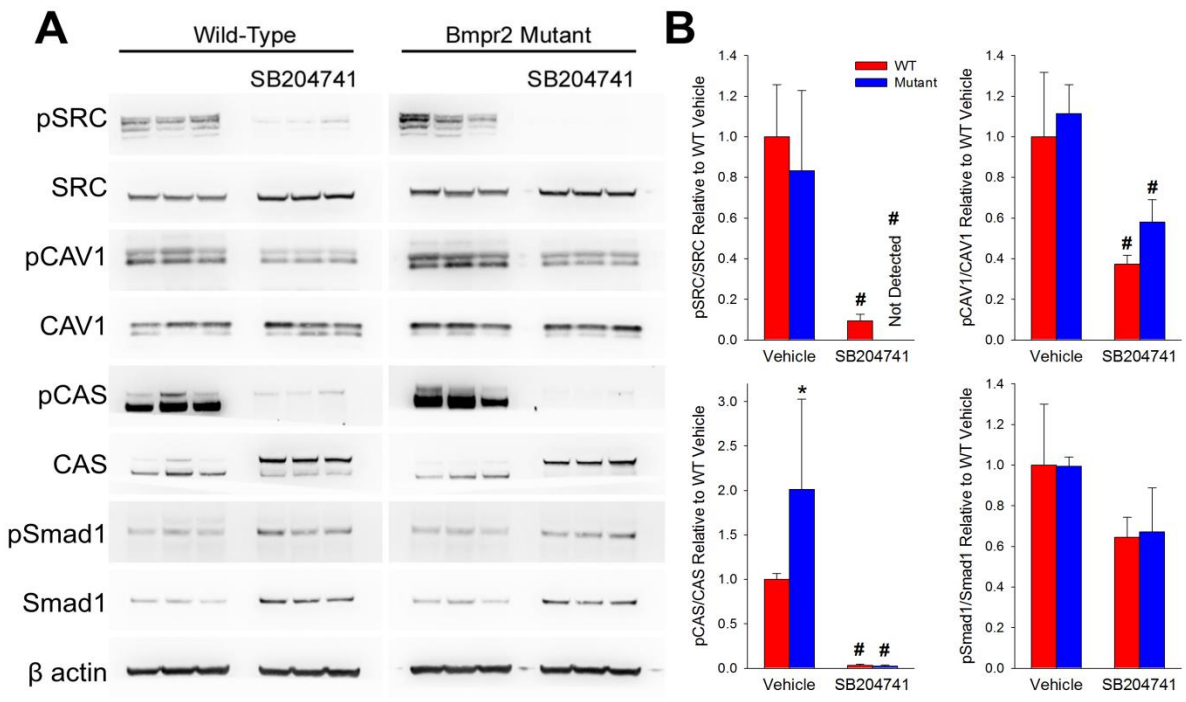


**Figure 3.4: SB204741 reduces Src phosphorylation and downstream activation *in vivo*.**
(A) Western blots from Bmpr2 mutant or WT mice whole lung treated with SB204741 or vehicle. Bmpr2 mutants show increased phosphorylation of Src target CAS; Src activity and phosphorylation is reduced with SB204741 treatment. (B) Densitometry for pSRC, pCAS, and pCAV1 phosphorylation. Values are normalized to total protein and β-actin (i.e. pSRC/SRC/β-actin). n=3, *p<0.05 compared to WT, #p<0.05 compared to vehicle treated.

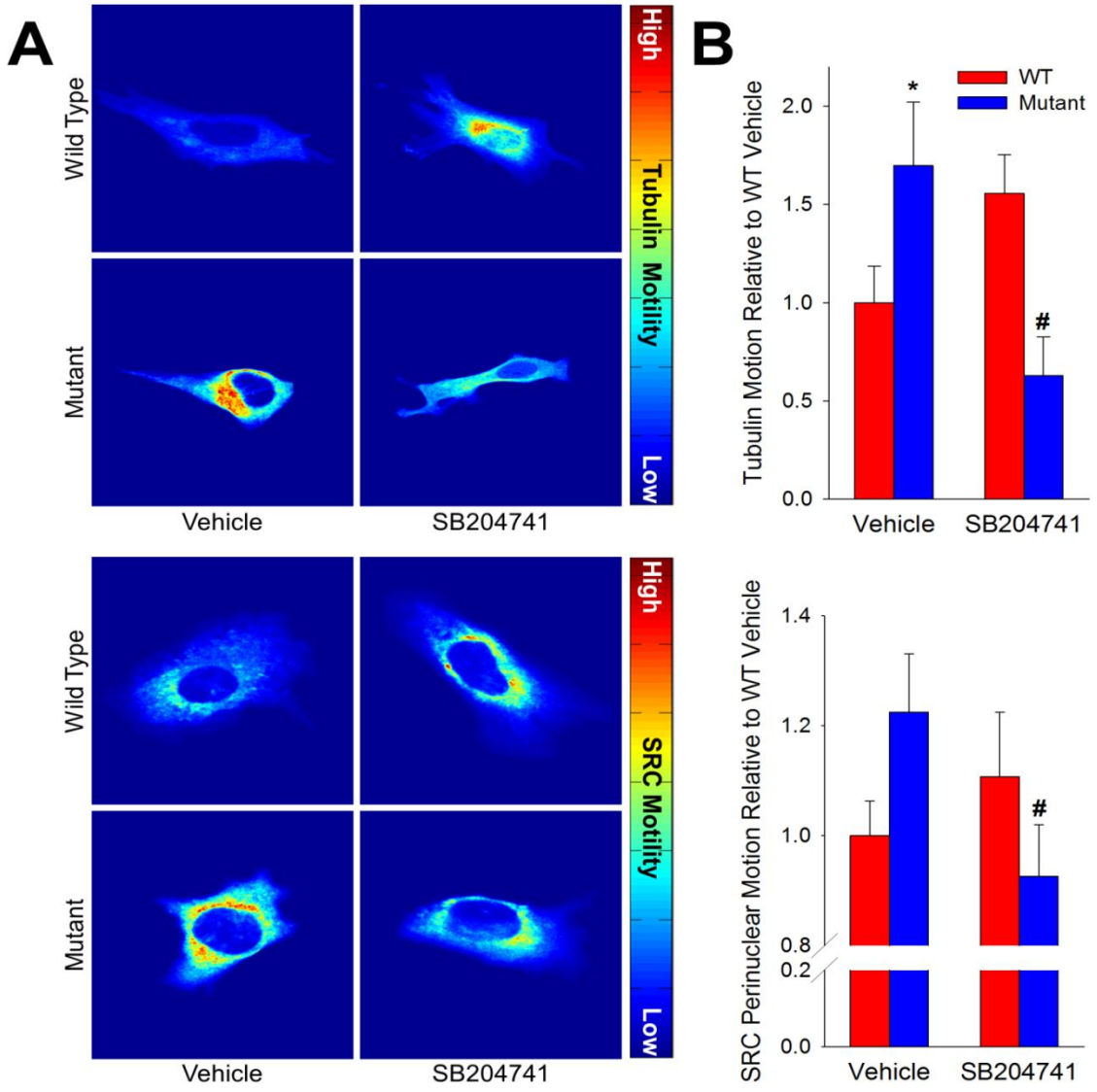


**Figure 3.5: 5-HT$_{2B}$ antagonism restricts motion of pSrc and tubulin in PAECs.**
(A) SB204741 reduces tubulin and perinuclear Src motility, both of which are increased in mutant microvascular endothelial cells. Eularian analysis of fluorescently labeled tubulin and Src in endothelial cells shows elevated motility in vehicle treated mutant cells, as well as a significant decrease in motility in mutants cells treated with SB204741. Values are expressed as mean ± standard error. n=5-10, *p<0.05 compared to WT, #p<0.05 compared to vehicle treated.

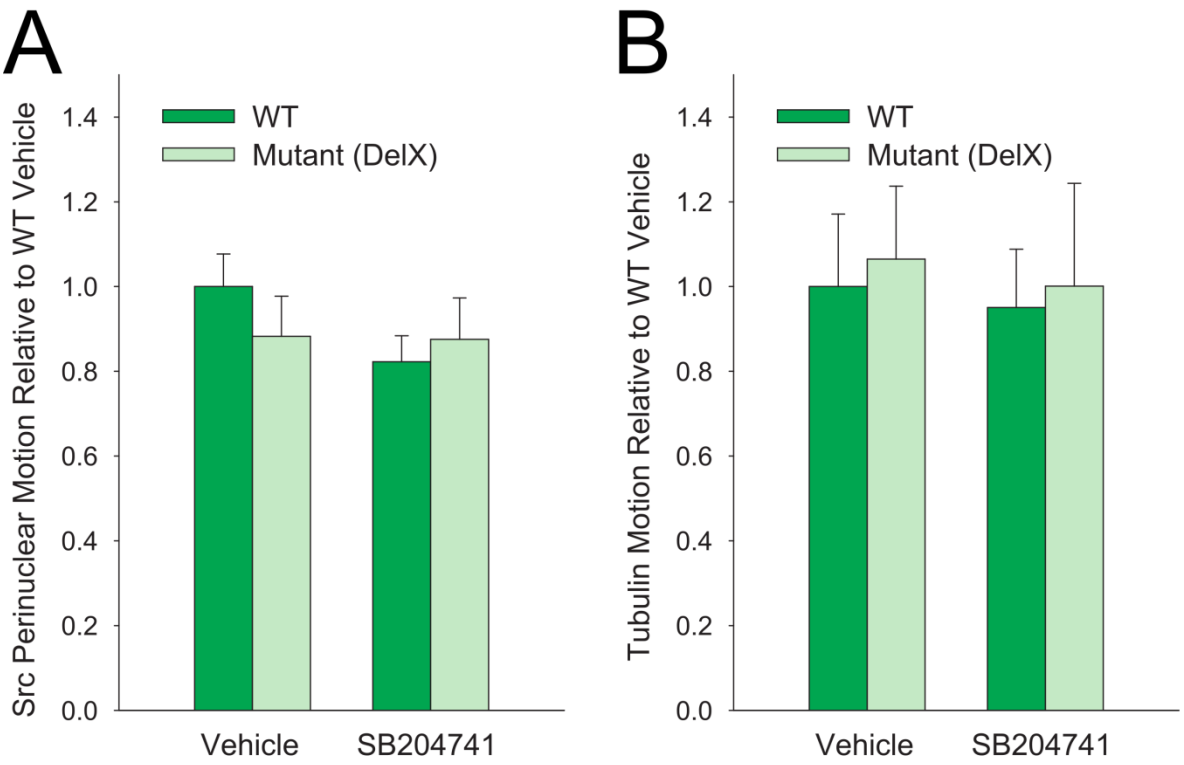


**Figure 3.6: 5-HT$_{2B}$ antagonism does not affect pSrc or tubulin motion in Bmpr2$^{Delx}$ PASMCs.** SB204741 treatment of PASMCs with the inducible DelX4 mutation in Bmpr2 does not alter (A) perinuclear pSrc motility or (B) tubulin motility. Values are expressed as mean ± standard error. n=5-10.

5-HT$_{2B}$ Modulates Muscle Contractility Genes in Bmpr2 Mutant Mice

To further examine molecular changes in Bmpr2 mutant mice caused by chronic 5-HT$_{2B}$ antagonism, Affymetrix gene expression profiling was performed on pools of lung RNA from mice with and without Bmpr2 mutation and with and without SB204741 treatment. Principal components analysis found that all four groups were well separated, but with changes in principal components with SB204741 treatment that were nearly diametrically opposed in control and Bmpr2 mutant mice (Figure 3.7 A). Each principal component corresponds to a list of genes that are roughly coregulated, with the first principal component (PC1) being the cluster of genes that explains the largest part of the variance across samples, PC2 being the gene group explaining the next most variance, etc. The analysis was performed without identifying gene groups *a priori*; the grouping of the samples is thus a natural result of gene expression

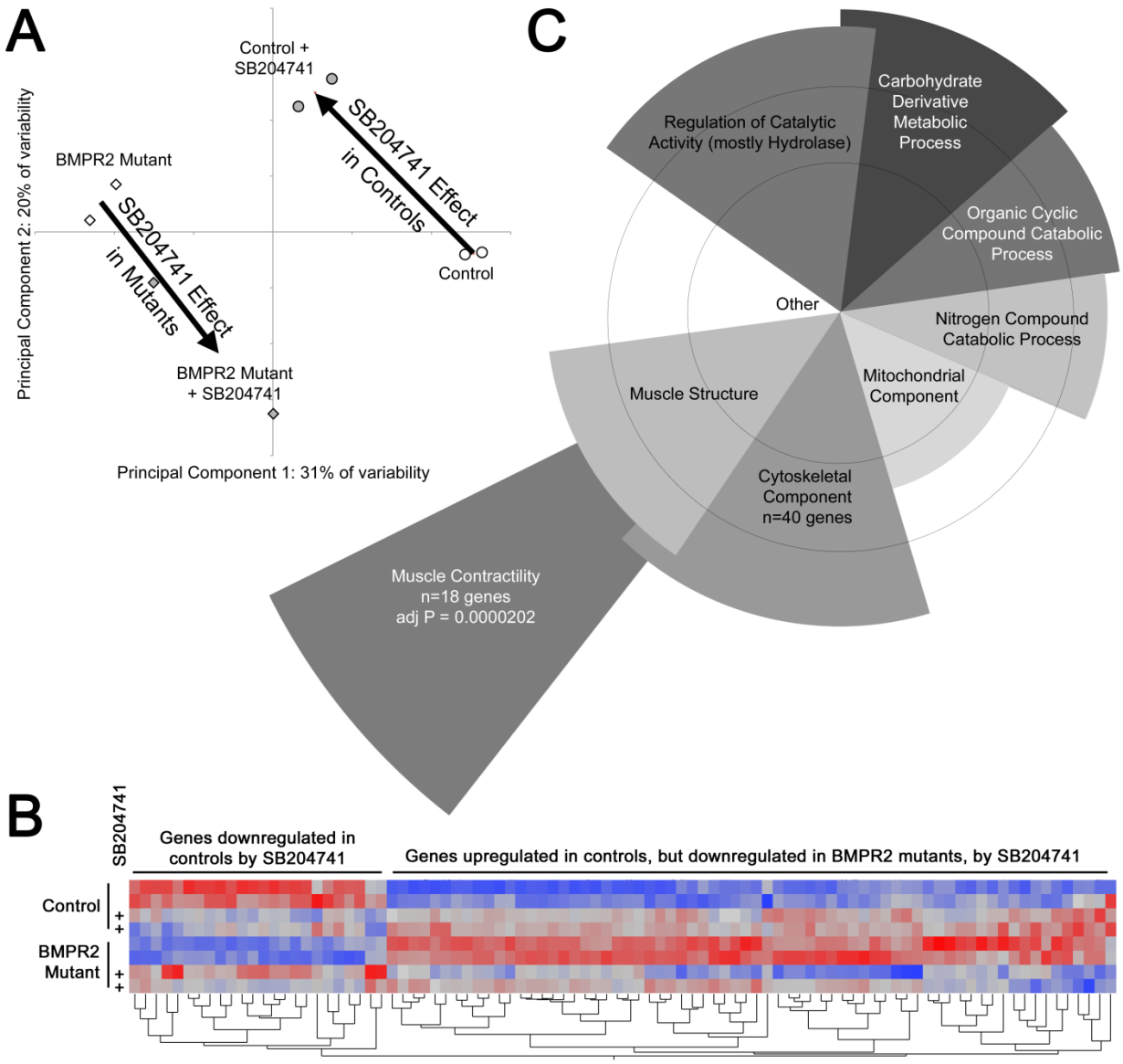


**Figure 3.7: Effect of SB204741 treatment on gene expression in the lungs of Bmpr2 mutant mice.** (A): Principal components analysis found a strong difference between Bmpr2 mutants and controls along Principal Component 1 (PC1). Treatment with SB204741 caused nearly opposite changes in PC vector in control and mutant mouse lungs (large arrows). Circles and diamonds refer to individual arrays for control and Bmpr2 mutants respectively: open and filled shading are for vehicle and SB204741 treatment respectively. (B): Heat map of normalized gene expression for 100 genes most affected by SB204741 treatment. Each column is a gene, with rows treatment/genotype groups. Red corresponds to high expression and blue to low. In general, SB204741 eliminates differences between control and Bmpr2 mutant mice, by moving gene expression in opposite directions (Bmpr2 mutants become more like controls, but controls become more like Bmpr2 mutants). (C): Representative examples of significantly overrepresented gene ontology groups. Angular width of each wedge is proportional to the number of genes altered by SB204741 in the group as a fraction of the 234 with a 95% confidence of change of over 20%. Radius is proportional to –log of the p-value (so longer is more significant). Circles correspond to multiple comparisons adjusted p=0.05 and p=0.01. Overlap is approximate, and demonstrates that most genes belong to more than one ontology group (lower level ontology groups not shown).

differences, rather than the result of selection. These data thus suggest opposite effects of drug in wild-type and Bmpr2 mutant mice. This differential effect can also be seen in a heatmap of the 100 genes most affected by SB204741, in which the direction of gene expression change is different in control and Bmpr2 mutant mice (Figure 3.6 B, Appendix Table A.1). When these 100 genes most affected by SB024741 are separated into statistically overrepresented gene ontology groups, the most statistically significant group is muscle contractility genes (Figure 3.7 C), although there are additional metabolic, muscle structure, and cytoskeletal component groups that are also statistically overrepresented. Categories of genes are similar to those seen in the lungs of 5HTT-/- mice reported previously, although 5HTT-/- lungs also had changes in inflammatory and cell differentiation pathways not seen in inhibition of one receptor alone.[232] Ion channel genes were noticeably absent from the list of genes differentially regulated in these samples; this may be because they are lost in using whole lung, or because changes were functional rather than expression, or because the mechanism here is related to structure, rather than control, of the cytoskeleton.

Some of the genes in these categories that are regulated in the opposite direction between Bmpr2 mutant and control mice include contractility genes (RhoA, Gamma Actin, and Myosin Light Chain 12a) and microtubule trafficking genes (Tubulin α1b, Wnt inhibitor Sfrp1, and Collagen 6a1) (Figure 3.8 A). However, there are additional muscle contractility and structure genes that are suppressed in both Bmpr2 mutant and control cells, including a ryanodine receptor, titin, troponin t2, myozenin 2, carbonic anhydrase 3, and sarcolipin (Figure 3.8 B). In summary, gene expression arrays on mouse lung indicate discrepant effects of SB204741 between control and Bmpr2 mutant lungs, but with effects concentrating on muscle structure, contractility, and energetics. Note that levels of 5-$HT_{2B}$ was not different due to Bmpr2 mutation or 5-$HT_{2B}$ antagonism.

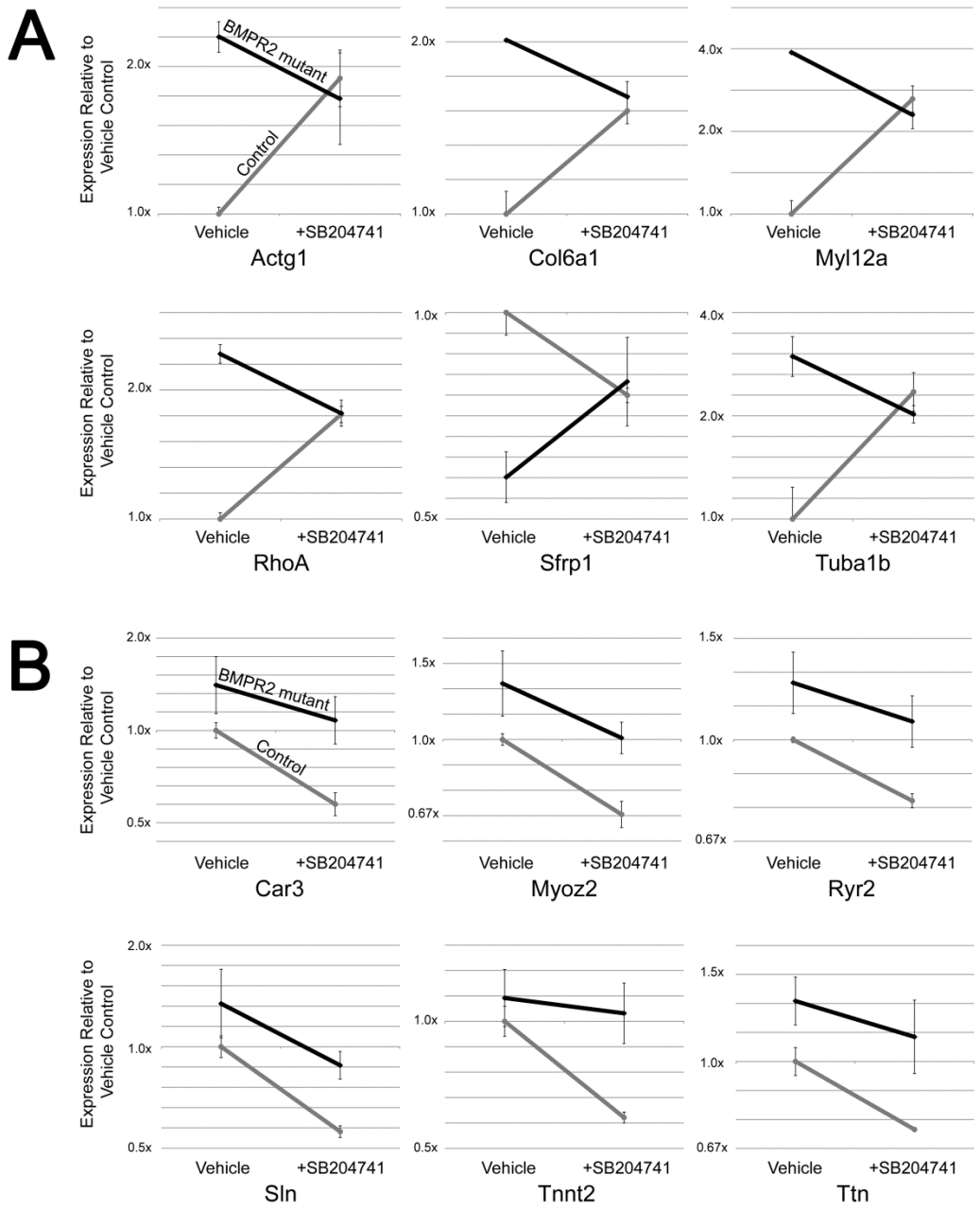


**Figure 3.8: Cytoskeletal contractility genes are altered by 5-HT$_{2B}$ antagonism.**
(A) SB204741 causes convergence of expression of most specific genes in the cytoskeletal component ontology group from Figure 5B between control and BMPR2 mutant lungs. (B) SB204741 results in reduced expression of most genes in the muscle contractility gene ontology group, which was the most statistically significant group in Figure 3.7 B. This brings expression levels of BMPR2 mutant mice to control levels. Error bars are standard deviation. Grey lines are from control mice; black lines are from BMPR2 mutant mice in both A and B.

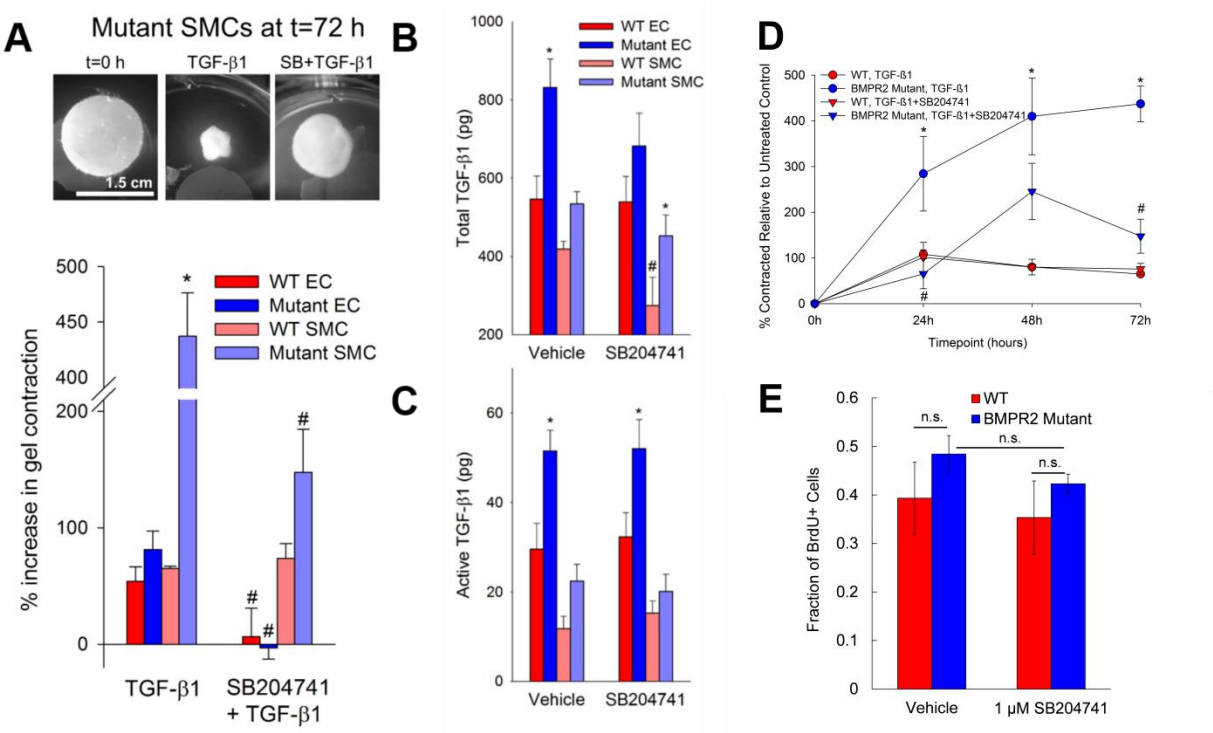


**Figure 3.9: SB204741 inhibits contractility of mutant microvascular cells in response to TGF-β1.** (A) Mutant microvascular smooth muscle cells exhibit a nearly five-fold increase in TGF-β1 induced contractility compared to their WT counterparts after 72 hours of treatment. TGF-β1 induced contractility in mutant microvascular smooth muscle cells is prevented when cells are treated concurrently with SB204741. (D) A similar effect is observed at earlier timepoints, and the effect is not likely due to inhibition of cell proliferation (E). Mutant cells synthesize (B) and activate (C) higher amounts of TGF-β1 than WT, and neither TGF-β1 synthesis nor activation is changed in mutant cells by SB204741. Values are expressed as mean ± standard error. n = 3-12 per group, *p<0.05 compared to WT, #p<0.05 compared to no treatment. Significance determined by a two-way ANOVA followed by a Holm-Sidak post hoc test.

5-$HT_{2B}$ Modulates Contraction in Bmpr2 Mutant Smooth Muscle

To determine whether these observed gene expression changes could produce a functional outcome *in vitro*, both pulmonary microvascular endothelial cells and smooth muscle cells cultured from control and Bmpr2 mutant mice were used in a gel contraction assay. Control and Bmpr2 mutant endothelial cells had comparable levels of contraction in response to exogenously added TGF-β1; in both cases this was suppressed by incubation with SB204741 (Figure 3.9 A). However, Bmpr2 mutant smooth cells had approximately five times the level of contraction in response to TGF-β1 as did control cells, and while control smooth muscle cell contractility was not affected by SB204741, contractility in Bmpr2 mutant cells was nearly normalized (Figure 3.9 A). Similar effects were observed at earlier timepoints (24 and 48 hours, Figure 3.9 D). Additionally, this effect was not likely due to differences in proliferation, as 5-HT2B has no effect on DNA synthesis as measured by BrdU incorporation (Figure 3.9 E). Total and active TGF-β1 was also increased in both endothelial and smooth muscle cells from Bmpr2 mutants but SB204741 did not appreciably alter these increases (Figure 3.9 B, C).

*Discussion*

These results suggest that 5-$HT_{2B}$ antagonism can prevent the onset of heritable PAH by preventing the translocation and downstream activity of phosphorylated Src due to Bmpr2 mutation (Figure 3.10). Wild-type Bmpr2 normally binds but does not phosphorylate Src, with binding occurring in a long cytoplasmic tail that is unique to Bmpr2 among TGFβ-superfamily receptors.[186] Mutations in the tail domain of Bmpr2 results in an increase in both phosphorylation and downstream activity of Src (Figure 3.4 A, B).[180,187] Here, we show that 5-$HT_{2B}$ antagonism prevents the Bmpr2 mutation-mediated increase in Src signaling (Figure 3.4 A, B) through inhibition of Src transport (Figure 3.5 A, B). Further, inhibition of Src translocation leads to modulation of cytoskeletal genes and functions through both direct (CAS and CAV1 mediated) and transcriptionally regulated targets (Figures 3.7 and 3.8).[233,234] Functionally,

Bmpr2 mutation leads to vascular stiffening *in vivo* (Figure 3.3), increased vascular cell contraction (Figure 3.9), increased inflammatory infiltration (Figure 3.1 C, D) and elevated pulmonary vascular resistance (Figure 3.1 A). This work thus demonstrates all of the elements present in Figure 3.10 and establishes Src activation as the primary target for preventing heritable PAH, and a strong candidate as the common signaling mechanism between drug-induced and heritable PAH.

One of the most interesting features of this data set is the finding that the effect of 5-$HT_{2B}$ inhibition is for many metrics completely opposite in WT and Bmpr2 mutant mice. This includes cellular infiltrate (Figure 3.1 C, D), vessel stiffness (Figure 3.3), Src motion (Figure 3.5), and patterns of gene expression (Figures 3.7 and 3.8). These strikingly discordant activities strongly suggest that the downstream signaling that arises from Bmpr2 mutation and 5-$HT_{2B}$ agonism/antagonism is very direct (Figure 3.10). The most straightforward explanation of this is that Src transport is dependent on its phosphorylation state or perhaps directly related to its Bmpr2 binding.

Bmpr2 mutation appears to alter TGF-β1 expression and activation in both endothelial and smooth muscle cells (Figure 3.9 B and C), but 5-$HT_{2B}$ antagonism does not suppress this expression or activation appreciably. Thus, the mechanism of preventing cell contraction likely involves an intracellular target of the 5-$HT_{2B}$ receptor. Previously, we found that TGF-β1 ligand binding led to Src phosphorylation directly from TGF-β1 type I receptor activation in heart valve cells.[190] 5-$HT_{2B}$ antagonism also prevented the downstream targeting of both CAS and p38 by TGF-β1-mediated Src phosphorylation. In the current study, we see a similar response – 5-$HT_{2B}$ antagonism physically restricts Src translocation and downstream activation of CAS and CAV1 and this prevents Bmpr2 mutation-induced vascular stiffening and smooth muscle cell contraction. This mechanism does not appear to mitogenic in nature, as 5-$HT_{2B}$ antagonism has no effect on DNA synthesis in isolated smooth muscle cells.

The ability of a 5-$HT_{2B}$ antagonist to prevent PAH by restricting downstream Src activity (but not phosphorylation) calls into question the inability of receptor tyrosine kinase inhibitors, such as imatinib or nilotinib, to effectively treat PAH clinically.[235] Presumably, these other inhibitors are non-specific, targeting multiple tyrosine kinases, and with their systemic delivery result in multiple alterations to signaling pathways that are important in maintaining cellular homeostasis in organs besides the lungs. Conversely, 5-$HT_{2B}$ offers a unique target for the treatment of PAH since it is largely restricted to the heart, lungs, liver, and gut with minimal expression in the brain and no known neurological function.

Although both serotonergic anorexigens and Bmpr2 mutation are associated with PAH, it is important to note that the relative risk associated with Bmpr2 mutations is much higher; roughly 100x for aminorex and 100,000x for Bmpr2 mutation. One explanation for this dramatic difference in risk is that Bmpr2 binds and signals through multiple mechanisms unrelated to Src, including through LIMK, SMAD transcription factors, TCTEX1, and potentially other targets through binding to type 1 receptors.[236] These mechanisms each confer additional risk of PAH. For instance, loss of SMAD signaling results in smooth muscle cell transition to a synthetic state, with significant attendant vascular dysfunction.

It is instructive to compare our results with 5-$HT_{2B}$ antagonists in Bmpr2 mutant mice with a recent study in which serotonin transporter (SERT) knockout was not protective against sugen/hypoxia induced PAH in rats.[237] Sugen/hypoxia can be thought of primarily as a model of severe endothelial damage with attendant remodeling, whereas although Bmpr2 mutants can develop significant endothelial lesions, these are rare and late in both mice[217] and humans.[238] This difference suggests that serotonin inhibition is not important in regulation of proliferation and remodeling, but rather plays an important role in initiating events and perhaps continuing underlying molecular pathologies.

While this study is the first to demonstrate a potential drug strategy for preventing heritable PAH in an animal model with the human-derived genetic mutation, it leaves several

questions unanswered. In which cell type are these signaling defects most important? Vascular endothelium and smooth muscle, and a variety of circulating cell types are all potentially important targets[239]; the answer may be a combination of these. What are the intermediate systems through which 5-$HT_{2B}$ regulates Src translocation? Moreover, because this was purely a prevention study, it is not clear that 5-$HT_{2B}$ antagonism would be capable of reversing established PAH. Further, because of the paradoxical effects of 5-$HT_{2B}$ antagonism in WT mice, it may not be a suitable point of intervention to correct the Src defects in idiopathic PAH patients, although it may be beneficial in heritable patients. The present study, combined with existing literature showing that most of these defects are present in human PAH patients, suggests that this will be a viable therapeutic avenue, but multiple questions remain as to the best method and timing of intervention.

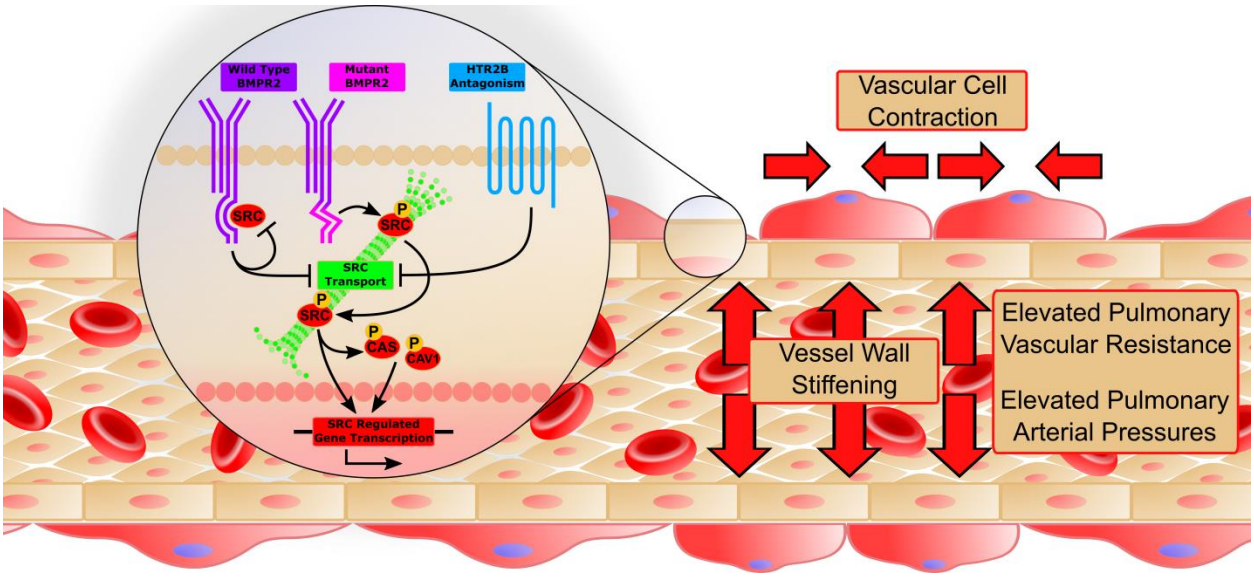


**Figure 3.10: A proposed molecular mechanism for 5-$HT_{2B}$ antagonism to prevent heritable PAH.** Mutations in the tail domain of Bmpr2 result in increased Src transport and signaling. Antagonism of 5-$HT_{2B}$ inhibits the translocation of Src and decreases Src signaling, causing a decrease in expression of Src regulated genes. Functionally, this results in increased small vessel compliance, reduced inflammatory infiltrate, and decreased vascular smooth muscle contractility which together contribute to a restoration in mean pulmonary arterial pressures.

# CHAPTER 4: BONE-MARROW DERIVED PRO-ANGIOGENIC CELLS MEDIATE PATHOLOGIC BIOMECHANICAL REMODELING DURING PULMONARY HYPERTENSION THROUGH SEROTONIN 2B RECEPTOR SIGNALING

Text and figures adapted in part from:

Bloodworth NC, et al. *Bone-Marrow Derived Pro-Angiogenic Cells Mediate Pathologic Biomechanical Remodeling During Pulmonary Hypertension through Serotonin 2B Receptor Signaling*. In preparation.

## *Introduction*

Pulmonary arterial hypertension (PAH) is an insidious illness of the pulmonary vasculature with exceptionally high morbidity and mortality and no effective treatment options for those afflicted.[18] The thickening and stiffening of pulmonary arterioles, a consequence of active vessel remodeling, is the hallmark pathologic feature of PAH and ultimately responsible for much of its deleterious hemodynamic phenotype.[29] While native endovascular cells contribute directly to this process, research in the last few years has provided compelling evidence for myeloid cell involvement as well.[192,193] Bone marrow derived proangiogenic cells (BM-PACs) are a subtype of myeloid cell that are believed to contribute directly to small vessel remodeling. Although a definitive class of surface markers for BM-PACs does not exist, these cells are generally described as expressing some combination of endothelial, hematopoietic, or stem cell markers (such as VEGFR2, Tie2, CD31, CXCR4, CD34, CD133, and cKit).[191,240] Their presence in peripheral blood has been well-correlated with PAH in a number of studies[202–204,241], and BM derived cells with endothelial or progenitor cell markers have been noted to embed themselves in the walls of remodeled vessels.[200–202] While BM-PACs are not believed to proliferate and occlude pulmonary vessels themselves, they are hypothesized to promote pathologic vasculogenic-like processes in neighboring endovascular cells via paracrine signaling

processes.[199] The exact function of these cells in PAH remains obscure however, and to date no one study has definitively established their role in promoting (or abrogating) disease.

The molecular mechanisms whereby BM-PACs might act to influence the progression of vascular remodeling are equally opaque. Cell surface receptors that mediate the mediate the mobilization, recruitment, proliferation and function of BM-PACs to the lung vasculature following hypoxic injury include traditional chemokine receptors such as CXCR4 and CXCR7 and their ligand SDF-1[241–243], as well as HIF-1 inducible factors such as erythropoietin and SCF.[191,201] One recent seminal study in particular has implicated the necessity of the serotonin 2B receptor (5-$HT_{2B}$) in the myeloid contribution to PAH – by selectively ablating 5-$HT_{2B}$ from the bone marrow, the authors were able to completely prevent the development of hypoxic pulmonary hypertension, while peripheral expression (or absence) had little effect on disease.[239] Interestingly, mice lacking 5-$HT_{2B}$ had similar metrics of hematopoiesis with a notable exception of fewer $CD31^{+}CD11b^{-}$ cells in the bone marrow and peripheral circulation, identified by the authors as immature proangiogenic or endothelial-like cells.

We hypothesized that BM-derived PACs contribute directly to small vessel stiffening and remodeling through a 5-$HT_{2B}$ dependent mechanism. By selectively ablating BM-PACs utilizing a transgenic mouse model we successfully prevented the development of elevated pulmonary pressures following hypoxic vascular injury. BM-PAC ablation also reduced markers of small vessel remodeling and restored vessel wall compliance to normal levels. We then illustrate the effectiveness of 5-$HT_{2B}$ antagonism in preventing PAH in the same disease model and, through lineage tracing of hematopoietic cells, show reduced recruitment and altered gene expression profiles of BM-PACs in animals treated with a pharmacologic inhibitor of 5-$HT_{2B}$.

*Methods*

Bone Marrow Transplantation and Transgenic Mouse Models

All mouse experiments were approved by the Vanderbilt Institutional Animal Care and Use Committee prior to their initiation. Cogenic (CD45.1 expressing) 6-12 week old C57BL/6 mice were given a lethal 12 Gy dose of radiation prior to transplant from a $Cs^{137}$ source, followed by retro-orbital administration of $5x10^5$ bone marrow cells isolated from an age- and sex-matched transgenic donor. For the ablation of BM-PACs, C57BL/6 donor mice were bred to express a tamoxifen-inducible Cre expression under the control of the 5' endothelial specific stem cell leukemia (SCL) promoter and diphtheria toxin under control of the ROSA26 promoter, preceded by a floxed-STOP codon to prevent transcription in the absence of Cre expression (endothelial SCL-$Cre^{ERT2}$/$DTa^{fl/-}$). For lineage tracing, we used C57BL/6 donor mice expressing a Tie2-promoter driven Cre and ROSA26-promoter driven YFP preceded by a floxed STOP codon (Tie2-Cre/$YFP^{fl/-}$, fluorescently labeling all hematopoietic cells regardless of lineage[244]). Donor cells were given 10 weeks for engraftment prior to the initiation of experiments.

Induction of PAH and Hemodynamic Phenotyping

To induce PAH, we administered the vascular endothelial growth factor receptor 2 (VEGFR2) inhibitor SU5416 (Tocris Biosciences) at 20 mg/kg/week intraperitoneally (IP) while mice were maintained in hypoxia (10% $O_2$) for 3 weeks. Inhibition of VEGFR2 in combination with hypoxia results in hypoxic vascular injury and a proliferative, vascular remodeling response mimicking PAH pathology.[245] Control animals were maintained on room air while receiving vehicle injections (0.5% carboxymethylcellulose, 0.4% polysorbate, 0.9% benzyl alcohol (Sigma-Aldrich) in 0.9% sterile saline). In order to ablate BM-derived PACs, SCL-$Cre^{ERT2}$/$DTa^{fl/-}$ recipient mice were simultaneously given 2 mg of tamoxifen (Sigma-Aldrich) IP every other day or vehicle injections (10% ethanol in sunflower oil, Sigma-Aldrich). For lineage tracing of BM-PACs, Tie2-Cre/$YFP^{fl/-}$ recipient mice were implanted with subcutaneous Alzet pumps delivering the 5-$HT_{2B}$ antagonist SB204741 (Tocris Biosciences) (1 mg/kg/day) or vehicle (50%

dimethylsulfoxide (Sigma-Aldrich) and polyethyleneglycol-400 (Fisher Chemical)) prior to disease induction. After 3 weeks, mice were placed under surgical anesthesia (Avertin) and a catheter was inserted into the right heart via the right jugular vein in a closed-chested procedure to measure right ventricular systolic pressures (RVSP), as previously described.[221] Mice were euthanized with a fatal dose of phenobarbital followed by collection of biologic samples.

Immunohistochemistry

Lungs were isolated, flushed with PBS, inflated and embedded with optimal cutting temperature compound, flash frozen in liquid nitrogen, and sectioned. Prior to staining lung sections were fixed in a solution of 4% paraformaldehyde (Electron Microscopy Sciences) and 0.01% Triton in PBS. Sections were stained with FITC conjugated rat anti-mouse CD31 (CD31-FITC, BD Biosciences), Cy3 conjugated mouse monoclonal anti- α smooth muscle actin (αSMA-Cy3, Sigma-Aldrich), and DAPI. Lung sections from Tie2-Cre/YFP$^{fl/-}$ transplanted animals were also stained with AF647 conjugated anti-GFP (GFP-AF647, Thermo Fisher Scientific). The number of fully (>75% of vessel circumference) and partially muscularized αSMA-positive pulmonary arterioles (<100 μm diameter) were quantified from images taken using an Olympus microscope. In lung sections taken from Tie2-Cre/YFP$^{fl/-}$ transplanted animals, pulmonary arterioles were further evaluated for the presence of cells expressing both YFP and CD31, identified as BM-PACs.

Measurement of Pulmonary Arteriole Wall Elastic Modulus

Atomic force microscopy (AFM) of whole tissue sections was performed as described previously.[246] Fresh-frozen lung sections 10 μm thick were stained with CD31-FITC, αSMA-Cy3, and DAPI. Lung sections from Tie2-Cre/YFP$^{fl/-}$ transplanted animals were also stained with GFP-AF647. After staining sections were immersed in PBS and αSMA-positive vessels less than 100 μm in diameter were identified using a Nikon Eclipse Ti microscope. Vessels were then scanned using a Bioscope Catalyst AFM at a scanning frequency of 0.25 Hz and a scan

window size of 5-8 μm. A total of 16-32 vessels were scanned from three animals for each treatment group, across two sections of lung per animal.

Wall modulus values were calculated as the average value of two scans per vessel, each consisting of 16,384 individual measurements (128x128) spanning an approximately 25-50 $um^2$ area along the vessel wall. The mean value for each scan (in kPa) is used as a representative measurement for the entire scan window.

Flow Cytometric Characterization

Lung cells were obtained from digesting masticated lungs in a solution of 5% fetal bovine serum, 1 mg/mL collagenase type IV, and 0.02 mg/mL DNase I (Sigma-Aldrich) in RPMI 1640 medium for 45 minutes at 37$^{o}$C. Peripheral blood mononucleocytes (PBMCs) were isolated from blood drawn from the right jugular. Red blood cells (RBCs) were lysed using RBC lysis buffer (BioLegend). For quantifying the number of BM-PACs in the lungs and peripheral blood, both PBMCs and Lung cells were stained with anti- Ter119-Pacific Blue, CD11b-redFuor (Tonbo Biosciences), CD31-PECy7 (BioLegend), and DAPI (Thermo Fisher Scientific). To quantify engraftment, PBMCs were stained with anti- Ter119-Pacific Blue, CD45.1-PE (BD Biosciences), CD45.2-PerCPCy5.5 (Tonbo Biosciences), and DAPI. Flow cytometry was performed using a BD LSRFortessa and the data analyzed using FlowJo.

RNA Sequencing and Gene Ontology Analysis

Adult male C57BL/6 mice were maintained on vehicle for SB204741 in normoxia for 3 weeks as described, after which BM cells and PBMCs were collected. Briefly, the femurs and tibeas isolated and flushed with sterile PBS. Marrow cords were collected, disaggregated, and strained, and RBCs were lysed. BM cells and PBMCs were stained with anti- Ter119, Gr1, B220, and CD3 –PacificBlue (Tonbo Biosciences), as well as anti- CD45-FITC (eBioscience), CD31-PECy7, CD11b-redFluor, and DAPI. Live ($Ter119^{-}Gr1^{-}B220^{-}CD3^{-}$) $CD31^{+}CD11b^{-}$ cells were sorted using a BD FACSAria III and collected in PBS (>95% purity). A Qiagen RNeasy Micro kit was used for RNA isolation. Messenger RNA enrichment, cDNA library preparation,

and sequencing were performed by the Vanderbilt Technologies for Advanced Genomics center (VANTAGE). RNA was pooled from three animals, with each condition replicated independently two times.

Analysis of RNA-seq data was performed using the Amazon Elastic Compute Cloud. Standard quality control analyses on raw reads were done using FastQC v0.11.5, with quality trimming and adaptor removal performed using Trimmomatic v0.36 and read alignment performed using STAR v 2.5.2b. Raw read counts were normalized using the TMM method of library size normalization in edgeR, and differential expression was performed in limma (both Biocondutor v3.3).[247]

Differentially expressed genes ($p<0.01$) were selected for inclusion in the gene ontology (GO) enrichment analysis. A GO slim analysis was performed using the BinGO app in Cytoscape,[248,249] with GO annotation files downloaded from the GO consortium. GO enrichment analysis for GO biologic processes was performed using the Web-based GEne SeT AnaLysis Toolkit (WebGestalt).[223,250] Significantly enriched GO terms are defined as having a $p<0.05$ following a false discovery rate correction.

Single nucleotide polymorphisms (SNPs) correlated with negative clinical outcomes (6 minute walk test and right ventricle function) were identified from a cohort of PAH patients seen at Vanderbilt using the Synthetic Derivative, a de-identified database of patient data and genome sequences, and the Illumina Exome chip. Variants strongly correlated with negative clinical outcomes ($p<0.01$) were then mapped to regions of the genome to identify the genes likely affected using the Ensembl Variant Effect Predictor tool.[251] Mapped genes were compared to mouse homologues whose expression was significantly altered by SB204741 in order to identify any overlap.

*Results*

Ablation of BM-PACs Prevents the Development of PAH and Normalizes Metrics of Pulmonary Vascular Remodeling

To perform targeted ablation of BM-PACs, we transplanted cogenic age- and sex-matched C57BL/6 mice with BM isolated from a transgenic donor with both a tamoxifen-inducible, endothelial specific Cre and diphtheria toxin expression under control of a ROSA26 promoter proceeded by a lox-P flanked STOP codon (SCL-Cre$^{ERT2}$/DTa$^{fl/-}$). Endothelial specificity was achieved by placing Cre expression under the control of a 5'-endothelial specific enhancer region for the SCL promoter. These mice, developed previously to study the contribution of hematopoietic proangiogenic cells to tumor endothelium, display little expression of Cre in mature hematopoietic stem cells thus making them an ideal lineage-restricted driver strain.[252] After transplant and reconstitution (Figure 4.3), mice were placed in hypoxia with weekly SU5416 injections or normoxia and received either vehicle or tamoxifen injections for three weeks (Figure 4.1 A). Following right heart catheterization, mice treated with tamoxifen were found to have significantly lower pressures than their vehicle-treated counterparts (Figure 4.1 B). The number of muscularized small arteries increased in vehicle-treated mice following hypoxic vascular injury, while mice receiving tamoxifen had significantly fewer fully muscularized arteries (but an increased number of partially muscularized arteries) (Figure 4.1 C). Ablation of BM-PACs also normalized average pulmonary arteriole wall stiffness (as measured with AFM) when compared to vehicle treated controls (Figure 4.2 D-F). Similar alterations in mice transplanted with BM from mice with SCL-Cre$^{ERT2}$ alone and treated with hypoxia and tamoxifen were not observed, proving that diphtheria toxin expression and subsequent ablation of BM-PACs is necessary for of remission of the PAH phenotype (Figure 4.4).

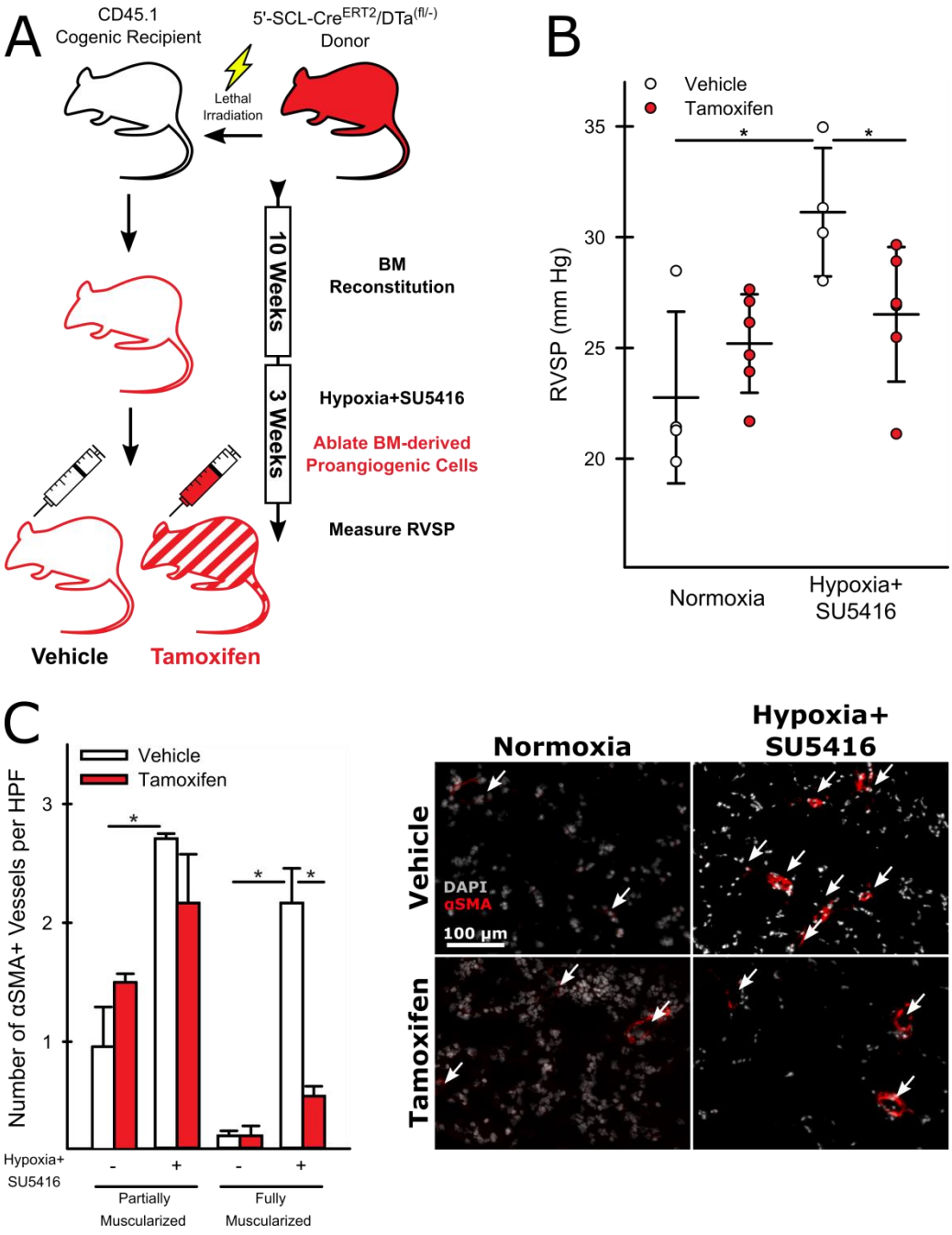


**Figure 4.1: Ablation of BM-derived proangiogenic cells reduces elevated RVSP and inhibits the muscularization of pulmonary arterioles.**
(A) Experimental approach. Cogenic age and sex-matched recipient animals were transplanted whole BM from endothelial-SCL-Cre$^{ERT2}$/DTa$^{(fl/-)}$ donors following lethal irradiation. After a 10 week reconstitution period, the mice were treated with SU5416+Hypoxia or room air and given either tamoxifen or vehicle to ablate BM-derived proangiogenic cells. (B) Tamoxifen-treated animals exposed to SU5416+Hypoxia had significantly decreased pressures compared to their vehicle treated counterparts (n=4-6, mean +/-S.E. *$p$<0.05 following 2-way ANOVA and Holm-Sidak post-hoc test). (C) The average number of fully, but not partially, muscularized arterioles (< 100 μm diameter) is significantly reduced in tamoxifen treated SU5416+Hypoxia animals compared to vehicle treated (n=3, mean+/- S.E. *$p$<0.05 following 2-way ANOVA and Holm-Sidak post-hoc test).

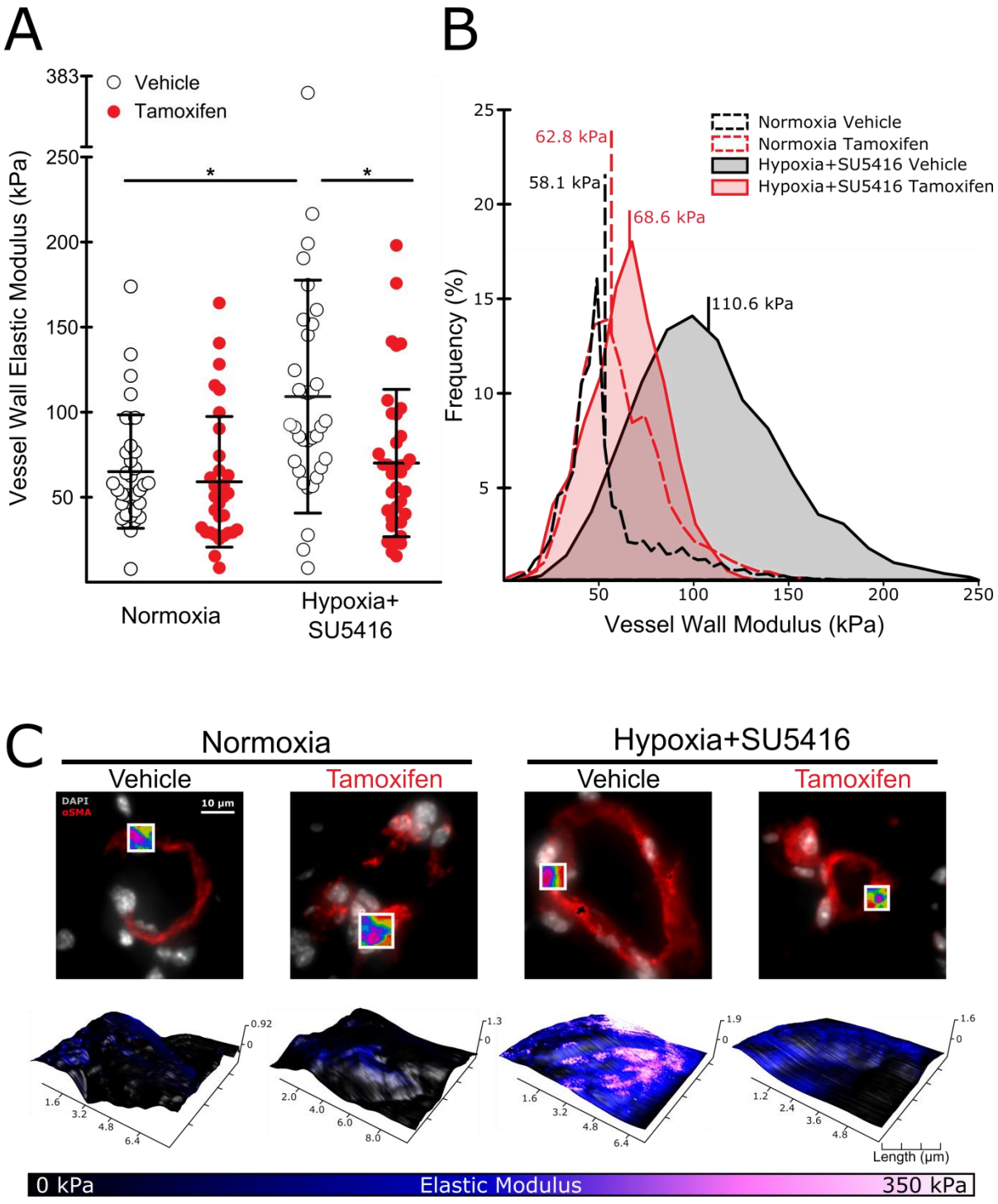


**Figure 4.2: BM-PAC ablation normalizes pulmonary arteriole stiffness.**
(A-C) The average elastic wall modulus of small pulmonary arterioles was significantly increased in animals exposed to SU5416+Hypoxia, while ablation of BM derived proangiogenic cells normalized arteriole stiffness. (A) Mean elastic wall modulus values for scanned vessels (n=16-24, mean +/-S.D. *$p$<0.05 following 2-way ANOVA and Holm-Sidak post-hoc test). (B) Representative modulus distributions and (C) scan windows for individual vessels.

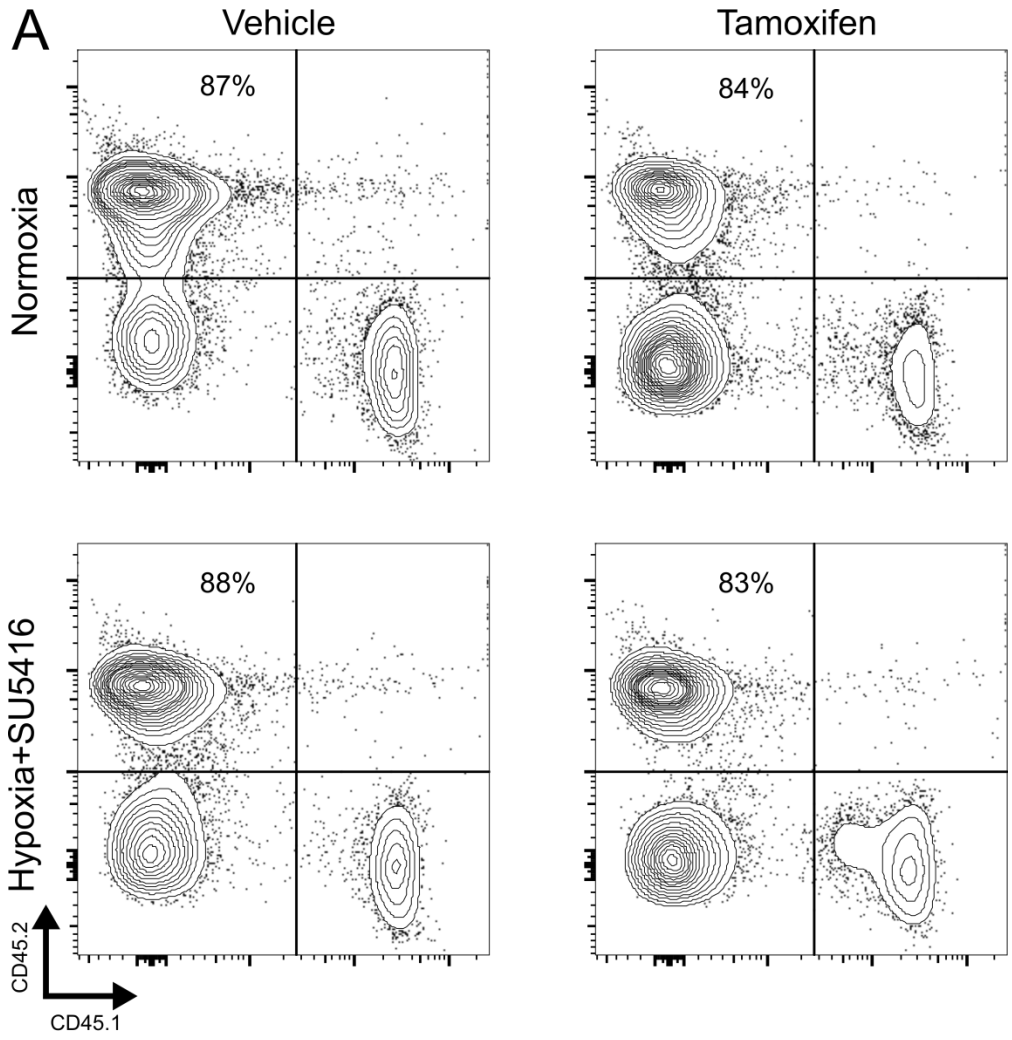


B

| Normoxia or SU5416+Hypoxia | Treatment | CD45.2 (Donor) (% of Total CD45) | Range (Low-High) (% of Total CD45) |
|---|---|---|---|
| Normoxia | Vehicle | 67.6% | 37% - 90% |
| Normoxia | Tamoxifen | 70.8% | 23% - 84% |
| SU5416+Hypoxia | Vehicle | 67.8% | 40% - 88% |
| SU5416+Hypoxia | Tamoxifen | 64.8% | 42% - 83% |

**Figure 4.3: Summary of engraftment efficiency for mice transplanted with BM from endothelial-SCL-CreERT2/DTa(fl/-) donor animals.**
(A) Representative flow plots for CD45.2 (donor allele) and CD45.1 (recipient allele) lymphocytes isolated from the peripheral blood of transplanted animals. (B) Tabulated summary of the engraftment efficiency, expressed as a percentage of donor CD45.2 cells out of the total number of CD45 cells. The average engraftment and engraftment range was comparable for all animals regardless of treatment group. ($p$>0.05 for all after two-way ANOVA and Holm-Sidak post-hoc test).

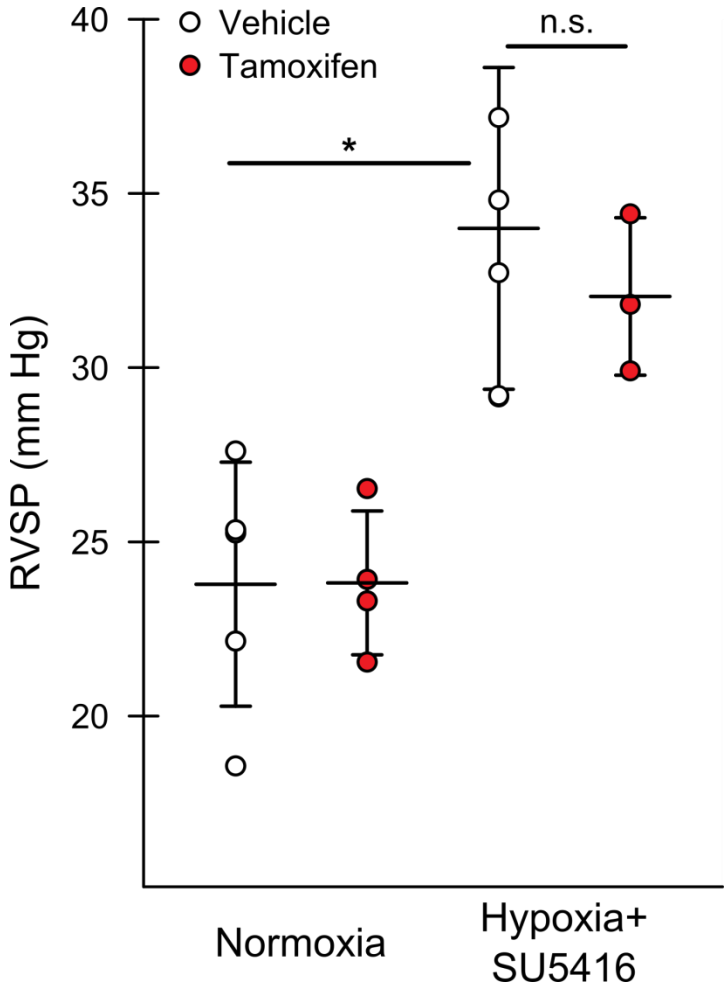


**Figure 4.4: Expression of diphtheria toxin is necessary to inhibit the development of PAH.** Mice transplanted with bone marrow cells expressing the tamoxifen inducible SCL-Cre but without expression of the floxed diphtheria toxin still develop pulmonary hypertension following Cre activation with tamoxifen. n=3-6, mean +/- S.E. *$p$<0.05, n.s. $p$>0.05 following two-way ANOVA and Holm-Sidak post-hoc test.

Pharmacologic Inhibition of 5-$HT_{2B}$ Prevents PAH and Vascular Remodeling

In order to determine if BM-PAC accumulation or function in the lungs was dependent on 5-HT2B signaling, we performed lineage tracing on BM-PACs using mice expressing both a Tie2-promoter driven Cre and a ROSA26-promoter driven fluorescent reporter (YFP) proceeded by a loxP-flanked STOP codon as BM donors. As Tie2 is expressed on hematopoietic stem cells, this model allowed us to positively identify all BM cells regardless of lineage.[244] We combined this approach with cell surface-labeling of $CD31^+CD11b^-$ negative BM-derived cells, a cell population containing BM-PACs and reported to be reduced in number in 5-$HT_{2B}$ deficient mice.[239,253] Engraftment efficiency was comparable between groups, as assessed by determining both the fraction of PBMCs that were $YFP^+$. The efficiency of Cre-mediated recombination was also comparable regardless of treatment, with the majority (>80%) of donor $CD45.2^+$ lymphocytes expressing YFP (Figure 4.5). Following transplantation and reconstitution, the mice were placed in either normoxia or hypoxia and subcutaneously implanted with an osmotic pump delivering the 5-$HT_{2B}$ antagonist SB204741 or vehicle for three weeks (Figure 4.6 A). Pharmacologic inhibition of 5-$HT_{2B}$ with SB204741 was sufficient to normalize RVSP as measured by right heart catheterization compared to vehicle treated controls (Figure 4.6 B). Treatment with SB204741 also reduced the number of fully (but not partially) muscularized arterioles (Figure 4.6 C). Measurements of pulmonary arteriole wall elastic modulus with AFM show a significant elevation in vascular stiffness for vehicle treated mice given SU5416 in hypoxia, with SB204741 treatment normalizing these values (Figure 4.7 D-F), recapitulating the results we observed when ablating BM-PACs.

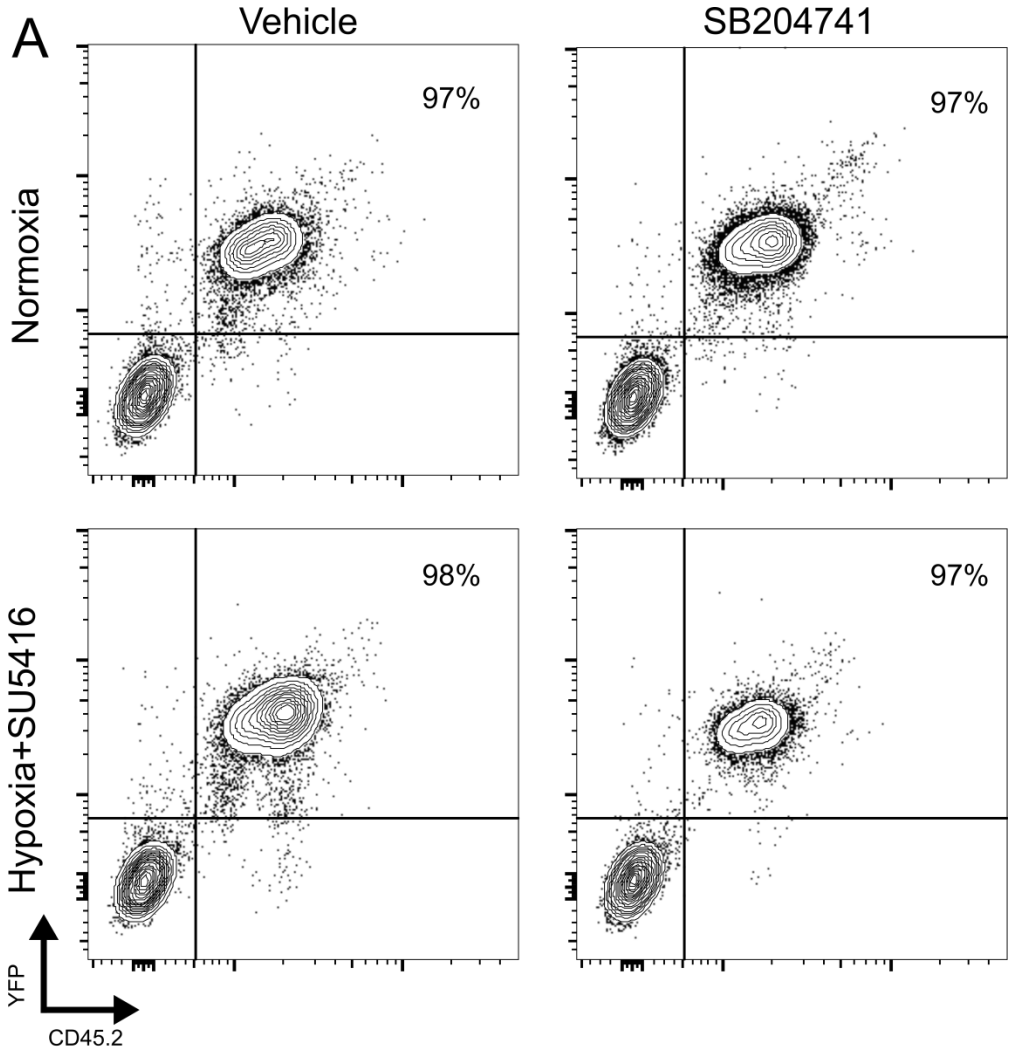


B

| Normoxia or SU5416+Hypoxia | Treatment | YFP+ (Donor) (% of Total PBMCs) | Range (Low-High) (% of Total PBMC) | YFP+ (% of CD45.2+) | Range (Low-High) (% of CD45.2+) |
|---|---|---|---|---|---|
| Normoxia | Vehicle | 57.4% | 24% - 82% | 84.2% | 46% - 99% |
| Normoxia | SB204741 | 46.7% | 13% - 64% | 87.0% | 75% - 100% |
| SU5416+Hypoxia | Vehicle | 41.8% | 14% - 58% | 68.8% | 35% - 99% |
| SU5416+Hypoxia | SB204741 | 58.9% | 28% - 88% | 84.5% | 33% - 100% |

**Figure 4.5: Summary of engraftment efficiency and hematopoietic cell labeling with YFP in transplanted mice.**
(A) Representative flow plots illustrating that donor lymphocytes ($CD45.2^+$) isolated from the lungs uniformly express YFP. (B) Tabulated summary of engraftment efficiency, expressed as a percentage of total peripheral blood mononucleocytes (PBMCs) that express YFP. The average engraftment efficiency was comparable for all animals regardless of treatment group ($p>0.05$ for all after two-way ANOVA and Holm-Sidak post-hoc test).

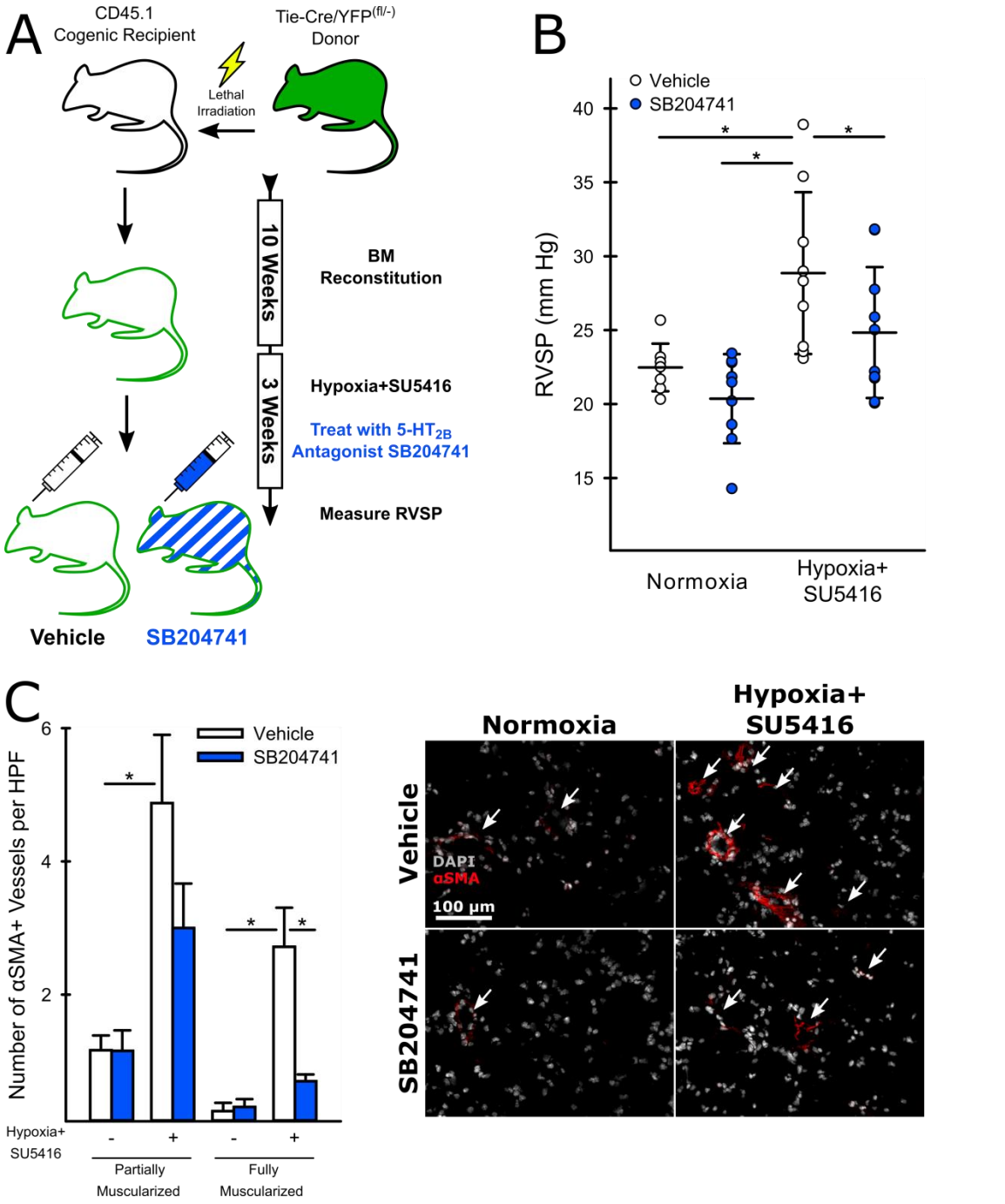


**Figure 4.6: Antagonism of the 5-HT$_{2B}$ receptor normalizes elevated RVSP and reduces the muscularization of pulmonary arterioles.**

(A) Experimental approach. Cogenic age and sex-matched recipient animals were transplanted whole BM from Tie2-Cre/YFP$^{(fl/-)}$ donors following lethal irradiation, effectively labelling all hematopoietic cells regardless of lineage. After a 10 week reconstitution period, the mice were exposed to SU5416+Hypoxia or room air for three weeks and simultaneously treated with either vehicle or the 5-HT$_{2B}$ antagonist SB204741. (B) Animals treated with SB204741 had a normalization of elevated RVSP compared to their vehicle treated counterparts (n=7-8, mean +/-S.E. *$p$<0.05 following 2-way ANOVA and Holm-Sidak post-hoc test). (C) SB204741 treated animals also had fewer fully, but not partially, muscularized pulmonary arterioles than vehicle treated mice (n=3, mean+/- S.E. *$p$<0.05 following 2-way ANOVA and Holm-Sidak post-hoc test).

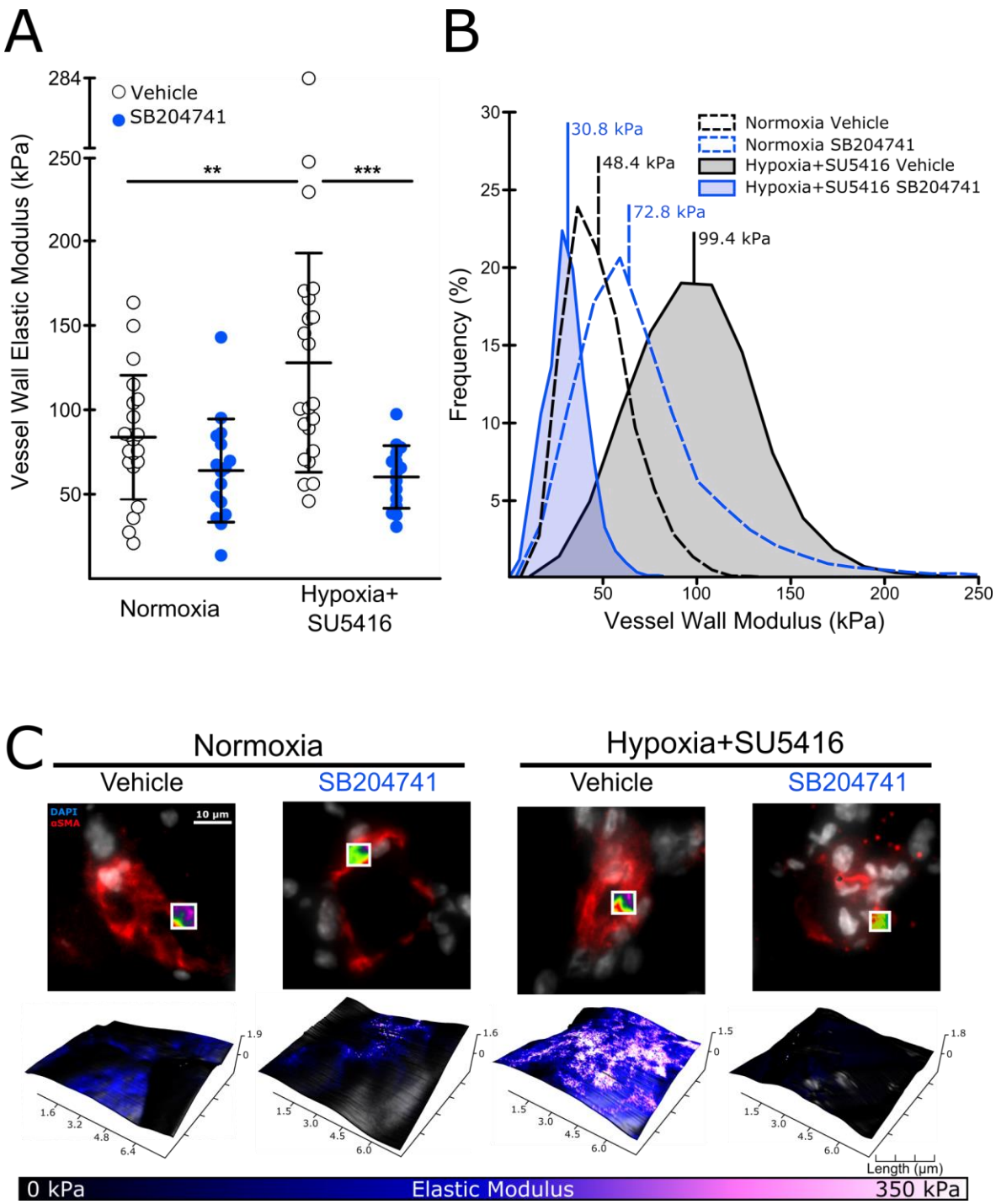


**Figure 4.7: 5-HT$_{2B}$ antagonism normalizes pulmonary arteriole stiffness.**
(D-F) The average elastic wall modulus of pulmonary arterioles was significantly elevated in animals exposed to SU5416+Hypoxia and normalized by treatment with SB20471. (D) Mean elastic wall modulus values for scanned vessels (n=16-24, mean +/-S.D. **$p$<0.01, ***$p$<0.001 following 2-way ANOVA and Holm-Sidak post-hoc test). (E) Representative modulus distributions and (F) scan windows for individual vessels.

Increased Numbers of BM-PACs in the Lungs and Walls of Remodeling Arterioles are Reduced by 5-$HT_{2B}$ Antagonism

We next quantified the number of BM-PACs in the lungs and peripheral blood following PAH induction and vehicle or SB204741 treatment. We found a significant reduction in the fraction of $YFP^+CD31^+CD11b^-$ cells in the peripheral blood in hypoxic animals treated with SB204741 (Figure 4.8 A). Additionally, there was a significant increase in the fraction of $YFP^+CD31^+CD11b^-$ cells in the lungs in vehicle treated hypoxic animals compared to vehicle treated controls. This fraction was reduced to normoxic levels in mice treated with SB204741 (Figure 4.8 B). Importantly, neither hypoxic vascular injury nor SB204741 treatment altered the total number of lung cells present, or the fraction of lung cells that expressed YFP+ (Figure 4.9 A – B), suggesting the absence of large scale inflammatory infiltrate. While cKit+ bone marrow derived cells previously been reported to accumulate in the walls of remodeled vessels and potentially mediate vessel remodeling in a 5-$HT_{2B}$ dependent manner,[200,203,239] we observed only a small and statistically non-significant increase in the fraction of bone-marrow derived cKit+ cells following hypoxia, with SB204741 exerting no measurable effects on the fraction present in the lungs. Approximately 10-15% of $YFP^+CD31^+CD11b^-$ cells expressed cKit, but this fraction was relatively consistent with all treatment conditions (Figure 4.9).

Quantification of lung immunostaining showed an increased number of $YFP^+CD31^+$ cells in the walls of remodeling (α-SMA positive) arterioles, as well as a larger fraction of pulmonary arterioles containing at least one positively identified $YFP^+CD31^+$ cell embedded in the vessel wall (Figure 4.10 A-B). Interestingly, pharmacologic antagonism of 5-$HT_{2B}$ in the absence of hypoxic vascular injury significantly increased the localization of BM-PACs to the walls of pulmonary arterioles, while leaving the total fraction of $YFP^+CD31^+CD11b^-$ cells unchanged (as evidenced by flow cytometry data).

We next assessed whether or not the presence or absence of BM-PACs was correlated with increased vessel wall stiffness. After determining the vessel wall elastic modulus using

AFM, we subdivided vessels into either positive or negative for $YFP^{+}CD31^{+}$ cells in the vessel wall. On average, the measured vessel wall elastic modulus was significantly higher for vessels with at least one positively identified $YFP^{+}CD31^{+}$ cell in vehicle treated hypoxic animals (Figure 4.11 C-D). While a significant fraction of vessels in SB204741 treated animals were identified as having greater than one $YFP^{+}CD31^{+}$ vessel, the presence or absence of these cells was not correlated with a significant difference in vessel stiffness in either hypoxic or normoxic conditions.

Finally, we assessed whether or not BM-PAC activity was necessary for the maintenance of the PAH phenotype. After transplant and reconstitution with bone marrow from SCL-$Cre^{ERT2}$/$DTa^{fl/-}$ donors, mice were placed in hypoxia with weekly SU5416 injections or normoxia for three weeks to induce PAH. After 3 weeks, mice were placed in normoxia and given either vehicle or tamoxifen injections to ablate BM-PACs (Figure 4.12 A). Following right heart catheterization, mice treated with tamoxifen were found to have significantly lower pressures than their vehicle-treated counterparts (Figure 4.12 B). The number of muscularized small arteries increased in vehicle-treated mice following hypoxic vascular injury, while mice receiving tamoxifen had significantly fewer fully and partially muscularized arteries (Figure 4.12 C). These results capitulated our initial findings in Figure 4.1, and indicate that the presence of BM-PACs is necessary for maintaining experimental pulmonary hypertension.

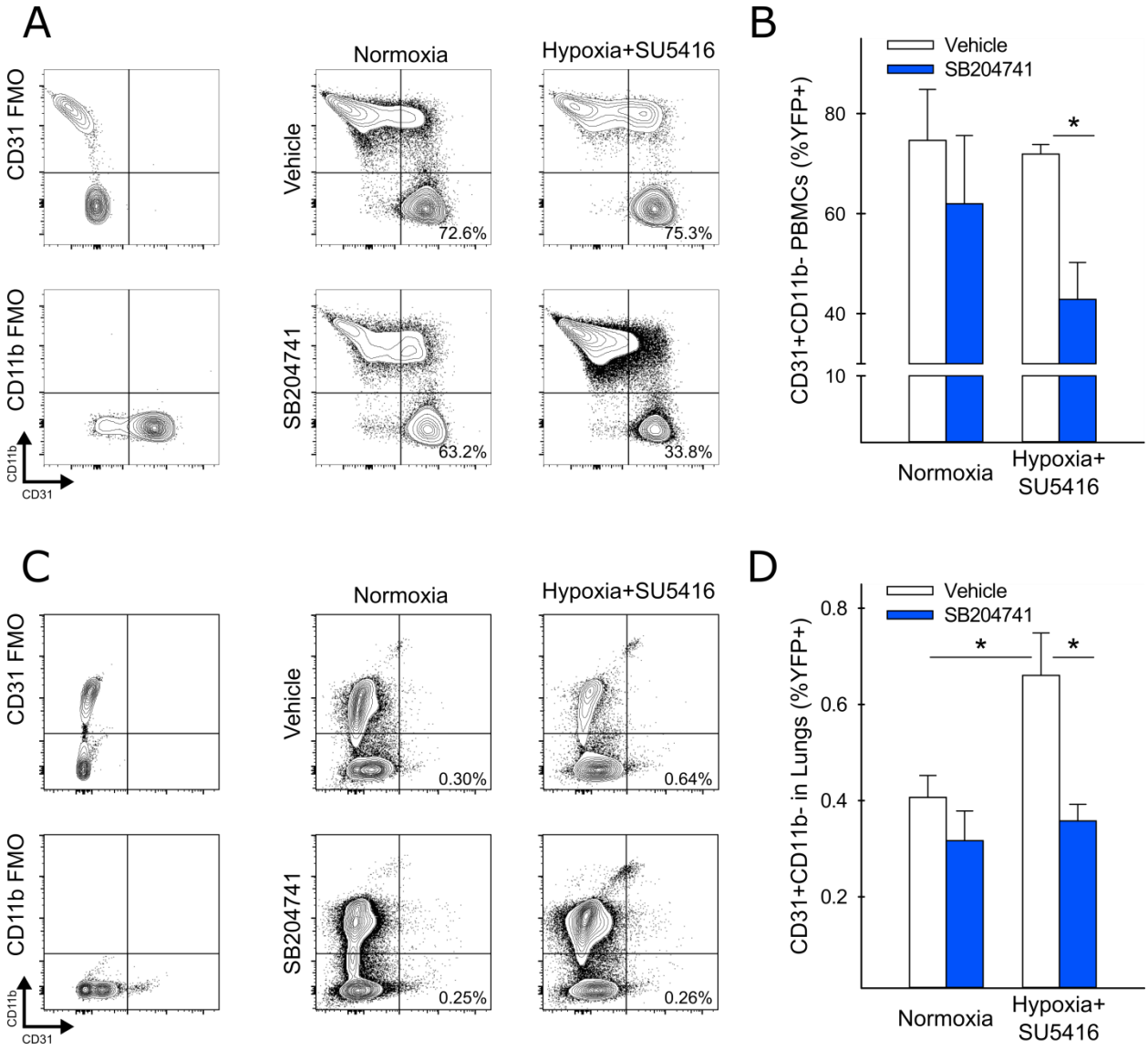


**Figure 4.8: 5-HT$_{2B}$ antagonism reduces the number of BM-derived proangiogenic cells in the lungs and peripheral blood following SU5416+Hypoxia.**
(A-B) Antagonism of 5-HT$_{2B}$ reduces the fraction of BM-derived CD31$^{+}$CD11b$^{-}$ cells in the peripheral circulation during normoxia (expressed as the percentage of total YFP labeled cells), but significantly reduces the fraction of these cells present in animals exposed to SU5416+Hypoxia (n=6-8, mean +/- S.E.). (C-D) The fraction of BM-derived CD31$^{+}$CD11b$^{-}$ cells is significantly elevated in the lungs of mice exposed to SU5416+Hypoxia, and reduced in mice treated with SB204741 (n=6-8, mean +/- S.E. *$p$<0.05 following 2-way ANOVA and Holm-Sidak post-hoc test). (A,C) Representative contour plots, gates, and percentages for each treatment condition.

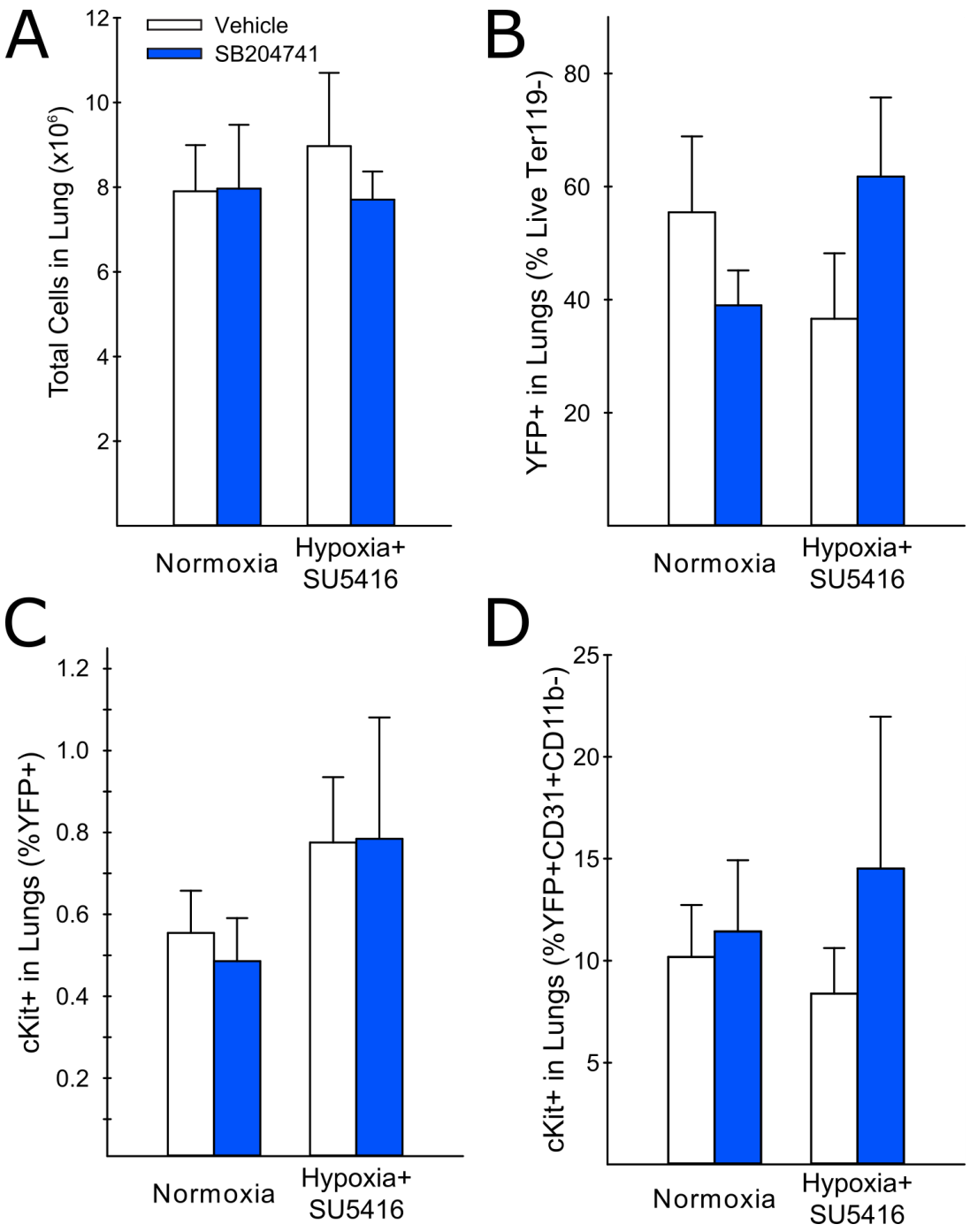


**Figure 4.9: Total cells, fraction of bone-marrow derived cells, and the fraction of cKit$^+$ bone-marrow derived cells are not altered by hypoxia or 5-HT$_{2B}$ antagonism.**
(A) The total number of cells does not change appreciably in the lung following hypoxic vascular injury or SB204741 treatment, as might be expected in a large inflammatory process. (B) The fraction of YFP$^+$ cells does not change significantly with SB204741 administration, suggesting the dug does not act to globally inhibit the migration or proliferation of hematopoietic cells in a nonspecific manner. (C) The fraction of bone-marrow derived cKit$^+$ cells is slightly increased in the lungs with hypoxia and SU5416 treatment, but this change is statistically insignificant and is further unaltered by SB204741.

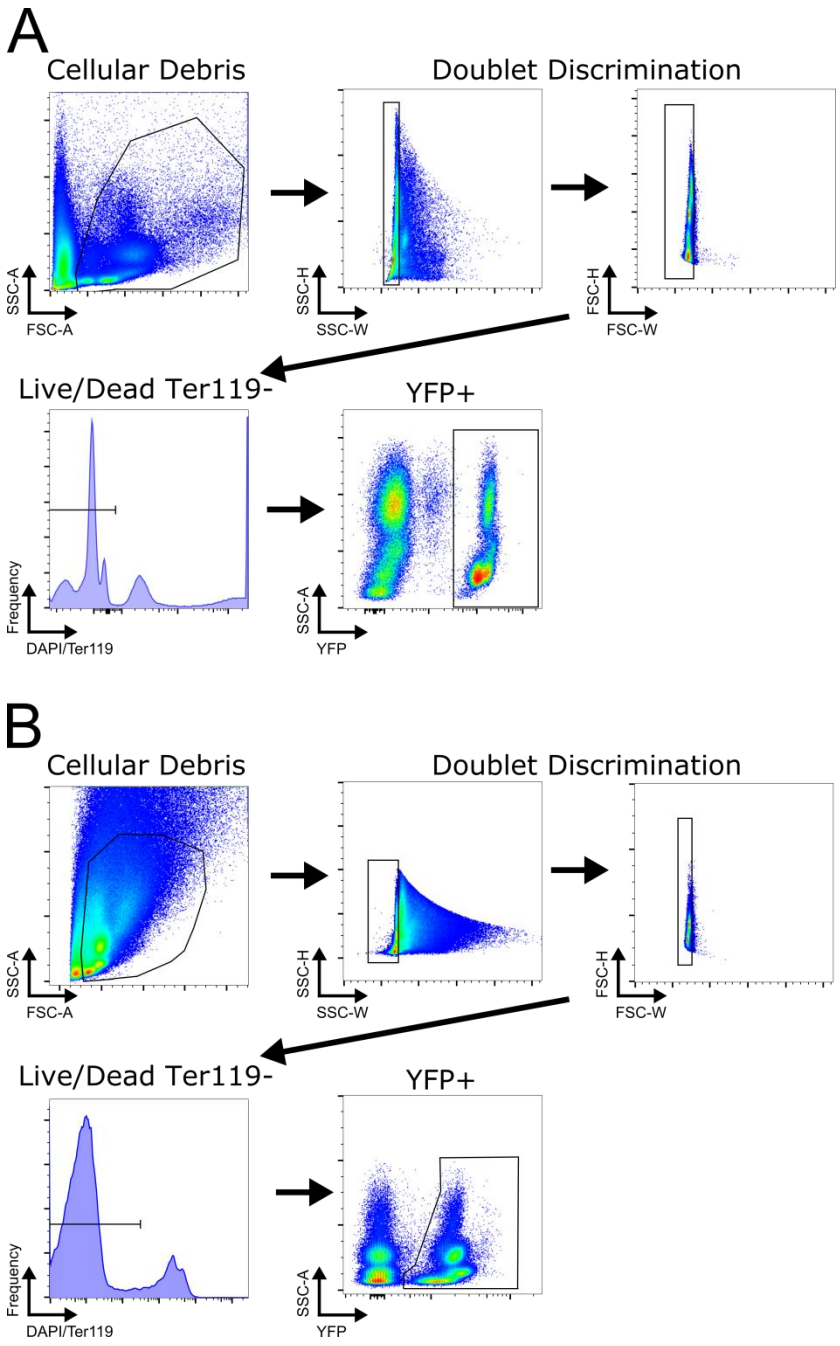


**Figure 4.10: Gating strategy for identification of BM-derived proangiogenic cells in mice transplanted with YFP-labeled hematopoietic cells.**
Representative flow plots illustrating the gating strategy used for identification of bone-marrow derived cells in (A) the peripheral blood and (B) the lung.

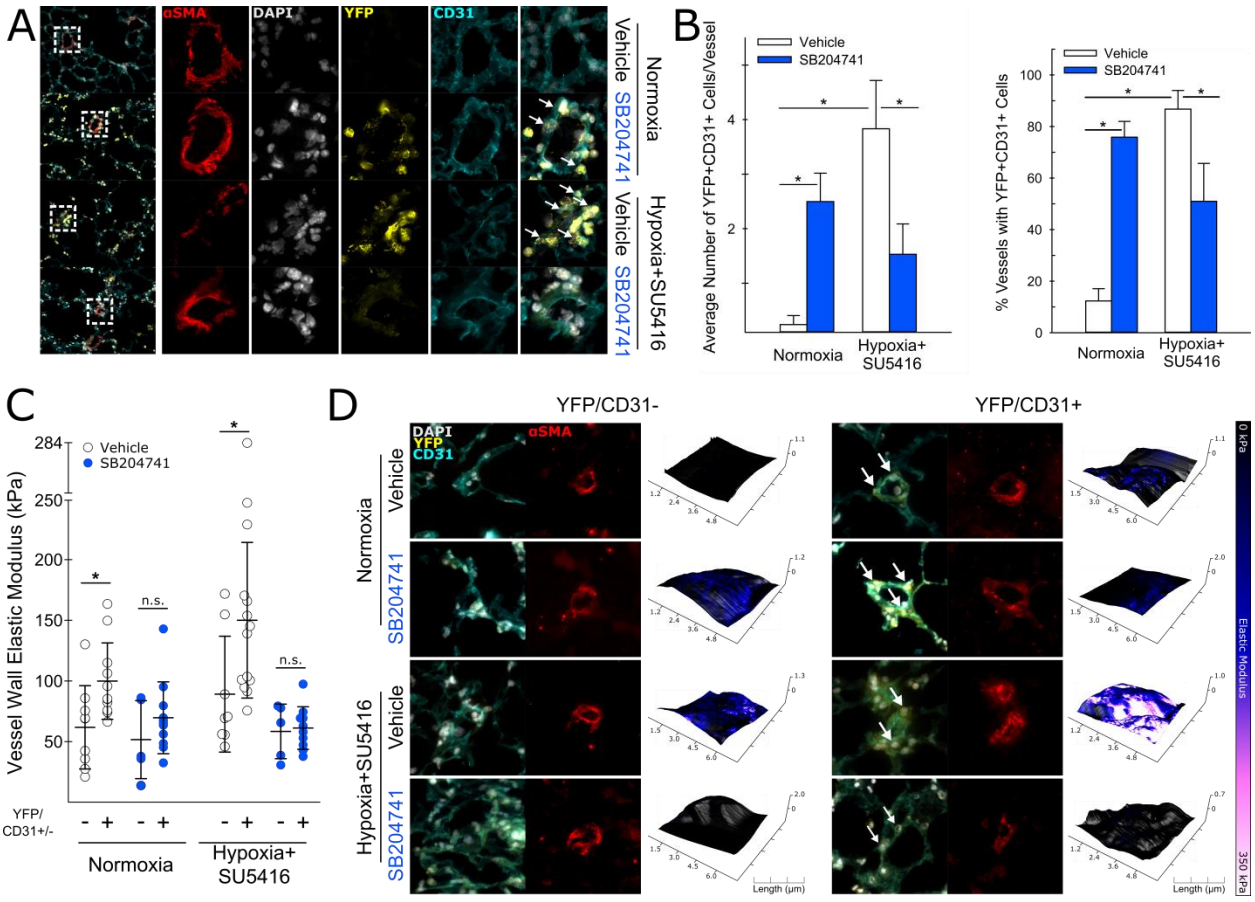


**Figure 4.11: 5-HT$_{2B}$ antagonism inhibits BM-PAC accumulation in the walls of muscularized and stiffened pulmonary arterioles.**

(A) Lung sections were incubated with fluorescently labeled antibodies specific for α-smooth muscle actin (αSMA) to identify pulmonary arterioles. Co-staining with DAPI, anti-GFP, and anti-CD31 allowed for the identification of CD31$^+$ bone-marrow derived cells. Representative images are shown for each treatment condition. (B) Both an increased number of BM-derived CD31$^+$ cells adjacent to remodeled vessels and an increased frequency of vessels with at least one BM-derived CD31$^+$ cell were observed adjacent to pulmonary arterioles in vehicle treated mice exposed to SU5416+Hypoxia (n=3-4 animals/group, mean +/- S.E. *$p$<0.05 following 2-way ANOVA and Holm-Sidak post-hoc test). (C) In normoxic and SU5416+hypoxia treated animals, αSMA+ arterioles with at least one adjacent BM-derived CD31$^+$ cell were significantly stiffer than those without adjacent BM-derived CD31$^+$ cells. In either case, SB204741 treatment normalized the stiffness of the vessel walls (n=4-13, mean +/- S.E. *$p$<0.05 following 2-way ANOVA and Holm-Sidak post-hoc test). (D) Representative images of scanned vessels without YFP$^+$CD31$^+$ (left) or with at least one YFP$^+$CD31$^+$ cell present in the vessel wall (right) for each treatment condition.

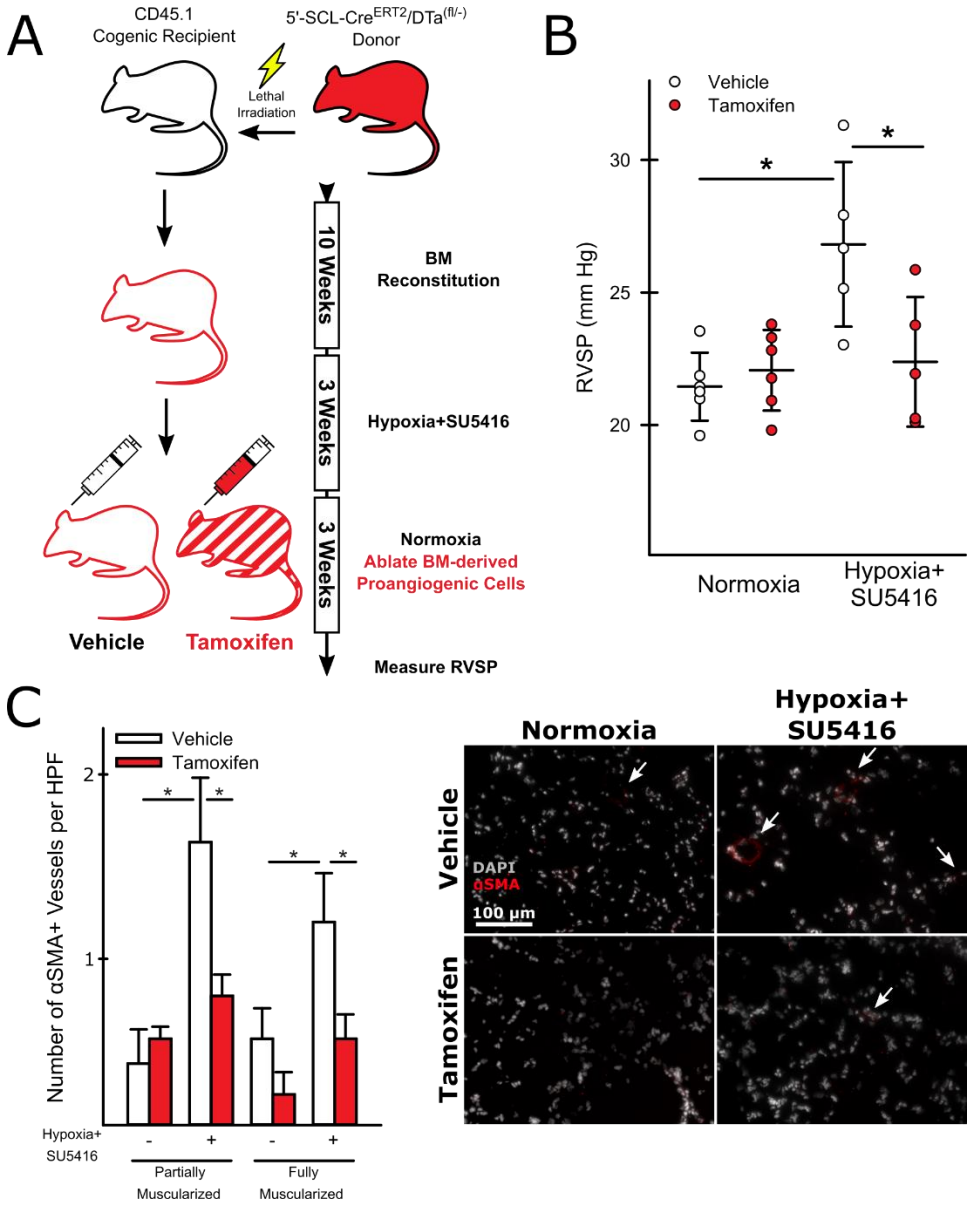


**Figure 4.12: Ablation of BM-derived proangiogenic cells reverses experimental pulmonary hypertension.**

(A) Experimental approach. Cogenic age and sex-matched recipient animals were transplanted whole BM from endothelial-SCL-Cre$^{ERT2}$/DTa$^{(fl/-)}$ donors following lethal irradiation. After a 10 week reconstitution period, the mice were treated with SU5416+Hypoxia or room air to induce pulmonary hypertension. After 3 weeks, animals were place on room air and given either tamoxifen or vehicle to ablate BM-derived proangiogenic cells. (B) Tamoxifen-treated animals exposed to SU5416+Hypoxia had significantly decreased pressures compared to their vehicle treated counterparts (n=5-6, mean +/-S.E. *$p$<0.05 following 2-way ANOVA and Holm-Sidak post-hoc test). (C) The average number of fully and partially, muscularized arterioles (< 100 μm diameter) is significantly reduced in tamoxifen treated SU5416+Hypoxia animals compared to vehicle treated (n=3, mean+/- S.E. *$p$<0.05 following 2-way ANOVA and Holm-Sidak post-hoc test).

5-$HT_{2B}$ Antagonism Alters the Expression Profile of BM-PACs

In order to determine how 5-$HT_{2B}$ antagonism might alter the function or phenotype of BM-PACs, we performed RNA sequencing on BM-PACs isolated from mice treated with either vehicle or SB204741 in normoxic conditions. After 3 weeks of treatment, RNA from ($Ter119^-Gr1^-B220^-CD3^-$) $CD31^+CD11b^-$ cells isolated from either the BM or peripheral blood was sequenced (Figure 4.14), and a gene ontology (GO) enrichment analysis performed on significantly differentially expressed genes ($p<0.01$) (shown in green in Figure 4.12 A and 4.13 A). The results of both a GO slim analysis and full GO Biologic Process analysis for BM-PACs isolated from both BM and peripheral blood are show in Figure 4.12 and 4.13, respectively. The GO slim analysis was notable for a significant enrichment of genes broadly regulating immunologic processes, cytoskeletal regulation and cell motility, and cell differentiation. A more detailed GO enrichment analysis for all biological process categories indicated that, in BM-PACs isolated from BM, 5-$HT_{2B}$ antagonism altered phosphorylation events associated with cellular metabolism, processes involved in cell development and differentiation, and cell motility and migration (Figure 4.12 B-C, Table A.4). Contrastingly in peripheral blood isolated BM-PACs, genes regulating cytokine production and response, cell motility and migration, and cell division were significantly enriched (Figure 4.13 B-C, Table A.5).

Following enrichment analysis, we compared our list of genes whose expression in BM-PACs was significantly altered by 5-$HT_{2B}$ antagonism to a list of SNPs affecting genes in humans negatively associated with clinical metrics of PAH (a worsened 6-minute walk test or right ventricle function). In BM-isolated BM-PACs, the expression of 3 genes regulating production of mitochondrial NADH (mt-nd1, mt-nd2, and mt-nd3) were significantly altered by 5-$HT_{2B}$ antagonism and had associated SNPs correlated with worsened 6-minute walk tests. In peripheral blood isolated BM-PACs, the expression of the clock gene Per3 was similarly altered by 5-$HT_{2B}$ antagonism and had a SNP associated with negative outcomes in the right ventricle function test. These results are summarized in Table 4.1.

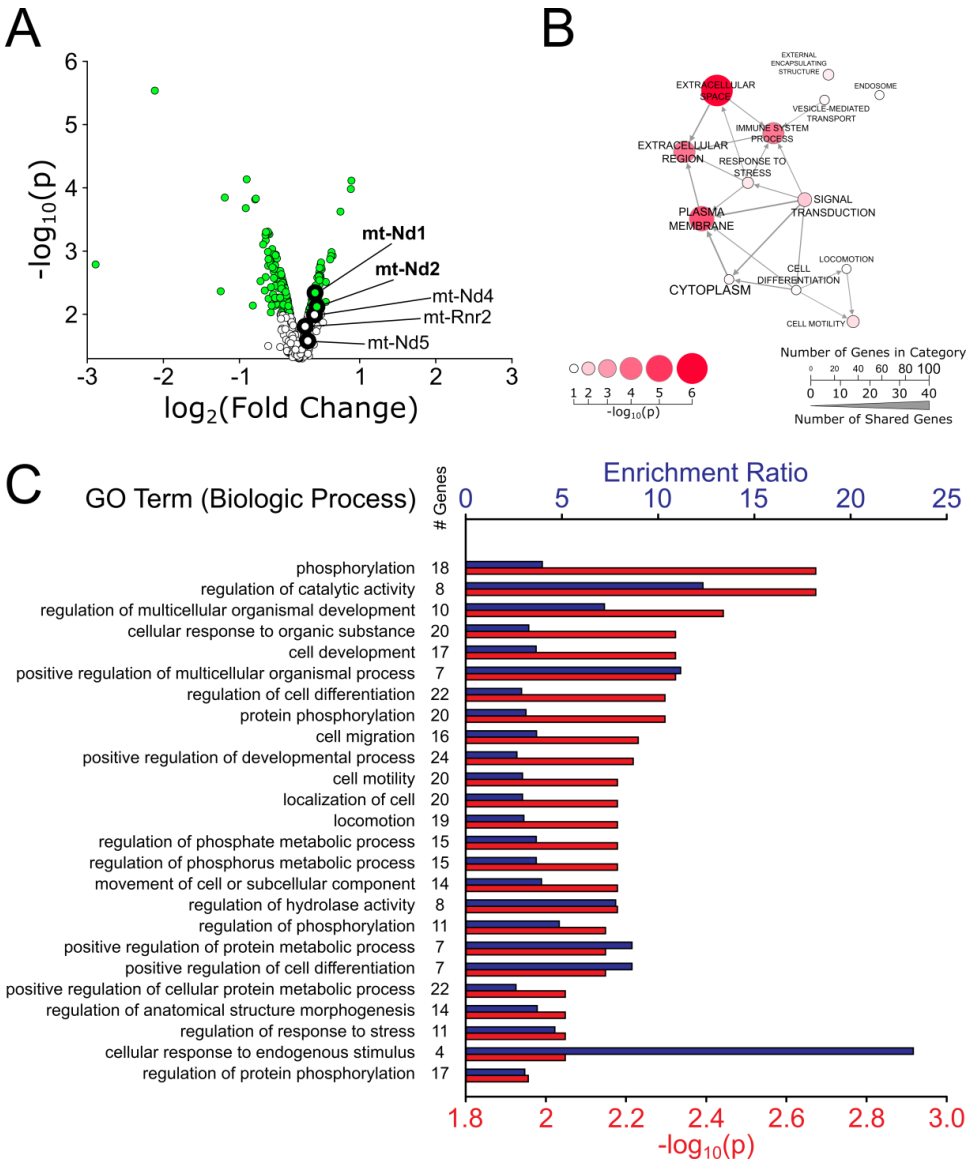


**Figure 4.13: Transcriptome analysis of proangiogenic cells isolated from BM reveals differential gene expression profiles in normoxic mice treated with either vehicle or SB204741.**
(A) Volcano plots displaying significantly up- and down-regulated genes in ($Ter119^-Gr1^-B220^-CD3^-$) $CD31^+CD11b^-$ cells isolated from BM. Genes in green were used in a subsequent gene ontology (GO) enrichment analysis. Labeled genes are included in table 4.1. (B) GO slim analysis for BM- isolated cells suggests 5-$HT_{2B}$ antagonism alters processes broadly associated with immunological regulation, signal transduction and differentiation. Results are presented as a directed acyclic graph, with the size and color of each node corresponding to the $-\log_{10}$ of the adjusted p-value. The size of the text for each node correlates to the number of genes in that GO category, and the thickness of each connecting arrow represents the number of shared genes between categories. The arrow direction signifies the parent/child relationship between categories. All categories are significantly enriched (adjusted $p<0.05$). (C) The top 25 most significantly altered GO biological process categories. Red bars correspond to $-\log_{10}$ of the adjusted p value, while blue bars represent the enrichment ratio (the number of differentially expressed genes found to belong to that category divided by the number of genes expected in that category by random chance alone). The results suggest processes regulating protein and metabolite phosphorylation and cell differentiation are altered by 5-$HT_{2B}$ antagonism.

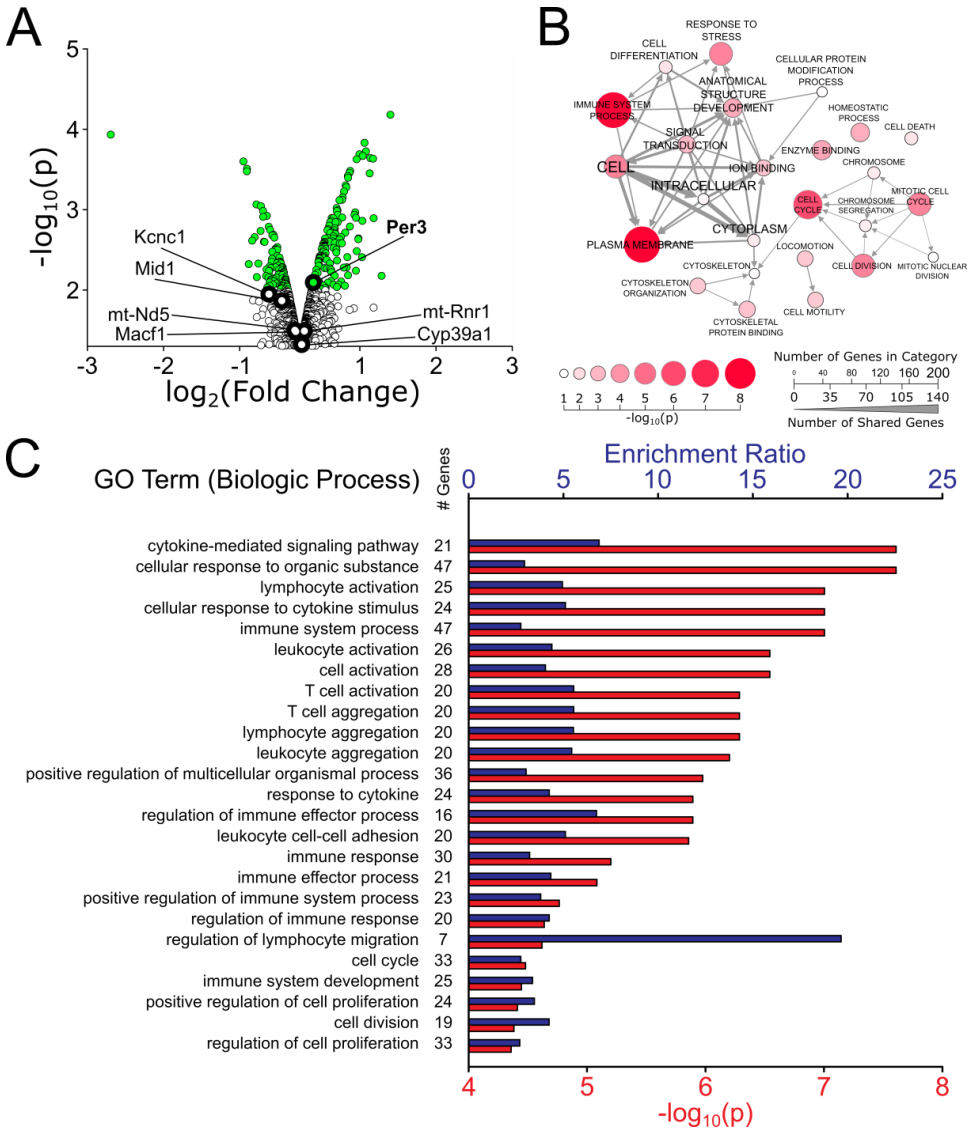


**Figure 4.14: Transcriptome analysis of proangiogenic cells isolated from the peripheral blood reveals differential gene expression profiles in normoxic mice treated with either vehicle or SB204741.**
(A) Volcano plots displaying significantly up- and down-regulated genes in ($Ter119^-Gr1^-B220^-CD3^-$) $CD31^+CD11b^-$ cells isolated from peripheral blood. Genes in green were used in a subsequent gene ontology (GO) enrichment analysis. Labeled genes are included in table 4.1. (B) GO slim analysis for peripheral blood-isolated cells suggests 5-$HT_{2B}$ antagonism alters processes broadly associated with immunological regulation, signal transduction and alterations to cytoskeletal regulation and locomotion more pronounced in peripheral blood isolated PACs. Results are presented as a directed acyclic graph, with the size and color of each node corresponding to the –log10 of the adjusted p-value. The size of the text for each node correlates to the number of genes in that GO category, and the thickness of each connecting arrow represents the number of shared genes between categories. The arrow direction signifies the parent/child relationship between categories. All categories are significantly enriched (adjusted $p<0.05$). (C) The top 25 most significantly altered GO biological process categories. Red bars correspond to –log10 of the adjusted p value, while blue bars represent the enrichment ratio (the number of differentially expressed genes found to belong to that category divided by the number of genes expected in that category by random chance alone). The results suggest processes regulating cytokine production and signaling and cell proliferation and migration are altered by 5-$HT_{2B}$ antagonism.

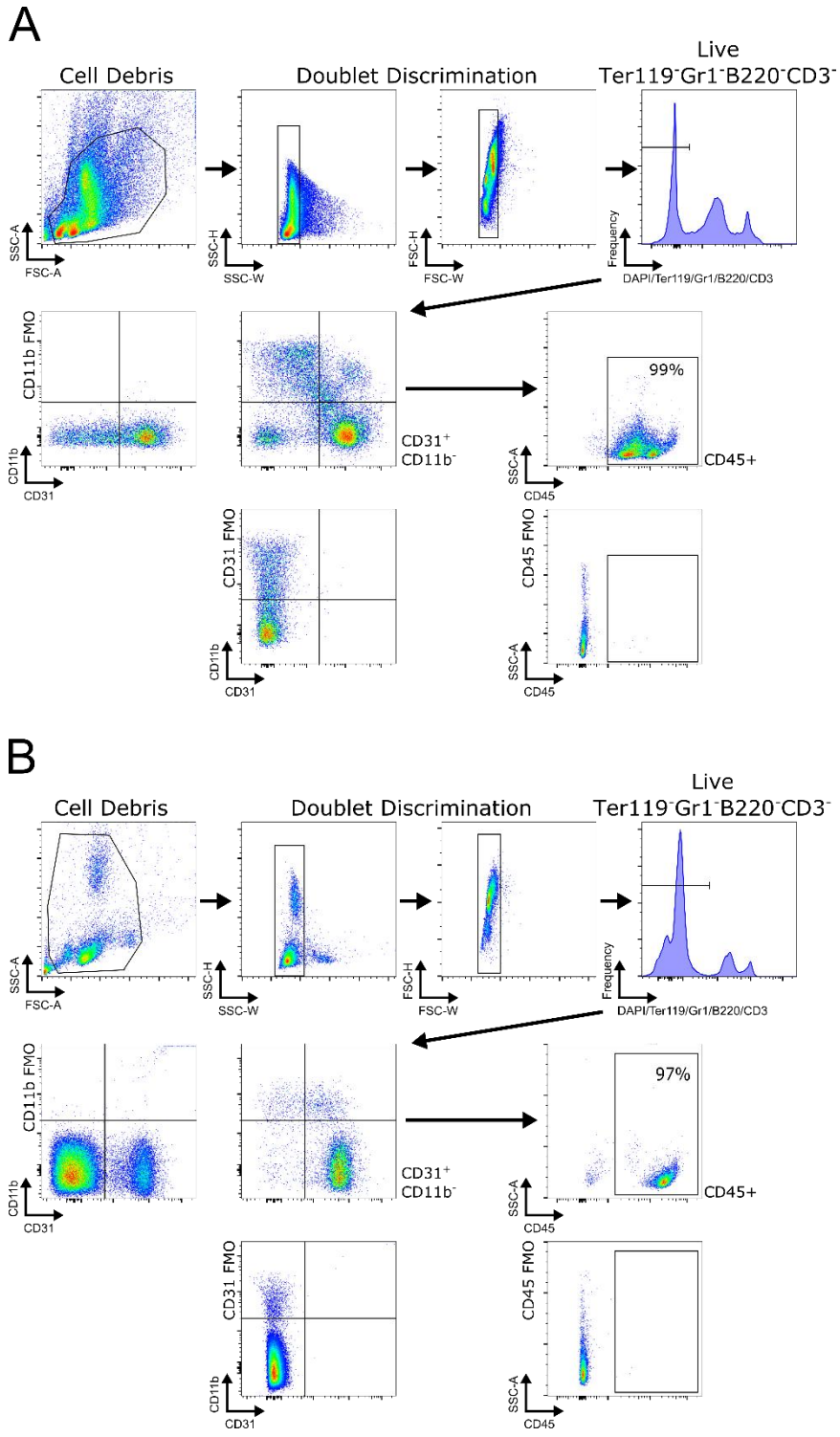


**Figure 4.15: Surface-maker characterization of proangiogenic cells isolated for RNA-seq using FACS.** Representative flow plots illustrating the gating strategy used to isolate BM-PACs for RNA-seq from both (A) bone marrow and (B) peripheral blood. 95-99% of BM-PACs from both BM and peripheral blood were $CD45^+$, confirming their hematopoietic origin.

| Tissue | Gene | $-\log_{10}(p)$ | $\log_2(FC)$ | Included in Significantly Enriched GO Term | PAH SNP ID | Predicted Impact | Human Homolog | Clinical Symptom Association |
|---|---|---|---|---|---|---|---|---|
| **BM** | mt-Nd1 | 2.3 | 0.42 | | rs28625645 | Upstream Gene Variant | MT-ND1 | 6-Minute Walk Test |
| **PBMC** | Per3 | 2.1 | 0.39 | GO:0042752 (Regulation of Circadian Rhythm) | rs228682 | Intron Variant | PER3 | Right Ventricle Function |
| **BM** | mt-Nd2 | 2.1 | 0.44 | GO:0016310 (Phosphorylation) | rs28625645 | Upstream Gene Variant | MT-ND2 | 6-Minute Walk Test |
| **BM** | mt-Nd4 | 2.0 | 0.41 | | rs28359178 | Downstream Gene Variant | MT-ND4 | 6-Minute Walk Test |
| PBMC | Kcnc1 | 1.9 | -0.61 | | rs2283249 | Intron Variant | KCNC1 | Right Ventricle Function |
| PBMC | Mid1 | 1.9 | -0.44 | | rs5979356 | Intron Variant | MID1 | Right Ventricle Function |
| BM | mt-Rnr2 | 1.8 | 0.29 | | rs28625645 | Upstream Gene Variant | MT-RNR2 | 6-Minute Walk Test |
| BM | mt-Nd5 | 1.5 | 0.32 | | rs28359178 | Missense Variant | MT-ND5 | 6-Minute Walk Test |
| PBMC | Macf1 | 1.5 | -0.27 | | rs2275767 | Intron Variant | MACF1 | 6-Minute Walk Test |
| PBMC | mt-Rnr1 | 1.5 | 0.28 | | rs28625645 | Upstream Gene Variant | MT-RNR1 | 6-Minute Walk Test |
| PBMC | Rad18 | 1.5 | -0.26 | | rs1714299 | Intron Variant | RAD18 | 6-Minute Walk Test |
| PBMC | Cyp39a1 | 1.3 | 0.24 | | rs2277119 | Missense Variant | CYP39A1 | 6-Minute Walk Test |

**Table 4.1: 5-$HT_{2B}$ antagonism alters expression of genes in BM-PACs associated with worsened clinical outcomes in PAH.**
An analysis of single nucleotide polymorphisms (SNPs) that correlate to a worsened clinical outcome in a cohort of PAH patients ($p<0.01$) revealed an overlap with 4 genes significantly altered by 5-$HT_{2B}$ antagonism in both BM- and peripheral blood-isolated PACs. Two of these genes were also included in significantly enriched GO terms.

*Discussion*

By utilizing a combination of genetically-targeted ablation and pharmacologic inhibition, we have illustrated for the first time that BM-PACs contribute directly to PAH pathogenesis and that the 5-$HT_{2B}$ receptor is a critical mediator of this contribution. While BM-PACs have long been suspected to influence vascular remodeling the evidence of their contribution has been largely correlative. This evidence stems primarily from observations that BM-derived cells expressing endothelial or progenitor surface markers accumulate in the walls of remodeled arterioles[200,201,254], and that increased or decreased numbers of these cells are found in the peripheral blood of PAH patients (depending on the surface markers employed for identification or patient cohort studied).[255–258] Pharmacologic blockade of chemokine receptors such as CXCR4 and CXCR7[203,242] and the progenitor cell marker cKit[239] has been successful in preventing PAH in animal models presumably by targeting subsets of this population, but the ubiquity of chemokine receptor expression among hematopoietic cell types (as well as native vascular endothelium)[259] and lack of specificity among tyrosine kinase receptor antagonists makes interpretation of these results difficult.

Employing an inducible endothelial-specific Cre developed for studying hematopoietic proangiogenic cells[252] allowed us to circumvent the problem of surface marker heterogeneity inherent in this population. By specifically targeting all bone-marrow derived cells with this

endothelial phenotype for destruction, we effectively prevented the development of PAH secondary to hypoxic vascular injury. Notably, while RVSP measurements and vascular stiffness were normalized following BM-PAC ablation, the number of partially muscularized arterioles remained elevated. This result is not entirely unsurprising considering that small artery muscularization is a natural adaptation to chronic hypoxia in the lung. The normalization of arteriole compliance following BM-PAC ablation is particularly notable, especially considering the important role arteriole stiffening plays in PAH pathogenesis. Recent evidence from mouse models and human patients suggests that small vessel stiffening is an early and perhaps initiating event in PAH pathogenesis.[57] Stiffer substrates induce metabolic reprogramming in native endothelial and smooth muscle cells, facilitating their transition to the proliferative and synthetic phenotype that predominates during active vascular remodeling.[60] It is possible that BM-PACs may be the cell type mediating this transition by directly modulating vascular stiffness.

The serotonin 2B receptor has long been recognized as a rate-limiting step in PAH pathogenesis, and more recently as an indispensable mediator of the hematopoietic contribution to disease.[173,239] We have previously shown that pharmacologic blockade of 5-$HT_{2B}$ is effective in preventing familial PAH using a genetic mouse model, and that 5-$HT_{2B}$ antagonism significantly normalizes the expression of genes regulating cytoskeletal maintenance and contractility in the lung.[246] Our results in the current study suggest that this effect may be secondary to the recruitment of BM-PACs following hypoxic vascular injury. 5-$HT_{2B}$ antagonism exerted similar effects on the PAH phenotype to BM-PAC ablation, effectively normalizing RVSP and metrics of pulmonary vessel remodeling (including vascular stiffness). 5-$HT_{2B}$ antagonism also reduced the fraction of $CD31^{+}CD11b^{-}$ BM-derived cells in circulation and in lung tissue during PAH, a cell population with enriched proangiogenic potential and previously reported to be reduced in the peripheral blood of 5-$HT_{2B}$ knockout mice.[239,253,260,261] This dual effect suggests that the 5-$HT_{2B}$ antagonist is exerting its effects in the bone marrow compartment by preventing the proliferation or differentiation of BM-PACs from a precursor population. The

results from our GO enrichment analysis complement these findings, indicating a significant alteration in genes regulating both cell differentiation and proliferation in BM- and peripheral blood-isolated BM-PACs. This is consistent with the previously published data showing that $CD34^+$ cells from 5-$HT_{2B}$ knockout mice and 5-$HT_{2B}$ antagonist treated human $CD34^+$ cells have reduced myeloerythroid differentiation potential.[239]

Also consistent with previous studies was our observation that $CD31^+$ BM-derived cells accumulate in the walls of muscularized arterioles following hypoxia and SU5416 treatment.[201,202,262] We also observed that vessels with at least one associated BM-derived $CD31^+$ cell were significantly stiffer in both normoxic and hypertensive animals. 5-$HT_{2B}$ antagonism reduced both the localization of $CD31^+$ BM-derived cells to the walls of remodeling arterioles and the stiffness of vessels with associated $CD31^+$ BM-derived cells. Surprisingly, in the absence of hypoxic vascular injury we found increased localization of these cells secondary to 5-$HT_{2B}$ antagonist treatment, despite the absence of observable changes in the total fraction of these cells as measured by flow cytometry. Despite this apparent increase in localization during normoxia, the normalization of vessel wall stiffness suggests that 5-$HT_{2B}$ antagonism also exerts direct, functional effects on this cell population, impairing their ability to induce vascular remodeling. Our GO enrichment results support this conclusion by showing alterations in cytokine production and signaling pathways secondary to 5-$HT_{2B}$ antagonism, the hypothesized mechanism whereby BM-PACs contribute to vessel remodeling.[199]

In the present study we have illustrated that BM-PACs are indispensable for the development of PAH and contribute directly to vascular remodeling. By implicating the 5-$HT_{2B}$ receptor as a critical mediator of the recruitment and function of these cells during hypoxic vascular injury, we have further defined the function of 5-$HT_{2B}$ signaling during PAH pathogenesis (Figure 4.14). This discovery provides additional impetus to pursue pharmacologic targeting of 5-$HT_{2B}$ as a potential therapy for PAH, and encourages further exploration of BM-

PAC function in vascular remodeling in the hopes of identifying novel molecular mediators of illness.

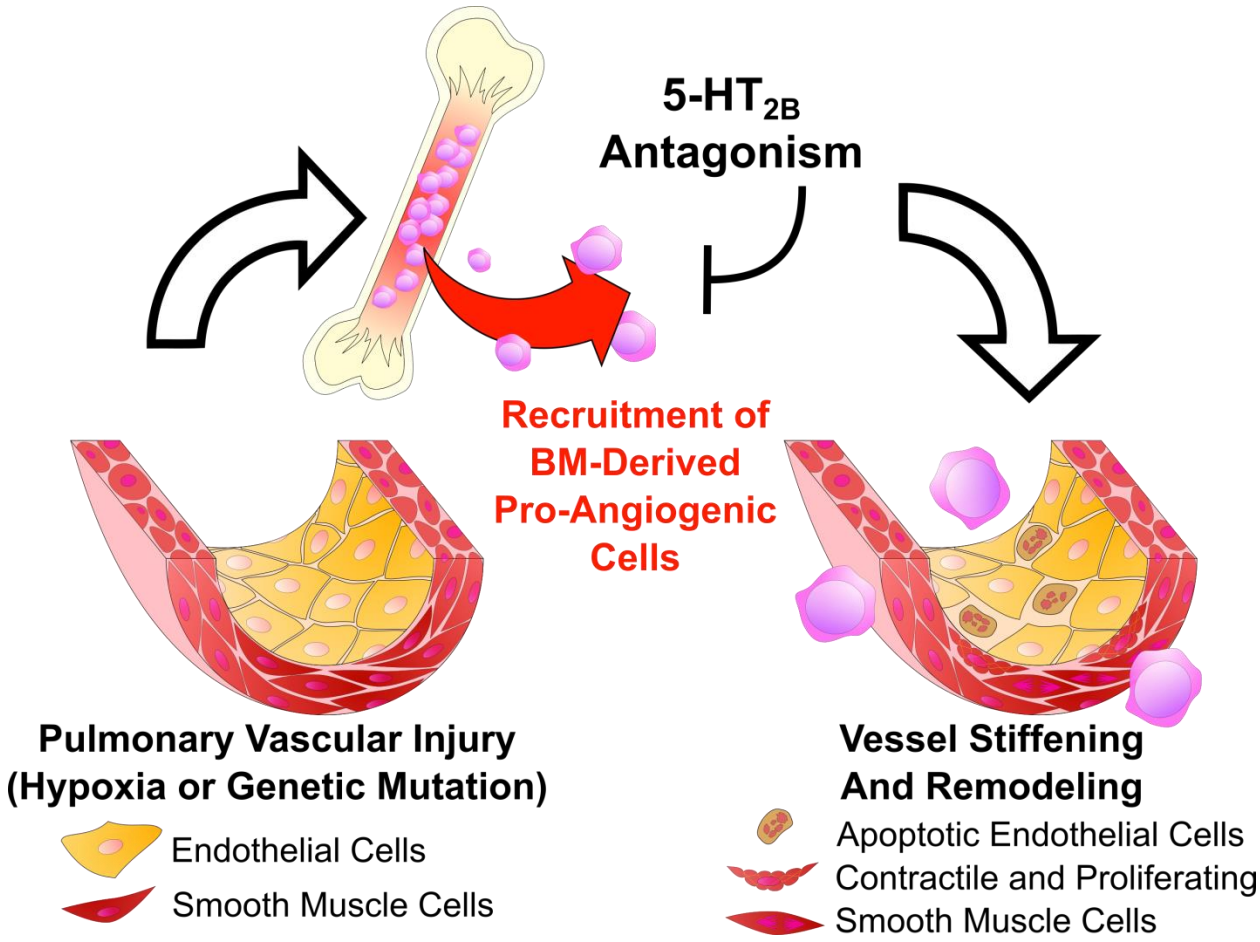


**Figure 4.14: A summary of BM-PAC function in PAH pathogenesis and the role of 5-HT$_{2B}$.**
BM-PACs are recruited to pulmonary arterioles following vascular injury where they mediate the stiffening and muscularization characteristic of small vessel remodeling. Intact 5-HT$_{2B}$ receptor signaling is necessary for their recruitment to and function in the lung vasculature, likely by mediating their differentiation in the bone marrow or production of cytokine mediators in the periphery.

# CHAPTER 5: IMPACT AND FUTURE DIRECTIONS

*Summary of Impact and Limitations*

In Chapter 3, we illustrated that Src motility and signaling is significantly dysregulated in Bmpr2-mutant pulmonary microvascular cells and animals, and that 5-$HT_{2B}$ antagonism corrects many of the deficits associated with this dysregulation. In Chapter 4 we proved that BM-PACs, a unique and poorly understood cell population, are responsible for mediating pathologic small vessel remodeling during PAH and that their function is dependent at least in part on intact 5-$HT_{2B}$ signaling. These discoveries provide additional insight into the mechanism and function of both the 5-$HT_{2B}$ receptor and the cellular mediators of small vessel remodeling.

Gene array data and GO analysis from Chapter 3 showed that 5-$HT_{2B}$ antagonism most significantly alters genes responsible for regulating cytoskeletal contractility in the lungs of Bmpr2 mutant animals. Our functional data suggests that the pharmacologic antagonist of 5-$HT_{2B}$, SB204741, can act directly on smooth muscle cells to counteract TGF-β1 mediated changes in cytoskeletal organization and function. Additionally, by preventing the recruitment of BM-PACs to the lungs during PAH as shown in Chapter 4, we show that 5-$HT_{2B}$ antagonism also functions indirectly to mediate these changes in cytoskeletal remodeling. Given our data and the fact that 5-$HT_{2B}$ is expressed natively in pulmonary endovascular cells and by cells of the hematopoietic system[239,263], it is likely that 5-$HT_{2B}$ antagonism exerts both direct and indirect effects on vascular remodeling by altering the function of multiple cell types.

Src signaling in PAH is a complex and poorly understood process. While elevated Src signaling is generally understood to contribute to pulmonary vascular remodeling, the effects are dependent on a number of factors including the isoform of Src that is activated.[263] Further complicating the picture are the disparate effects of various tyrosine kinase inhibitors on experimental pulmonary hypertension. Dasatinib, a tyrosine kinase inhibitor with Src inhibitory activity, is known to cause PAH.[263] In mice dasatinib, but not imatinib (another tyrosine kinase

inhibitor with less potent Src inhibition[264]), worsens experimental pulmonary hypertension.[265] While the exact mechanism is unclear, it could be due to excessive inhibition of Src. Imatinib has been studied previously as potential treatment for PAH. In phase 3 of the IMPRES clinical trial, some patients on standard treatment showed small but meaningful improvements in clinical outcomes when taking imatinib; however, the increase in adverse events (including subdural hematoma) was a cause for concern.[266] Our data suggests that in Bmpr2 mutant animals, upregulated Src motility leads to excessive Src signaling as a direct consequence of the R899X Bmpr2 mutation. We correlate increased Src signaling and motility with expression of the mutant Bmpr2 receptor and show a correction of both increased Src signaling and motility with 5-$HT_{2B}$ antagonism. By doing so, we directly implicate Src signaling as a pathologic mediator of PAH. Our study was specific to genetic PAH, and to a very specific Bmpr2 mutation – the deletion of tyrosine residue in the cytoplasmic tail domain. Given the diverse functions of the Bmpr2 tail domain, evolutionarily conserved and unique among the TGF-β superfamily of receptors, it is conceivable that our findings may not be broadly applicable outside of hereditary PAH.[146,186] This narrower scope could also explain the discrepancies in the literature regarding the conflicting reports of Src inhibition in PAH treatment. For the IMPRES study in particular the cohort of patients was not genotyped, making it impossible to know whether or not they possessed Bmpr2 mutations known to cause PAH. It is possible that patients with more severe disease who responded better to imatinib therapy may have done so due to the presence of a Bmpr2 mutation. It is also possible that 5-$HT_{2B}$ antagonism might depress Src signaling just enough to retain baseline function, whereas global disruption of Src signaling (as in the case of dasatinib) is excessive enough to cause serious adverse events.

While the findings that 5-$HT_{2B}$ antagonism corrects defects in Src signaling associated with the Bmpr2 mutation are both novel and compelling, the lack of mechanistic data limits the scope and interpretation of the work. Futhermore, the 5-$HT_{2B}$ antagonist used in the study (SB204741), while specific, also has small but measurable activity for the 5-$HT_{2A}$ receptor, an

important mediator of small vessel contractility and proliferation.[65] Additional approaches for targeting the 5-$HT_{2B}$ receptor including transcriptional silencing with siRNA, targeted genetic mutations, and other small molecule antagonists, would help to confirm the findings presented here.

Our work in Chapter 4 illustrates for the first time that BM-PACs contribute directly to small vessel remodeling. Additionally, we further clarify a role for the 5-$HT_{2B}$ receptor in the hematopoietic contribution to PAH by implicating 5-$HT_{2B}$ signaling directly in mediating the recruitment to and function of these cells in the pulmonary microvasculature. In the first part of our study, we relied on a genetic driver (SCL or Tal1 promoter tamoxifen-inducible Cre) to define the cell type to be ablated. In the second portion, we identified $CD31^{+}CD11b^{-}$ BM-derived cells as the cell type of interest. There is undoubtedly overlap between these two populations; CD31 alone is a sufficient marker to delineate a proangiogenic population of bone marrow cells,[253] and it is very likely that the $CD31^{+}CD11b^{-}$ cell population contains the SCL-expressing subpopulation. However, it is impossible to know the exact frequency and extent of this overlap, limiting our interpretation of the results. Future studies would benefit from the use of Cre-inducible fluorescent reporters specific to the SCL enhancer, allowing us to trace and isolate the exact cell population we ablated.

Further work on the exact mechanism of BM-PAC function in vascular remodeling also remains to be done. Our work identified several key pathways in BM-PACs altered by 5-$HT_{2B}$ antagonism, including those regulating cell differentiation and the production and response to cytokines. While it is likely BM-PACs exert their ill effects via production of cytokines and signaling factors[199], the identify of these factors and the mechanism whereby they are produced and exert their effects remain obscure. As our study relied on systemic inhibition of 5-$HT_{2B}$ with a small molecule antagonist, it is also unclear as to how exactly 5-$HT_{2B}$ mediates the function of these cells and their presence in the lung. The GO results could potentially be due to

downstream alterations in the transcriptional profile of these cells, with 5-$HT_{2B}$ antagonism primarily mediating its effects in their progenitor population.

*Future Directions*

Further studies targeting the 5-$HT_{2B}$ receptor using transgenic animals and targeted genetic ablation would be helpful in further determining how 5-$HT_{2B}$ acts to mediate Src signaling and transport and interact with Bmpr2. By breeding mice expressing both the rtTA2 and TETO7-$Bmpr2^{R899X}$ mutant genes as well as two copies of either a non-functional 5-$HT_{2B}$ gene or wild-type 5-$HT_{2B}$, ($Bmpr2^{R899X}$/5-$HT2B^{-/-}$) we can perform both *in vitro* and, more importantly, *in vivo* experiments on isolated pulmonary microvascular cells to elucidate this mechanism of action. Transplantation of bone marrow from $Bmpr2^{R899X}$/5-$HT2B^{-/-}$ into Bmpr2 mutant mice with functional 5-$HT_{2B}$ receptors and vise-versa will also help connect aims 1 and 2, broadening the impact and scope of the work by tying the Bmpr2 mutation to BM-PAC function and 5-$HT_{2B}$ inhibition to its correction, potentially through a Src-dependent mechanism. We have already produced the first generation of these animals as of the writing of this dissertation.

New transgenic mouse models could also be utilized to further interrogate how 5-$HT_{2B}$ modulates the function of BM-PACs. We have recently acquired an unpublished mouse expressing a floxed 5-$HT_{2B}$ receptor. When crossed with a Cre expressing mouse, the 5-$HT_{2B}$ receptor will be functionally deleted from any cells expressing Cre. By selectively breeding mice that express the SCL $Cre^{ERT2}$ used in Chapter 4 and transplanting their bone marrow into that of wild-type mice, we can selectively ablate the 5-$HT_{2B}$ receptor from the same cell population ablated in Chapter 4. Reciprocal transplants using wild-type mice as donors and these transgenic animals as recipients will allow us to interrogate whether the 5-$HT_{2B}$ receptor functions to directly modulate BM-PAC function, or if the effect is secondary to its function on other cell types.

Our work opens important avenues to the therapeutic targeting of 5-$HT_{2B}$ for the treatment of PAH. While 5-$HT_{2B}$ inhibition has long been identified as a potential therapeutic avenue for PAH[173], intervention with systemically administered pharmacologic antagonists has the potential for undesirable side effects in the central nervous system.[267] By working to design 5-$HT_{2B}$ inhibitors that do not cross the blood brain barrier, we can develop therapeutic interventions with minimal side effects. Our work also implies that correction of PAH could be achievable with (relatively) simple gene-therapy strategies. Introducing inactivating mutations in 5-$HT_{2B}$ in the hematopoietic stem cells of PAH patients could potentially be curative, allowing the treatment of PAH with autologous bone marrow transplantation. The recent advent of CRISPR/Cas9 endonuclease gene editing technology allows targeted mutations to be introduced into predetermined regions of the genome with high fidelity and specificity. This technology has already been used to mutate genes in both mouse and human hematopoietic stem cells.[267] Additionally, we have developed and validated guide RNAs that specifically target exon 2 of 5-$HT_{2B}$. Future studies evaluating the efficacy of this targeting strategy for the correction of PAH in mice would be an important first step in their translation into humans.

BIBLIOGRAPHY


1. George MG, Schieb LJ, Ayala C, Talwalkar A, Levant S. Pulmonary Hypertension Surveillance. *Chest*. 2014;146(2):476-495.

2. Macchia A, Marchioli R, Tognoni G, et al. Systematic review of trials using vasodilators in pulmonary arterial hypertension: why a new approach is needed. *Am Heart J*. 2010;159(2):245-257.

3. Preston IR. Properly diagnosing pulmonary arterial hypertension. *Am J Cardiol*. 2013;111(8 Suppl):2C-9C.

4. Simonneau G, Gatzoulis MA, Adatia I, et al. Updated clinical classification of pulmonary hypertension. *J Am Coll Cardiol*. 2013;62(25 Suppl):D34-D41.

5. Badesch DB, Raskob GE, Elliott CG, et al. Pulmonary Arterial Hypertension. *Chest*. 2010;137(2):376-387.

6. Humbert M, Sitbon O, Yaïci A, et al. Survival in incident and prevalent cohorts of patients with pulmonary arterial hypertension. *Eur Respir J*. 2010;36(3):549-555.

7. Benza RL, Miller DP, Gomberg-Maitland M, et al. Predicting survival in pulmonary arterial hypertension: insights from the Registry to Evaluate Early and Long-Term Pulmonary Arterial Hypertension Disease Management (REVEAL). *Circulation*. 2010;122(2):164-172.

8. D'Alonzo GE, Barst RJ, Ayres SM, et al. Survival in patients with primary pulmonary hypertension. Results from a national prospective registry. *Ann Intern Med*. 1991;115(5):343-349.

9. Lai Y-C, Potoka KC, Champion HC, Mora AL, Gladwin MT. Pulmonary arterial hypertension: the clinical syndrome. *Circ Res*. 2014;115(1):115-30.

10. Thenappan T, Ryan JJ, Archer SL. Evolving epidemiology of pulmonary arterial hypertension. *Am J Respir Crit Care Med*. 2012;186(8):707-9.

11. Chen Y-F, Jowett S, Barton P, et al. Clinical and cost-effectiveness of epoprostenol, iloprost, bosentan, sitaxentan and sildenafil for pulmonary arterial hypertension within their licensed indications: a systematic review and economic evaluation. *Health Technol Assess*. 2009;13(49):1-320.

12. Umar S, Rabinovitch M, Eghbali M. Estrogen paradox in pulmonary hypertension: current controversies and future perspectives. *Am J Respir Crit Care Med*. 2012;186(2):125-31.

13. Humbert M, Sitbon O, Chaouat A, et al. Pulmonary Arterial Hypertension in France. *Am J Respir Crit Care Med*. 2006;173(9):1023-1030.

14. McLaughlin V V, Archer SL, Badesch DB, et al. ACCF/AHA 2009 expert consensus document on pulmonary hypertension: a report of the American College of Cardiology

Foundation Task Force on Expert Consensus Documents and the American Heart Association: developed in collaboration with the American College. *Circulation*. 2009;119(16):2250-2294.

15. Shimoda LA, Laurie SS. Vascular remodeling in pulmonary hypertension. *J Mol Med (Berl)*. 2013;91(3):297-309.

16. McLaughlin V V, McGoon MD. Pulmonary arterial hypertension. *Circulation*. 2006;114(13):1417-31.

17. Macchia A, Marchioli R, Marfisi R, et al. A meta-analysis of trials of pulmonary hypertension: a clinical condition looking for drugs and research methodology. *Am Heart J*. 2007;153(6):1037-1047.

18. Sutendra G, Michelakis ED. Pulmonary arterial hypertension: challenges in translational research and a vision for change. *Sci Transl Med*. 2013;5(208):208sr5.

19. Bloodworth NC, West JD, Merryman WD. Microvessel mechanobiology in pulmonary arterial hypertension: cause and effect. *Hypertension*. 2015;65(3):483-9.

20. Mahapatra S, Nishimura RA, Oh JK, McGoon MD. The prognostic value of pulmonary vascular capacitance determined by Doppler echocardiography in patients with pulmonary arterial hypertension. *J Am Soc Echocardiogr*. 2006;19(8):1045-1050.

21. Mahapatra S, Nishimura RA, Sorajja P, Cha S, McGoon MD. Relationship of pulmonary arterial capacitance and mortality in idiopathic pulmonary arterial hypertension. *J Am Coll Cardiol*. 2006;47(4):799-803.

22. Brittain EL, Pugh ME, Wheeler LA, et al. Shorter survival in familial versus idiopathic pulmonary arterial hypertension is associated with hemodynamic markers of impaired right ventricular function. *Pulm Circ*. 2013;3(3):589-598.

23. Su Z, Tan W, Shandas R, Hunter KS. Influence of distal resistance and proximal stiffness on hemodynamics and RV afterload in progression and treatments of pulmonary hypertension: a computational study with validation using animal models. *Comput Math Methods Med*. 2013;2013:618326.

24. Li M, Tan Y, Stenmark KR, Tan W. High Pulsatility Flow Induces Acute Endothelial Inflammation through Overpolarizing Cells to Activate NF-κB. *Cardiovasc Eng Technol*. 2013;4(1):26-38.

25. Tan Y, Tseng P-O, Wang D, et al. Stiffening-Induced High Pulsatility Flow Activates Endothelial Inflammation via a TLR2/NF-κB Pathway. *PLoS One*. 2014;9(7):e102195.

26. Wang Z, Chesler NC. Pulmonary vascular wall stiffness: An important contributor to the increased right ventricular afterload with pulmonary hypertension. *Pulm Circ*. 2011;1(2):212-223.

27. Scott D, Tan Y, Shandas R, Stenmark KR, Tan W. High pulsatility flow stimulates smooth muscle cell hypertrophy and contractile protein expression. *Am J Physiol Lung Cell Mol Physiol*. 2013;304(1):L70-L81.

28. Saouti N, Westerhof N, Helderman F, et al. RC time constant of single lung equals that of both lungs together: a study in chronic thromboembolic pulmonary hypertension. *Am J*

*Physiol Heart Circ Physiol*. 2009;297(6):H2154-H2160.

29. Rabinovitch M. Molecular pathogenesis of pulmonary arterial hypertension. *J Clin Invest*. 2012;122(12):4306-4313.

30. Milnor WR, Bergel DH, Bargainer JD. Hydraulic power associated with pulmonary blood flow and its relation to heart rate. *Circ Res*. 1966;19(3):467-480.

31. Milnor WR, Conti CR, Lewis KB, O'Rourke MF. Pulmonary arterial pulse wave velocity and impedance in man. *Circ Res*. 1969;25(6):637-649.

32. Nichols WW, Conti CR, Walker WE, Milnor WR. Input impedance of the systemic circulation in man. *Circ Res*. 1977;40(5):451-458.

33. Saouti N, Westerhof N, Helderman F, et al. Right ventricular oscillatory power is a constant fraction of total power irrespective of pulmonary artery pressure. *Am J Respir Crit Care Med*. 2010;182(10):1315-1320.

34. Lankhaar J-W, Westerhof N, Faes TJC, et al. Pulmonary vascular resistance and compliance stay inversely related during treatment of pulmonary hypertension. *Eur Heart J*. 2008;29(13):1688-1695.

35. Saouti N, Westerhof N, Postmus PE, Vonk-Noordegraaf A. The arterial load in pulmonary hypertension. *Eur Respir Rev*. 2010;19(117):197-203.

36. Lammers S, Scott D, Hunter K, Tan W, Shandas R, Stenmark KR. Mechanics and function of the pulmonary vasculature: implications for pulmonary vascular disease and right ventricular function. *Compr Physiol*. 2012;2(1):295-319.

37. Gan CT-J, Lankhaar J-W, Westerhof N, et al. Noninvasively assessed pulmonary artery stiffness predicts mortality in pulmonary arterial hypertension. *Chest*. 2007;132(6):1906-1912.

38. Lankhaar J-W, Westerhof N, Faes TJC, et al. Quantification of right ventricular afterload in patients with and without pulmonary hypertension. *Am J Physiol Heart Circ Physiol*. 2006;291(4):H1731-H1737.

39. Zuckerman BD, Orton EC, Latham LP, Barbiere CC, Stenmark KR, Reeves JT. Pulmonary vascular impedance and wave reflections in the hypoxic calf. *J Appl Physiol*. 1992;72(6):2118-2127.

40. Castelain V, Hervé P, Lecarpentier Y, Duroux P, Simonneau G, Chemla D. Pulmonary artery pulse pressure and wave reflection in chronic pulmonary thromboembolism and primary pulmonary hypertension. *J Am Coll Cardiol*. 2001;37(4):1085-1092.

41. Hunter KS, Lee P-F, Lanning CJ, et al. Pulmonary vascular input impedance is a combined measure of pulmonary vascular resistance and stiffness and predicts clinical outcomes better than pulmonary vascular resistance alone in pediatric patients with pulmonary hypertension. *Am Heart J*. 2008;155(1):166-174.

42. Tuchscherer HA, Vanderpool RR, Chesler NC. Pulmonary vascular remodeling in isolated mouse lungs: effects on pulsatile pressure-flow relationships. *J Biomech*. 2007;40(5):993-1001.

43. Kobs RW, Chesler NC. The mechanobiology of pulmonary vascular remodeling in the congenital absence of eNOS. *Biomech Model Mechanobiol*. 2006;5(4):217-225.

44. Kobs RW, Muvarak NE, Eickhoff JC, Chesler NC. Linked mechanical and biological aspects of remodeling in mouse pulmonary arteries with hypoxia-induced hypertension. *Am J Physiol Heart Circ Physiol*. 2005;288(3):H1209-H1217.

45. Laskey WK, Ferrari VA, Palevsky HI, Kussmaul WG. Pulmonary artery hemodynamics in primary pulmonary hypertension. *J Am Coll Cardiol*. 1993;21(2):406-412.

46. Furuno Y, Nagamoto Y, Fujita M, Kaku T, Sakurai S, Kuroiwa A. Reflection as a cause of mid-systolic deceleration of pulmonary flow wave in dogs with acute pulmonary hypertension: comparison of pulmonary artery constriction with pulmonary embolisation. *Cardiovasc Res*. 1991;25(2):118-124.

47. Lalande S, Yerly P, Faoro V, Naeije R. Pulmonary vascular distensibility predicts aerobic capacity in healthy individuals. *J Physiol*. 2012;590(Pt 17):4279-4288.

48. Reusser M, Hunter KS, Lammers SR, Stenmark KR. Validation of a pressure diameter method for determining modulus and strain of collagen engagement for long branches of bovine pulmonary arteries. *J Biomech Eng*. 2012;134(5):54501.

49. Chesler NC, Argiento P, Vanderpool R, D'Alto M, Naeije R. How to measure peripheral pulmonary vascular mechanics. *Conf Proc IEEE Eng Med Biol Soc*. 2009;2009:173-176.

50. Linehan JH, Haworth ST, Nelin LD, Krenz GS, Dawson CA. A simple distensible vessel model for interpreting pulmonary vascular pressure-flow curves. *J Appl Physiol*. 1992;73(3):987-994.

51. Nihill MR, McNamara DG, Vick RL. The effects of increased blood viscosity on pulmonary vascular resistance. *Am Heart J*. 1976;92(1):65-72.

52. Blyth KG, Syyed R, Chalmers J, et al. Pulmonary arterial pulse pressure and mortality in pulmonary arterial hypertension. *Respir Med*. 2007;101(12):2495-2501.

53. Stergiopulos N, Westerhof N. Determinants of Pulse Pressure. *Hypertension*. 1998;32(3):556-559.

54. Li M, Scott DE, Shandas R, Stenmark KR, Tan W. High pulsatility flow induces adhesion molecule and cytokine mRNA expression in distal pulmonary artery endothelial cells. *Ann Biomed Eng*. 2009;37(6):1082-1092.

55. Humphrey JD. Mechanisms of arterial remodeling in hypertension: coupled roles of wall shear and intramural stress. *Hypertension*. 2008;52(2):195-200.

56. Stenmark KR, Fagan KA, Frid MG. Hypoxia-induced pulmonary vascular remodeling: cellular and molecular mechanisms. *Circ Res*. 2006;99(7):675-691.

57. Liu F, Haeger CM, Dieffenbach PB, et al. Distal vessel stiffening is an early and pivotal mechanobiological regulator of vascular remodeling and pulmonary hypertension. *JCI insight*. 2016;1(8).

58. Bertero T, Cottrill KA, Lu Y, et al. Matrix Remodeling Promotes Pulmonary Hypertension through Feedback Mechanoactivation of the YAP/TAZ-miR-130/301 Circuit. *Cell Rep*.

2015;13(5):1016-1032.

59. Nave AH, Mi ikova I, Niess G, et al. Lysyl Oxidases Play a Causal Role in Vascular Remodeling in Clinical and Experimental Pulmonary Arterial Hypertension. *Arterioscler Thromb Vasc Biol*. 2014;34(7):1446-1458.

60. Bertero T, Oldham WM, Cottrill KA, et al. Vascular stiffness mechanoactivates YAP/TAZ-dependent glutaminolysis to drive pulmonary hypertension. *J Clin Invest*. 2016;126(9):3313-3335.

61. Tuder RM. Pathology of pulmonary arterial hypertension. *Semin Respir Crit Care Med*. 2009;30(4):376-385.

62. Lambers C, Roth M, Zhong J, et al. The interaction of endothelin-1 and TGF-β1 mediates vascular cell remodeling. *PLoS One*. 2013;8(8):e73399.

63. Tang W-L, Guo H, Yang J, Chen B, Wang X. Suppression of tissue inhibitors of metalloproteinases may reverse severe pulmonary arterial hypertension. *Cytotherapy*. 2011;13(4):499-502.

64. Rogers NM, Yao M, Sembrat J, et al. Cellular, pharmacological, and biophysical evaluation of explanted lungs from a patient with sickle cell disease and severe pulmonary arterial hypertension. *Pulm Circ*. 2013;3(4):936-951.

65. Thomas M, Ciuclan L, Hussey MJ, Press NJ. Targeting the serotonin pathway for the treatment of pulmonary arterial hypertension. *Pharmacol Ther*. 2013;138(3):409-417.

66. Chow KS, Jun D, Helm KM, Wagner DH, Majka SM. Isolation & characterization of Hoechst(low) CD45(negative) mouse lung mesenchymal stem cells. *J Vis Exp*. 2011;(56):e3159.

67. Rabinovitch M, Guignabert C, Humbert M, Nicolls MR. Inflammation and immunity in the pathogenesis of pulmonary arterial hypertension. *Circ Res*. 2014;115(1):165-175.

68. Paulin R, Michelakis ED. The metabolic theory of pulmonary arterial hypertension. *Circ Res*. 2014;115(1):148-164.

69. Chow M-J, Turcotte R, Lin CP, Zhang Y. Arterial extracellular matrix: a mechanobiological study of the contributions and interactions of elastin and collagen. *Biophys J*. 2014;106(12):2684-2692.

70. Tabima DM, Roldan-Alzate A, Wang Z, Hacker TA, Molthen RC, Chesler NC. Persistent vascular collagen accumulation alters hemodynamic recovery from chronic hypoxia. *J Biomech*. 2012;45(5):799-804.

71. Ooi CY, Wang Z, Tabima DM, Eickhoff JC, Chesler NC. The role of collagen in extralobar pulmonary artery stiffening in response to hypoxia-induced pulmonary hypertension. *Am J Physiol Heart Circ Physiol*. 2010;299(6):H1823-H1831.

72. Wang Z, Chesler NC. Role of collagen content and cross-linking in large pulmonary arterial stiffening after chronic hypoxia. *Biomech Model Mechanobiol*. 2012;11(1-2):279-289.

73. Botney MD, Kaiser LR, Cooper JD, et al. Extracellular matrix protein gene expression in

atherosclerotic hypertensive pulmonary arteries. *Am J Pathol*. 1992;140(2):357-364.

74. Botney MD, Liptay MJ, Kaiser LR, Cooper JD, Parks WC, Mecham RP. Active collagen synthesis by pulmonary arteries in human primary pulmonary hypertension. *Am J Pathol*. 1993;143(1):121-129.

75. Prosser IW, Stenmark KR, Suthar M, Crouch EC, Mecham RP, Parks WC. Regional heterogeneity of elastin and collagen gene expression in intralobar arteries in response to hypoxic pulmonary hypertension as demonstrated by in situ hybridization. *Am J Pathol*. 1989;135(6):1073-1088.

76. Ciuclan L, Bonneau O, Hussey M, et al. A novel murine model of severe pulmonary arterial hypertension. *Am J Respir Crit Care Med*. 2011;184(10):1171-1182.

77. Stenmark KR, Nozik-Grayck E, Gerasimovskaya E, et al. The adventitia: Essential role in pulmonary vascular remodeling. *Compr Physiol*. 2011;1(1):141-161.

78. Frid MG, Kale VA, Stenmark KR. Mature vascular endothelium can give rise to smooth muscle cells via endothelial-mesenchymal transdifferentiation: in vitro analysis. *Circ Res*. 2002;90(11):1189-1196.

79. Zhu P, Huang L, Ge X, Yan F, Wu R, Ao Q. Transdifferentiation of pulmonary arteriolar endothelial cells into smooth muscle-like cells regulated by myocardin involved in hypoxia-induced pulmonary vascular remodelling. *Int J Exp Pathol*. 2006;87(6):463-474.

80. Piera-Velazquez S, Jimenez SA. Molecular mechanisms of endothelial to mesenchymal cell transition (EndoMT) in experimentally induced fibrotic diseases. *Fibrogenesis Tissue Repair*. 2012;5(Suppl 1 Proceedings of Fibroproliferative disorders: from biochemical analysis to targeted therapiesPetro E Petrides and David Brenner):S7.

81. Vieillard-Baron A, Frisdal E, Eddahibi S, et al. Inhibition of matrix metalloproteinases by lung TIMP-1 gene transfer or doxycycline aggravates pulmonary hypertension in rats. *Circ Res*. 2000;87(5):418-425.

82. Vieillard-Baron A, Frisdal E, Raffestin B, et al. Inhibition of matrix metalloproteinases by lung TIMP-1 gene transfer limits monocrotaline-induced pulmonary vascular remodeling in rats. *Hum Gene Ther*. 2003;14(9):861-869.

83. Frisdal E, Gest V, Vieillard-Baron A, et al. Gelatinase expression in pulmonary arteries during experimental pulmonary hypertension. *Eur Respir J*. 2001;18(5):838-845.

84. Lepetit H, Eddahibi S, Fadel E, et al. Smooth muscle cell matrix metalloproteinases in idiopathic pulmonary arterial hypertension. *Eur Respir J*. 2005;25(5):834-842.

85. Benisty JI, Folkman J, Zurakowski D, et al. Matrix metalloproteinases in the urine of patients with pulmonary arterial hypertension. *Chest*. 2005;128(6 Suppl):572S.

86. Safdar Z, Tamez E, Chan W, et al. Circulating Collagen Biomarkers as Indicators of Disease Severity in Pulmonary Arterial Hypertension. *JACC Heart Fail*. 2014;2(4):412-421.

87. George J, D'Armiento J. Transgenic expression of human matrix metalloproteinase-9 augments monocrotaline-induced pulmonary arterial hypertension in mice. *J Hypertens*. 2011;29(2):299-308.

88. Wagenseil JE, Mecham RP. Vascular extracellular matrix and arterial mechanics. *Physiol Rev*. 2009;89(3):957-989.

89. Sokolis DP, Kefaloyannis EM, Kouloukoussa M, Marinos E, Boudoulas H, Karayannacos PE. A structural basis for the aortic stress-strain relation in uniaxial tension. *J Biomech*. 2006;39(9):1651-1662.

90. Cowan KN, Jones PL, Rabinovitch M. Elastase and matrix metalloproteinase inhibitors induce regression, and tenascin-C antisense prevents progression, of vascular disease. *J Clin Invest*. 2000;105(1):21-34.

91. Rabinovitch M, Bothwell T, Hayakawa BN, et al. Pulmonary artery endothelial abnormalities in patients with congenital heart defects and pulmonary hypertension. A correlation of light with scanning electron microscopy and transmission electron microscopy. *Lab Invest*. 1986;55(6):632-653.

92. Ferruzzi J, Collins MJ, Yeh AT, Humphrey JD. Mechanical assessment of elastin integrity in fibrillin-1-deficient carotid arteries: implications for Marfan syndrome. *Cardiovasc Res*. 2011;92(2):287-295.

93. Fonck E, Prod'hom G, Roy S, Augsburger L, Rüfenacht DA, Stergiopulos N. Effect of elastin degradation on carotid wall mechanics as assessed by a constituent-based biomechanical model. *Am J Physiol Heart Circ Physiol*. 2007;292(6):H2754-H2763.

94. Shifren A, Durmowicz AG, Knutsen RH, Faury G, Mecham RP. Elastin insufficiency predisposes to elevated pulmonary circulatory pressures through changes in elastic artery structure. *J Appl Physiol*. 2008;105(5):1610-1619.

95. Durmowicz AG, Parks WC, Hyde DM, Mecham RP, Stenmark KR. Persistence, re-expression, and induction of pulmonary arterial fibronectin, tropoelastin, and type I procollagen mRNA expression in neonatal hypoxic pulmonary hypertension. *Am J Pathol*. 1994;145(6):1411-1420.

96. Clifford PS, Ella SR, Stupica AJ, et al. Spatial distribution and mechanical function of elastin in resistance arteries: a role in bearing longitudinal stress. *Arterioscler Thromb Vasc Biol*. 2011;31(12):2889-2896.

97. Cowan KN, Heilbut A, Humpl T, Lam C, Ito S, Rabinovitch M. Complete reversal of fatal pulmonary hypertension in rats by a serine elastase inhibitor. *Nat Med*. 2000;6(6):698-702.

98. Timmins LH, Wu Q, Yeh AT, Moore JE, Greenwald SE. Structural inhomogeneity and fiber orientation in the inner arterial media. *Am J Physiol Heart Circ Physiol*. 2010;298(5):H1537-H1545.

99. Rothman A, Davidson S, Wiencek RG, et al. Vascular histomolecular analysis by sequential endoarterial biopsy in a shunt model of pulmonary hypertension. *Pulm Circ*. 2013;3(1):50-57.

100. Zeinali-Davarani S, Chow M-J, Turcotte R, Zhang Y. Characterization of biaxial mechanical behavior of porcine aorta under gradual elastin degradation. *Ann Biomed Eng*. 2013;41(7):1528-1538.

101. Fu L, Zhou A, Shen J, Zhao W, Li F. Effect of elastase inhibitor on pulmonary hypertension induced by monocrotaline. *Zhonghua Er Ke Za Zhi*. 2004;42(5):375-378.

102. Thompson K, Rabinovitch M. Exogenous leukocyte and endogenous elastases can mediate mitogenic activity in pulmonary artery smooth muscle cells by release of extracellular-matrix bound basic fibroblast growth factor. *J Cell Physiol*. 1996;166(3):495-505.

103. Izikki M, Guignabert C, Fadel E, et al. Endothelial-derived FGF2 contributes to the progression of pulmonary hypertension in humans and rodents. *J Clin Invest*. 2009;119(3):512-523.

104. Merklinger SL, Jones PL, Martinez EC, Rabinovitch M. Epidermal growth factor receptor blockade mediates smooth muscle cell apoptosis and improves survival in rats with pulmonary hypertension. *Circulation*. 2005;112(3):423-431.

105. Alenghat FJ, Ingber DE. Mechanotransduction: all signals point to cytoskeleton, matrix, and integrins. *Sci STKE*. 2002;2002(119):pe6.

106. Katsumi A, Orr AW, Tzima E, Schwartz MA. Integrins in mechanotransduction. *J Biol Chem*. 2004;279(13):12001-12004.

107. Gao YZ, Saphirstein RJ, Yamin R, Suki B, Morgan KG. Aging Impairs Smooth Muscle Mediated Regulation of Aortic Stiffness: A Defect in Shock Absorption Function? *Am J Physiol Heart Circ Physiol*. 2014:H1252-H1261.

108. Hong Z, Sun Z, Li Z, Mesquitta W-T, Trzeciakowski JP, Meininger GA. Coordination of fibronectin adhesion with contraction and relaxation in microvascular smooth muscle. *Cardiovasc Res*. 2012;96(1):73-80.

109. Nagayama K, Adachi A, Matsumoto T. Heterogeneous response of traction force at focal adhesions of vascular smooth muscle cells subjected to macroscopic stretch on a micropillar substrate. *J Biomech*. 2011;44(15):2699-2705.

110. Umesh A, Paudel O, Cao Y-N, Myers AC, Sham JSK. Alteration of pulmonary artery integrin levels in chronic hypoxia and monocrotaline-induced pulmonary hypertension. *J Vasc Res*. 2011;48(6):525-537.

111. Welschoff J, Matthey M, Wenzel D. RGD peptides induce relaxation of pulmonary arteries and airways via β3-integrins. *FASEB J*. 2014;28(5):2281-2292.

112. Balasubramanian L, Lo C-M, Sham JSK, Yip K-P. Remanent cell traction force in renal vascular smooth muscle cells induced by integrin-mediated mechanotransduction. *Am J Physiol Cell Physiol*. 2013;304(4):C382-C391.

113. Umesh A, Thompson MA, Chini EN, Yip K-P, Sham JSK. Integrin ligands mobilize Ca2+ from ryanodine receptor-gated stores and lysosome-related acidic organelles in pulmonary arterial smooth muscle cells. *J Biol Chem*. 2006;281(45):34312-34323.

114. Heerkens EHJ, Shaw L, Ryding A, et al. alphaV integrins are necessary for eutrophic inward remodeling of small arteries in hypertension. *Hypertension*. 2006;47(2):281-287.

115. Kwapiszewska G, Wygrecka M, Marsh LM, et al. Fhl-1, a new key protein in pulmonary hypertension. *Circulation*. 2008;118(11):1183-1194.

116. de Jesus Perez VA, Yuan K, Orcholski ME, et al. Loss of adenomatous poliposis coli-α3 integrin interaction promotes endothelial apoptosis in mice and humans. *Circ Res*. 2012;111(12):1551-1564.

117. Saphirstein RJ, Gao YZ, Jensen MH, et al. The focal adhesion: a regulated component of aortic stiffness. *PLoS One*. 2013;8(4):e62461.

118. Martinez-Lemus LA, Hill MA, Bolz SS, Pohl U, Meininger GA. Acute mechanoadaptation of vascular smooth muscle cells in response to continuous arteriolar vasoconstriction: implications for functional remodeling. *FASEB J*. 2004;18(6):708-710.

119. Kim HR, Gallant C, Leavis PC, Gunst SJ, Morgan KG. Cytoskeletal remodeling in differentiated vascular smooth muscle is actin isoform dependent and stimulus dependent. *Am J Physiol Cell Physiol*. 2008;295(3):C768-C778.

120. Sehgel NL, Zhu Y, Sun Z, et al. Increased vascular smooth muscle cell stiffness: a novel mechanism for aortic stiffness in hypertension. *Am J Physiol Heart Circ Physiol*. 2013;305(9):H1281-H1287.

121. Gunst SJ, Zhang W. Actin cytoskeletal dynamics in smooth muscle: a new paradigm for the regulation of smooth muscle contraction. *Am J Physiol Cell Physiol*. 2008;295(3):C576-C587.

122. Newman JH, Wheeler L, Lane KB, et al. Mutation in the gene for bone morphogenetic protein receptor II as a cause of primary pulmonary hypertension in a large kindred. *N Engl J Med*. 2001;345(5):319-324.

123. Nichols WC, Koller DL, Slovis B, et al. Localization of the gene for familial primary pulmonary hypertension to chromosome 2q31-32. *Nat Genet*. 1997;15(3):277-280.

124. Deng Z, Morse JH, Slager SL, et al. Familial primary pulmonary hypertension (gene PPH1) is caused by mutations in the bone morphogenetic protein receptor-II gene. *Am J Hum Genet*. 2000;67(3):737-744.

125. Morse JH, Jones AC, Barst RJ, Hodge SE, Wilhelmsen KC, Nygaard TG. Mapping of familial primary pulmonary hypertension locus (PPH1) to chromosome 2q31-q32. *Circulation*. 1997;95(12):2603-2606.

126. Atkinson C, Stewart S, Upton PD, et al. Primary pulmonary hypertension is associated with reduced pulmonary vascular expression of type II bone morphogenetic protein receptor. *Circulation*. 2002;105(14):1672-1678.

127. West J, Austin E, Fessel JP, Loyd J, Hamid R. Rescuing the BMPR2 signaling axis in pulmonary arterial hypertension. *Drug Discov Today*. 2014;19(8):1241-1245.

128. Thomson JR, Machado RD, Pauciulo MW, et al. Sporadic primary pulmonary hypertension is associated with germline mutations of the gene encoding BMPR-II, a receptor member of the TGF-beta family. *J Med Genet*. 2000;37(10):741-745.

129. Lane KB, Machado RD, Pauciulo MW, et al. Heterozygous germline mutations in BMPR2, encoding a TGF-beta receptor, cause familial primary pulmonary hypertension. *Nat Genet*. 2000;26(1):81-84.

130. Harrison RE, Flanagan JA, Sankelo M, et al. Molecular and functional analysis identifies

ALK-1 as the predominant cause of pulmonary hypertension related to hereditary haemorrhagic telangiectasia. *J Med Genet*. 2003;40(12):865-871.

131. El-Bizri N, Guignabert C, Wang L, et al. SM22alpha-targeted deletion of bone morphogenetic protein receptor 1A in mice impairs cardiac and vascular development, and influences organogenesis. *Development*. 2008;135(17):2981-2991.

132. Vanderpool RR, El-Bizri N, Rabinovitch M, Chesler NC. Patchy deletion of Bmpr1a potentiates proximal pulmonary artery remodeling in mice exposed to chronic hypoxia. *Biomech Model Mechanobiol*. 2013;12(1):33-42.

133. Long L, Crosby A, Yang X, et al. Altered bone morphogenetic protein and transforming growth factor-beta signaling in rat models of pulmonary hypertension: potential for activin receptor-like kinase-5 inhibition in prevention and progression of disease. *Circulation*. 2009;119(4):566-576.

134. Roy S, Samanta K, Chakraborti T, Chowdhury A, Chakraborti S. Role of TGF-β1 and TNF-α in IL-1β mediated activation of proMMP-9 in pulmonary artery smooth muscle cells: Involvement of an aprotinin sensitive protease. *Arch Biochem Biophys*. 2011;513(1):61-69.

135. Roca H, Varsos ZS, Sud S, Craig MJ, Ying C, Pienta KJ. CCL2 and interleukin-6 promote survival of human CD11b+ peripheral blood mononuclear cells and induce M2-type macrophage polarization. *J Biol Chem*. 2009;284(49):34342-34354.

136. Vergadi E, Chang MS, Lee C, et al. Early macrophage recruitment and alternative activation are critical for the later development of hypoxia-induced pulmonary hypertension. *Circulation*. 2011;123(18):1986-1995.

137. Steiner MK, Syrkina OL, Kolliputi N, Mark EJ, Hales CA, Waxman AB. Interleukin-6 overexpression induces pulmonary hypertension. *Circ Res*. 2009;104(2):236-244.

138. Hagen M, Fagan K, Steudel W, et al. Interaction of interleukin-6 and the BMP pathway in pulmonary smooth muscle. *Am J Physiol Lung Cell Mol Physiol*. 2007;292(6):L1473-L1479.

139. Paulin R, Meloche J, Bonnet S. STAT3 signaling in pulmonary arterial hypertension. *JAK-STAT*. 2012;1(4):223-233.

140. Channick RN, Sitbon O, Barst RJ, Manes A, Rubin LJ. Endothelin receptor antagonists in pulmonary arterial hypertension. *J Am Coll Cardiol*. 2004;43(12 Suppl S):62S-67S.

141. Shaw L, Ahmed S, Austin C, Taggart MJ. Inhibitors of actin filament polymerisation attenuate force but not global intracellular calcium in isolated pressurised resistance arteries. *J Vasc Res*. 2003;40(1):1-10.

142. Cipolla MJ, Gokina NI, Osol G. Pressure-induced actin polymerization in vascular smooth muscle as a mechanism underlying myogenic behavior. *FASEB J*. 2002;16(1):72-76.

143. Staiculescu MC, Galiñanes EL, Zhao G, et al. Prolonged vasoconstriction of resistance arteries involves vascular smooth muscle actin polymerization leading to inward remodelling. *Cardiovasc Res*. 2013;98(3):428-436.

144. Gamell C, Osses N, Bartrons R, et al. BMP2 induction of actin cytoskeleton

reorganization and cell migration requires PI3-kinase and Cdc42 activity. *J Cell Sci*. 2008;121(Pt 23):3960-3970.

145. Johnson JA, Hemnes AR, Perrien DS, et al. Cytoskeletal defects in Bmpr2-associated pulmonary arterial hypertension. *Am J Physiol Lung Cell Mol Physiol*. 2012;302(5):L474-L484.

146. Foletta VC, Lim MA, Soosairajah J, et al. Direct signaling by the BMP type II receptor via the cytoskeletal regulator LIMK1. *J Cell Biol*. 2003;162(6):1089-1098.

147. Tang DD, Gunst SJ. The small GTPase Cdc42 regulates actin polymerization and tension development during contractile stimulation of smooth muscle. *J Biol Chem*. 2004;279(50):51722-51728.

148. Li F-H, Xia W, Li A-W, Zhao C-F, Sun R-P. Inhibition of rho kinase attenuates high flow induced pulmonary hypertension in rats. *Chin Med J (Engl)*. 2007;120(1):22-29.

149. Abe K, Shimokawa H, Morikawa K, et al. Long-term treatment with a Rho-kinase inhibitor improves monocrotaline-induced fatal pulmonary hypertension in rats. *Circ Res*. 2004;94(3):385-393.

150. Abe K, Tawara S, Oi K, et al. Long-term inhibition of Rho-kinase ameliorates hypoxia-induced pulmonary hypertension in mice. *J Cardiovasc Pharmacol*. 2006;48(6):280-285.

151. Yasuda T, Tada Y, Tanabe N, Tatsumi K, West J. Rho-kinase inhibition alleviates pulmonary hypertension in transgenic mice expressing a dominant-negative type II bone morphogenetic protein receptor gene. *Am J Physiol Lung Cell Mol Physiol*. 2011;301(5):L667-L674.

152. Ohashi K, Nagata K, Maekawa M, Ishizaki T, Narumiya S, Mizuno K. Rho-associated kinase ROCK activates LIM-kinase 1 by phosphorylation at threonine 508 within the activation loop. *J Biol Chem*. 2000;275(5):3577-3582.

153. Sumi T, Matsumoto K, Shibuya A, Nakamura T. Activation of LIM kinases by myotonic dystrophy kinase-related Cdc42-binding kinase alpha. *J Biol Chem*. 2001;276(25):23092-23096.

154. Edwards DC, Sanders LC, Bokoch GM, Gill GN. Activation of LIM-kinase by Pak1 couples Rac/Cdc42 GTPase signalling to actin cytoskeletal dynamics. *Nat Cell Biol*. 1999;1(5):253-259.

155. Larkin EK, Newman JH, Austin ED, et al. Longitudinal analysis casts doubt on the presence of genetic anticipation in heritable pulmonary arterial hypertension. *Am J Respir Crit Care Med*. 2012;186(9):892-6.

156. Fantozzi I, Platoshyn O, Wong AH, et al. Bone morphogenetic protein-2 upregulates expression and function of voltage-gated K+ channels in human pulmonary artery smooth muscle cells. *Am J Physiol Lung Cell Mol Physiol*. 2006;291(5):L993-1004.

157. Song Y, Jones JE, Beppu H, Keaney JF, Loscalzo J, Zhang Y-Y. Increased susceptibility to pulmonary hypertension in heterozygous BMPR2-mutant mice. *Circulation*. 2005;112(4):553-562.

158. Lawrie A, Spiekerkoetter E, Martinez EC, et al. Interdependent serotonin transporter and

receptor pathways regulate S100A4/Mts1, a gene associated with pulmonary vascular disease. *Circ Res*. 2005;97(3):227-235.

159. Greenway S, van Suylen RJ, Du Marchie Sarvaas G, et al. S100A4/Mts1 produces murine pulmonary artery changes resembling plexogenic arteriopathy and is increased in human plexogenic arteriopathy. *Am J Pathol*. 2004;164(1):253-262.

160. Dees C, Akhmetshina A, Zerr P, et al. Platelet-derived serotonin links vascular disease and tissue fibrosis. *J Exp Med*. 2011;208(5):961-972.

161. Eddahibi S, Guignabert C, Barlier-Mur A-M, et al. Cross talk between endothelial and smooth muscle cells in pulmonary hypertension: critical role for serotonin-induced smooth muscle hyperplasia. *Circulation*. 2006;113(15):1857-64.

162. Guilluy C, Eddahibi S, Agard C, et al. RhoA and Rho kinase activation in human pulmonary hypertension: role of 5-HT signaling. *Am J Respir Crit Care Med*. 2009;179(12):1151-8.

163. Penumatsa KC, Fanburg BL. Transglutaminase 2-mediated serotonylation in pulmonary hypertension. *Am J Physiol Lung Cell Mol Physiol*. 2014;306(4):L309-L315.

164. Wei L, Warburton RR, Preston IR, et al. Serotonylated fibronectin is elevated in pulmonary hypertension. *Am J Physiol Lung Cell Mol Physiol*. 2012;302(12):L1273-L1279.

165. Santhanam L, Tuday EC, Webb AK, et al. Decreased S-nitrosylation of tissue transglutaminase contributes to age-related increases in vascular stiffness. *Circ Res*. 2010;107(1):117-125.

166. Jung SM, Jandu S, Steppan J, et al. Increased tissue transglutaminase activity contributes to central vascular stiffness in eNOS knockout mice. *Am J Physiol Heart Circ Physiol*. 2013;305(6):H803-H810.

167. Spiekerkoetter E, Alvira CM, Kim Y-M, et al. Reactivation of gammaHV68 induces neointimal lesions in pulmonary arteries of S100A4/Mts1-overexpressing mice in association with degradation of elastin. *Am J Physiol Lung Cell Mol Physiol*. 2008;294(2):L276-L289.

168. Kim Y-M, Haghighat L, Spiekerkoetter E, et al. Neutrophil elastase is produced by pulmonary artery smooth muscle cells and is linked to neointimal lesions. *Am J Pathol*. 2011;179(3):1560-1572.

169. Long L, MacLean MR, Jeffery TK, et al. Serotonin increases susceptibility to pulmonary hypertension in BMPR2-deficient mice. *Circ Res*. 2006;98(6):818-827.

170. Liu Y, Ren W, Warburton R, Toksoz D, Fanburg BL. Serotonin induces Rho/ROCK-dependent activation of Smads 1/5/8 in pulmonary artery smooth muscle cells. *FASEB J*. 2009;23(7):2299-306.

171. Rothman RB, Baumann MH, Savage JE, et al. Evidence for possible involvement of 5-HT(2B) receptors in the cardiac valvulopathy associated with fenfluramine and other serotonergic medications. *Circulation*. 2000;102(23):2836-2841.

172. Porvasnik SL, Germain S, Embury J, et al. PRX-08066, a novel 5-hydroxytryptamine

receptor 2B antagonist, reduces monocrotaline-induced pulmonary arterial hypertension and right ventricular hypertrophy in rats. *J Pharmacol Exp Ther*. 2010;334(2):364-372.

173. Launay J-M, Hervé P, Peoc'h K, et al. Function of the serotonin 5-hydroxytryptamine 2B receptor in pulmonary hypertension. *Nat Med*. 2002;8(10):1129-1135.

174. Bonhaus DW, Flippin LA, Greenhouse RJ, et al. RS-127445: a selective, high affinity, orally bioavailable 5-HT2B receptor antagonist. *Br J Pharmacol*. 1999;127(5):1075-1082.

175. MacLean MR, Deuchar GA, Hicks MN, et al. Overexpression of the 5-hydroxytryptamine transporter gene: effect on pulmonary hemodynamics and hypoxia-induced pulmonary hypertension. *Circulation*. 2004;109(17):2150-2155.

176. Zopf DA, das Neves LAA, Nikula KJ, Huang J, Senese PB, Gralinski MR. C-122, a novel antagonist of serotonin receptor 5-HT2B, prevents monocrotaline-induced pulmonary arterial hypertension in rats. *Eur J Pharmacol*. 2011;670(1):195-203.

177. Bakhshi FR, Mao M, Shajahan AN, et al. Nitrosation-dependent caveolin 1 phosphorylation, ubiquitination, and degradation and its association with idiopathic pulmonary arterial hypertension. *Pulm Circ*. 2013;3(4):816-830.

178. Weigand L, Sylvester JT, Shimoda LA. Mechanisms of endothelin-1-induced contraction in pulmonary arteries from chronically hypoxic rats. *Am J Physiol Lung Cell Mol Physiol*. 2006;290(2):L284-L290.

179. Karoor V, Oka M, Walchak SJ, Hersh LB, Miller YE, Dempsey EC. Neprilysin regulates pulmonary artery smooth muscle cell phenotype through a platelet-derived growth factor receptor-dependent mechanism. *Hypertension*. 2013;61(4):921-930.

180. Paulin R, Meloche J, Jacob MH, Bisserier M, Courboulin A, Bonnet S. Dehydroepiandrosterone inhibits the Src/STAT3 constitutive activation in pulmonary arterial hypertension. *Am J Physiol Heart Circ Physiol*. 2011;301(5):H1798-H1809.

181. Paulin R, Meloche J, Courboulin A, et al. Targeting cell motility in pulmonary arterial hypertension. *Eur Respir J*. 2014;43(2):531-544.

182. Pullamsetti SS, Berghausen EM, Dabral S, et al. Role of Src tyrosine kinases in experimental pulmonary hypertension. *Arterioscler Thromb Vasc Biol*. 2012;32(6):1354-1365.

183. Ishida T, Ishida M, Suero J, Takahashi M, Berk BC. Agonist-stimulated cytoskeletal reorganization and signal transduction at focal adhesions in vascular smooth muscle cells require c-Src. *J Clin Invest*. 1999;103(6):789-797.

184. Min J, Reznichenko M, Poythress RH, et al. Src modulates contractile vascular smooth muscle function via regulation of focal adhesions. *J Cell Physiol*. 2012;227(11):3585-3592.

185. Godinas L, Guignabert C, Seferian A, et al. Tyrosine kinase inhibitors in pulmonary arterial hypertension: a double-edge sword? *Semin Respir Crit Care Med*. 2013;34(5):714-724.

186. Wong WKP, Knowles JA, Morse JH. Bone morphogenetic protein receptor type II C-terminus interacts with c-Src: implication for a role in pulmonary arterial hypertension. *Am*

*J Respir Cell Mol Biol*. 2005;33(5):438-446.

187. Prewitt AR, Ghose S, Frump AL, et al. Heterozygous Null Bone Morphogenetic Protein Receptor Type 2 Mutations Promote Src-Dependent Caveolar Trafficking Defects and Endothelial Dysfunction in Pulmonary Arterial Hypertension. *J Biol Chem*. 2014.

188. Majka S, Hagen M, Blackwell T, et al. Physiologic and molecular consequences of endothelial Bmpr2 mutation. *Respir Res*. 2011;12(1):84.

189. Nebigil CG, Launay JM, Hickel P, Tournois C, Maroteaux L. 5-hydroxytryptamine 2B receptor regulates cell-cycle progression: cross-talk with tyrosine kinase pathways. *Proc Natl Acad Sci U S A*. 2000;97(6):2591-2596.

190. Hutcheson JD, Ryzhova LM, Setola V, Merryman WD. 5-HT(2B) antagonism arrests non-canonical TGF-β1-induced valvular myofibroblast differentiation. *J Mol Cell Cardiol*. 2012;53(5):707-714.

191. Farha S, Asosingh K, Xu W, et al. Hypoxia-inducible factors in human pulmonary arterial hypertension: a link to the intrinsic myeloid abnormalities. *Blood*. 2011;117(13):3485-93.

192. Asosingh K, Farha S, Lichtin A, et al. Pulmonary vascular disease in mice xenografted with human BM progenitors from patients with pulmonary arterial hypertension. *Blood*. 2012;120(6):1218-27.

193. Yan L, Chen X, Talati M, et al. Bone Marrow–derived Cells Contribute to the Pathogenesis of Pulmonary Arterial Hypertension. *Am J Respir Crit Care Med*. 2016;193(8):898-909.

194. Vergadi E, Chang MS, Lee C, et al. Early Macrophage Recruitment and Alternative Activation Are Critical for the Later Development of Hypoxia-Induced Pulmonary Hypertension. *Circulation*. 2011;123(18):1986-1995.

195. Tian W, Jiang X, Tamosiuniene R, et al. Blocking Macrophage Leukotriene B4 Prevents Endothelial Injury and Reverses Pulmonary Hypertension. *Sci Transl Med*. 2013;5(200):200ra117-200ra117.

196. El Kasmi KC, Pugliese SC, Riddle SR, et al. Adventitial Fibroblasts Induce a Distinct Proinflammatory/Profibrotic Macrophage Phenotype in Pulmonary Hypertension. *J Immunol*. 2014;193(2):597-609.

197. Talati M, West J, Zaynagetdinov R, et al. BMP pathway regulation of and by macrophages. Waisman A, ed. *PLoS One*. 2014;9(4):e94119.

198. Tamosiuniene R, Tian W, Dhillon G, et al. Regulatory T Cells Limit Vascular Endothelial Injury and Prevent Pulmonary Hypertension. *Circ Res*. 2011;109(8):867-879.

199. Lanzola E, Farha S, Erzurum SC, Asosingh K. Bone marrow-derived vascular modulatory cells in pulmonary arterial hypertension. *Pulm Circ*. 2013;3(4):781-91.

200. Montani D, Perros F, Gambaryan N, et al. C-kit-positive cells accumulate in remodeled vessels of idiopathic pulmonary arterial hypertension. *Am J Respir Crit Care Med*. 2011;184(1):116-23.

201. Satoh K, Kagaya Y, Nakano M, et al. Important role of endogenous erythropoietin system

in recruitment of endothelial progenitor cells in hypoxia-induced pulmonary hypertension in mice. *Circulation*. 2006;113(11):1442-50.

202. Toshner M, Voswinckel R, Southwood M, et al. Evidence of dysfunction of endothelial progenitors in pulmonary arterial hypertension. *Am J Respir Crit Care Med*. 2009;180(8):780-7.

203. Gambaryan N, Perros F, Montani D, et al. Targeting of c-kit+ haematopoietic progenitor cells prevents hypoxic pulmonary hypertension. *Eur Respir J*. 2011;37(6):1392-1399.

204. Foris V, Kovacs G, Marsh LM, et al. CD133+ cells in pulmonary arterial hypertension. *Eur Respir J*. 2016;48(2):459-469.

205. Takahashi M, Nakamura T, Toba T, Kajiwara N, Kato H, Shimizu Y. Transplantation of Endothelial Progenitor Cells into the Lung to Alleviate Pulmonary Hypertension in Dogs. *Tissue Eng*. 2004;10(5-6):771-779.

206. Luan Y, Zhang Z-H, Wei D-E, Lu Y, Wang Y-B. Effects of autologous bone marrow mononuclear cells implantation in canine model of pulmonary hypertension. *Circ J*. 2012;76(4):977-85.

207. Raoul W, Wagner-Ballon O, Saber G, et al. Effects of bone marrow-derived cells on monocrotaline- and hypoxia-induced pulmonary hypertension in mice. *Respir Res*. 2007;8(1):8.

208. Mirsky R, Jahn S, Koskenvuo JW, et al. Treatment of pulmonary arterial hypertension with circulating angiogenic cells. *AJP Lung Cell Mol Physiol*. 2011;301(1):L12-L19.

209. Zhao YD, Courtman DW, Deng Y, Kugathasan L, Zhang Q, Stewart DJ. Rescue of monocrotaline-induced pulmonary arterial hypertension using bone marrow-derived endothelial-like progenitor cells: efficacy of combined cell and eNOS gene therapy in established disease. *Circ Res*. 2005;96(4):442-50.

210. Wang X-X, Zhang F-R, Shang Y-P, et al. Transplantation of Autologous Endothelial Progenitor Cells May Be Beneficial in Patients With Idiopathic Pulmonary Arterial Hypertension. *J Am Coll Cardiol*. 2007;49(14):1566-1571.

211. Maclean MR, Dempsie Y. The serotonin hypothesis of pulmonary hypertension revisited. *Adv Exp Med Biol*. 2010;661:309-322.

212. Abenhaim L, Moride Y, Brenot F, et al. Appetite-suppressant drugs and the risk of primary pulmonary hypertension. International Primary Pulmonary Hypertension Study Group. *N Engl J Med*. 1996;335(9):609-16.

213. Gurtner HP. Aminorex and pulmonary hypertension. A review. *Cor Vasa*. 1985;27(2-3):160-71.

214. Eddahibi S, Adnot S, Frisdal E, Levame M, Hamon M, Raffestin B. Dexfenfluramine-associated changes in 5-hydroxytryptamine transporter expression and development of hypoxic pulmonary hypertension in rats. *J Pharmacol Exp Ther*. 2001;297(1):148-154.

215. Eddahibi S, Hanoun N, Lanfumey L, et al. Attenuated hypoxic pulmonary hypertension in mice lacking the 5-hydroxytryptamine transporter gene. *J Clin Invest*. 2000;105(11):1555-1562.

216. Keegan A, Morecroft I, Smillie D, Hicks MN, MacLean MR. Contribution of the 5-HT(1B) receptor to hypoxia-induced pulmonary hypertension: converging evidence using 5-HT(1B)-receptor knockout mice and the 5-HT(1B/1D)-receptor antagonist GR127935. *Circ Res*. 2001;89(12):1231-9.

217. West J, Harral J, Lane K, et al. Mice expressing BMPR2R899X transgene in smooth muscle develop pulmonary vascular lesions. *Am J Physiol Lung Cell Mol Physiol*. 2008;295(5):L744-L755.

218. Austin ED, Loyd JE. The Genetics of Pulmonary Arterial Hypertension. *Circ Res*. 2014;115(1):189-202.

219. Hutcheson JD, Setola V, Roth BL, Merryman WD. Serotonin receptors and heart valve disease--it was meant 2B. *Pharmacol Ther*. 2011;132(2):146-157.

220. Ebrahimkhani MR, Oakley F, Murphy LB, et al. Stimulating healthy tissue regeneration by targeting the 5-HT2B receptor in chronic liver disease. *Nat Med*. 2011;17(12):1668-1673.

221. Chen W-C, Park S-H, Hoffman C, et al. Right ventricular systolic pressure measurements in combination with harvest of lung and immune tissue samples in mice. *J Vis Exp*. 2013;(71):e50023.

222. Lane KL, Talati M, Austin E, et al. Oxidative injury is a common consequence of BMPR2 mutations. *Pulm Circ*. 2011;1(1):72-83.

223. Wang J, Duncan D, Shi Z, Zhang B. WEB-based GEne SeT AnaLysis Toolkit (WebGestalt): update 2013. *Nucleic Acids Res*. 2013;41(Web Server issue):W77-83.

224. Sewell-Loftin M-K, Brown CB, Baldwin HS, Merryman WD. A novel technique for quantifying mouse heart valve leaflet stiffness with atomic force microscopy. *J Heart Valve Dis*. 2012;21(4):513-20.

225. Sewell-Loftin MK, DeLaughter DM, Peacock JR, et al. Myocardial contraction and hyaluronic acid mechanotransduction in epithelial-to-mesenchymal transformation of endocardial cells. *Biomaterials*. 2014;35(9):2809-2815.

226. Parekh A, Ruppender NS, Branch KM, et al. Sensing and Modulation of Invadopodia across a Wide Range of Rigidities. *Biophys J*. 2011;100(3):573-582.

227. Abe M, Harpel JG, Metz CN, Nunes I, Loskutoff DJ, Rifkin DB. An assay for transforming growth factor-beta using cells transfected with a plasminogen activator inhibitor-1 promoter-luciferase construct. *Anal Biochem*. 1994;216(2):276-84.

228. Merryman WD, Liao J, Parekh A, Candiello JE, Lin H, Sacks MS. Differences in tissue-remodeling potential of aortic and pulmonary heart valve interstitial cells. *Tissue Eng*. 2007;13(9):2281-2289.

229. Hemnes AR, Brittain EL, Trammell AW, et al. Evidence for right ventricular lipotoxicity in heritable pulmonary arterial hypertension. *Am J Respir Crit Care Med*. 2014;189(3):325-34.

230. Talati M, Mutlak H, Lane K, et al. NF-κB Activation Exacerbates, but Is not Required for Murine Bmpr2-Related Pulmonary Hypertension. *Diseases*. 2014;2(2):148-167.

231. West J, Fagan K, Steudel W, et al. Pulmonary Hypertension in Transgenic Mice Expressing a Dominant-Negative BMPRII Gene in Smooth Muscle. *Circ Res*. 2004;94(8):1109-1114.

232. Crona D, Harral J, Adnot S, Eddahibi S, West J. Gene expression in lungs of mice lacking the 5-hydroxytryptamine transporter gene. *BMC Pulm Med*. 2009;9(1):19.

233. Yao Q, Liu B-Q, Li H, et al. C-terminal Src kinase (Csk)-mediated phosphorylation of eukaryotic elongation factor 2 (eEF2) promotes proteolytic cleavage and nuclear translocation of eEF2. *J Biol Chem*. 2014;289(18):12666-78.

234. Machiyama H, Hirata H, Loh XK, et al. Displacement of p130Cas from focal adhesions links actomyosin contraction to cell migration. *J Cell Sci*. 2014;127(Pt 16):3440-50.

235. Hu J, Xu Q, McTiernan C, Lai Y-C, Osei-Hwedieh D, Gladwin M. Novel Targets of Drug Treatment for Pulmonary Hypertension. *Am J Cardiovasc Drugs*. 2015;15(4):225-34.

236. Tada Y, Majka S, Carr M, et al. Molecular effects of loss of BMPR2 signaling in smooth muscle in a transgenic mouse model of PAH. *Am J Physiol Lung Cell Mol Physiol*. 2007;292(6):L1556-63.

237. De Raaf MA, Kroeze Y, Middelman A, et al. Serotonin transporter is not required for the development of severe pulmonary hypertension in the Sugen hypoxia rat model. *Am J Physiol - Lung Cell Mol Physiol*. 2015;309(10):ajplung.00127.2015.

238. Stacher E, Graham BB, Hunt JM, et al. Modern Age Pathology of Pulmonary Arterial Hypertension. *Am J Respir Crit Care Med*. 2012;186(3):261-272.

239. Launay J-M, Hervé P, Callebert J, et al. Serotonin 5-HT2B receptors are required for bone-marrow contribution to pulmonary arterial hypertension. *Blood*. 2012;119(7):1772-1780.

240. Rose JA, Erzurum S, Asosingh K. Biology and flow cytometry of proangiogenic hematopoietic progenitors cells. *Cytometry A*. 2015;87(1):5-19.

241. Wei L, Zhang B, Cao W, Xing H, Yu X, Zhu D. Inhibition of CXCL12/CXCR4 suppresses pulmonary arterial smooth muscle cell proliferation and cell cycle progression via PI3K/Akt pathway under hypoxia. *J Recept Signal Transduct Res*. 2014:1-11.

242. Young KC, Torres E, Hatzistergos KE, Hehre D, Suguihara C, Hare JM. Inhibition of the SDF-1/CXCR4 Axis Attenuates Neonatal Hypoxia-Induced Pulmonary Hypertension. *Circ Res*. 2009;104(11):1293-1301.

243. Marsboom G, Pokreisz P, Gheysens O, et al. Sustained endothelial progenitor cell dysfunction after chronic hypoxia-induced pulmonary hypertension. *Stem Cells*. 2008;26(4):1017-26.

244. Tang Y, Harrington A, Yang X, Friesel RE, Liaw L. The contribution of the Tie2+ lineage to primitive and definitive hematopoietic cells. *Genesis*. 2010;48(9):563-7.

245. Nicolls MR, Mizuno S, Taraseviciene-Stewart L, et al. New models of pulmonary hypertension based on VEGF receptor blockade-induced endothelial cell apoptosis. *Pulm Circ*. 2012;2(4):434-442.

246. West JD, Carrier EJ, Bloodworth NC, et al. Serotonin 2B Receptor Antagonism Prevents Heritable Pulmonary Arterial Hypertension. *PLoS One*. 2016;11(2):e0148657.

247. Law CW, Alhamdoosh M, Su S, Smyth GK, Ritchie ME. RNA-seq analysis is easy as 1-2-3 with limma, Glimma and edgeR. *F1000Research*. 2016;5:1408.

248. Shannon P, Markiel A, Ozier O, et al. Cytoscape: a software environment for integrated models of biomolecular interaction networks. *Genome Res*. 2003;13(11):2498-504.

249. Maere S, Heymans K, Kuiper M. BiNGO: a Cytoscape plugin to assess overrepresentation of Gene Ontology categories in Biological Networks. *Bioinformatics*. 2005;21(16):3448-3449.

250. Gene Ontology Consortium: going forward. *Nucleic Acids Res*. 2015;43(D1):D1049-D1056.

251. Jian X, Boerwinkle E, Liu X, et al. In silico prediction of splice-altering single nucleotide variants in the human genome. *Nucleic Acids Res*. 2014;42(22):13534-13544.

252. Göthert JR, Gustin SE, van Eekelen JAM, et al. Genetically tagging endothelial cells in vivo: bone marrow-derived cells do not contribute to tumor endothelium. *Blood*. 2004;104(6):1769-77.

253. Kim H, Cho H-J, Kim S-W, et al. CD31+ cells represent highly angiogenic and vasculogenic cells in bone marrow: novel role of nonendothelial CD31+ cells in neovascularization and their therapeutic effects on ischemic vascular disease. *Circ Res*. 2010;107(5):602-14.

254. Majka SM, Skokan M, Wheeler L, et al. Evidence for cell fusion is absent in vascular lesions associated with pulmonary arterial hypertension. *AJP Lung Cell Mol Physiol*. 2008;295(6):L1028-L1039.

255. Smadja DM, Mauge L, Sanchez O, et al. Distinct patterns of circulating endothelial cells in pulmonary hypertension. *Eur Respir J*. 2010;36(6):1284-1293.

256. JunHui Z, XingXiang W, GuoSheng F, YunPeng S, FuRong Z, JunZhu C. Reduced number and activity of circulating endothelial progenitor cells in patients with idiopathic pulmonary arterial hypertension. *Respir Med*. 2008;102(7):1073-1079.

257. Diller G-P, van Eijl S, Okonko DO, et al. Circulating Endothelial Progenitor Cells in Patients With Eisenmenger Syndrome and Idiopathic Pulmonary Arterial Hypertension. *Circulation*. 2008;117(23):3020-3030.

258. Smadja DM, Gaussem P, Mauge L, et al. Circulating Endothelial Cells: A New Candidate Biomarker of Irreversible Pulmonary Hypertension Secondary to Congenital Heart Disease. *Circulation*. 2009;119(3):374-381.

259. Burns JM, Summers BC, Wang Y, et al. A novel chemokine receptor for SDF-1 and I-TAC involved in cell survival, cell adhesion, and tumor development. *J Exp Med*. 2006;203(9).

260. Wara AK, Croce K, Foo S, et al. Bone marrow-derived CMPs and GMPs represent highly functional proangiogenic cells: implications for ischemic cardiovascular disease. *Blood*. 2011;118(24):6461-6464.

261. Dudley AC, Udagawa T, Melero-Martin JM, et al. Bone marrow is a reservoir for proangiogenic myelomonocytic cells but not endothelial cells in spontaneous tumors. *Blood*. 2010;116(17):3367-71.

262. Asosingh K, Aldred MA, Vasanji A, et al. Circulating Angiogenic Precursors in Idiopathic Pulmonary Arterial Hypertension. *Am J Pathol*. 2008;172(3):615-627.

263. Ullmer C, Schmuck K, Kalkman HO, Lübbert H. Expression of serotonin receptor mRNAs in blood vessels. *FEBS Lett*. 1995;370(3):215-21.

264. Bantscheff M, Eberhard D, Abraham Y, et al. Quantitative chemical proteomics reveals mechanisms of action of clinical ABL kinase inhibitors. *Nat Biotechnol*. 2007;25(9):1035-1044.

265. Guignabert C, Phan C, Seferian A, et al. Dasatinib induces lung vascular toxicity and predisposes to pulmonary hypertension. *J Clin Invest*. 2016;126(9):3207-18.

266. Hoeper MM, Barst RJ, Bourge RC, et al. Imatinib mesylate as add-on therapy for pulmonary arterial hypertension: results of the randomized IMPRES study. *Circulation*. 2013;127(10):1128-1138.

267. Diaz SL, Doly S, Narboux-Nême N, et al. 5-HT2B receptors are required for serotonin-selective antidepressant actions. *Mol Psychiatry*. 2012;17(2):154-163.

# APPENDIX

| | Values Normalized to Controls (Differences are Log(2), so +1 = 2x change) | | | | | | | | | | | |
|---|---|---|---|---|---|---|---|---|---|---|---|---|
| Gene Symbol | Control | | | Control+SB | | | R899X | | | R899X+SB | | |
| Aagab | 1 | ± | 0.03 | -0.31 | ± | 0.17 | -0.49 | ± | 0.04 | -0.14 | ± | 0.03 |
| Acot2 | 1 | ± | 0.12 | -0.38 | ± | 0.02 | -0.61 | ± | 0.06 | -0.28 | ± | 0.02 |
| Actg1 | 1 | ± | 0.05 | 0.92 | ± | 0.19 | 1.20 | ± | 0.10 | 0.78 | ± | 0.31 |
| Aldh2 | 1 | ± | 0.11 | 1.07 | ± | 0.14 | 1.45 | ± | 0.22 | 0.91 | ± | 0.06 |
| Apln | 1 | ± | 0.05 | -0.45 | ± | 0.07 | -0.90 | ± | 0.01 | -0.50 | ± | 0.11 |
| Arsb | 1 | ± | 0.11 | 0.45 | ± | 0.03 | 1.00 | ± | 0.17 | 0.33 | ± | 0.05 |
| Atp5l | 1 | ± | 0.11 | 0.36 | ± | 0.04 | 0.22 | ± | 0.06 | -0.16 | ± | 0.02 |
| BC061237 | 1 | ± | 0.07 | 0.35 | ± | 0.06 | 0.42 | ± | 0.08 | 0.03 | ± | 0.18 |
| Bgn | 1 | ± | 0.06 | 0.74 | ± | 0.05 | 1.07 | ± | 0.03 | 0.71 | ± | 0.03 |
| Cd24a | 1 | ± | 0.24 | 0.63 | ± | 0.03 | 1.08 | ± | 0.09 | 0.42 | ± | 0.19 |
| Cldn3 | 1 | ± | 0.03 | -0.46 | ± | 0.01 | -0.65 | ± | 0.09 | -0.34 | ± | 0.10 |
| Col1a2 | 1 | ± | 0.05 | 0.63 | ± | 0.07 | 0.97 | ± | 0.13 | 0.31 | ± | 0.34 |
| Col6a1 | 1 | ± | 0.13 | 0.60 | ± | 0.07 | 1.01 | ± | 0.00 | 0.68 | ± | 0.09 |
| Copz1 | 1 | ± | 0.01 | -0.39 | ± | 0.13 | -0.64 | ± | 0.08 | -0.33 | ± | 0.06 |
| Cryab | 1 | ± | 0.04 | 0.72 | ± | 0.03 | 1.11 | ± | 0.02 | 0.66 | ± | 0.14 |
| Csrp1 | 1 | ± | 0.12 | -0.32 | ± | 0.01 | -0.52 | ± | 0.01 | -0.12 | ± | 0.10 |
| Cyp2s1 | 1 | ± | 0.02 | -0.34 | ± | 0.07 | -0.40 | ± | 0.02 | -0.06 | ± | 0.10 |
| Ect2 | 1 | ± | 0.30 | -0.31 | ± | 0.35 | -0.64 | ± | 0.02 | -0.21 | ± | 0.05 |
| Ehd1 | 1 | ± | 0.08 | 0.95 | ± | 0.05 | 1.51 | ± | 0.08 | 0.74 | ± | 0.13 |
| Fam107a | 1 | ± | 0.02 | 0.55 | ± | 0.02 | 0.95 | ± | 0.21 | 0.28 | ± | 0.41 |
| Ftl1 | 1 | ± | 0.01 | 1.04 | ± | 0.03 | 1.46 | ± | 0.04 | 0.86 | ± | 0.43 |
| Gabarap | 1 | ± | 0.11 | 0.71 | ± | 0.10 | 0.96 | ± | 0.11 | 0.61 | ± | 0.12 |
| Glul | 1 | ± | 0.05 | 0.33 | ± | 0.05 | 0.84 | ± | 0.00 | 0.43 | ± | 0.23 |
| Gm10021 | 1 | ± | 0.10 | 0.36 | ± | 0.07 | 0.53 | ± | 0.10 | 0.13 | ± | 0.08 |
| Gmcl1l | 1 | ± | 0.15 | 0.33 | ± | 0.02 | 0.37 | ± | 0.00 | -0.23 | ± | 0.14 |
| H3f3a | 1 | ± | 0.03 | 0.48 | ± | 0.05 | 0.67 | ± | 0.07 | 0.25 | ± | 0.19 |
| H3f3b | 1 | ± | 0.01 | 0.34 | ± | 0.02 | 0.62 | ± | 0.04 | 0.10 | ± | 0.20 |
| Hbb-b1 | 1 | ± | 0.26 | 1.53 | ± | 0.19 | 1.99 | ± | 0.22 | 1.59 | ± | 0.29 |
| Hbb-b1 | 1 | ± | 0.13 | 0.48 | ± | 0.24 | 1.07 | ± | 0.14 | 0.44 | ± | 0.54 |
| Hnrnph2 | 1 | ± | 0.06 | 0.41 | ± | 0.02 | 0.50 | ± | 0.01 | 0.15 | ± | 0.18 |
| Hnrnpk | 1 | ± | 0.17 | 1.05 | ± | 0.10 | 1.40 | ± | 0.18 | 1.05 | ± | 0.20 |
| Hsd3b7 | 1 | ± | 0.11 | -0.32 | ± | 0.06 | -0.48 | ± | 0.08 | -0.16 | ± | 0.17 |
| Ifna5 | 1 | ± | 0.09 | -0.38 | ± | 0.03 | -0.22 | ± | 0.04 | 0.37 | ± | 0.11 |
| Kpnb1 | 1 | ± | 0.09 | 0.35 | ± | 0.00 | 0.50 | ± | 0.05 | 0.16 | ± | 0.18 |
| Maf | 1 | ± | 0.13 | 0.94 | ± | 0.03 | 1.09 | ± | 0.08 | 0.57 | ± | 0.29 |
| Mbnl2 | 1 | ± | 0.02 | 0.58 | ± | 0.08 | 0.83 | ± | 0.06 | 0.39 | ± | 0.22 |
| Mcl1 | 1 | ± | 0.22 | 0.46 | ± | 0.03 | 0.66 | ± | 0.05 | 0.36 | ± | 0.23 |
| MGC107098 | 1 | ± | 0.17 | 0.50 | ± | 0.11 | 0.46 | ± | 0.02 | -0.11 | ± | 0.07 |
| Mir101c | 1 | ± | 0.10 | 0.59 | ± | 0.02 | 0.86 | ± | 0.02 | 0.43 | ± | 0.07 |
| Mir1938 | 1 | ± | 0.17 | -0.46 | ± | 0.03 | -1.24 | ± | 0.04 | -0.64 | ± | 0.04 |
| Mir28c | 1 | ± | 0.08 | 0.31 | ± | 0.09 | 0.39 | ± | 0.10 | -0.15 | ± | 0.36 |
| Mir3101 | 1 | ± | 0.03 | -0.32 | ± | 0.12 | -1.24 | ± | 0.20 | -0.86 | ± | 0.06 |
| Mir3473d | 1 | ± | 0.00 | 0.42 | ± | 0.02 | 0.86 | ± | 0.10 | 0.48 | ± | 0.14 |
| Mir5133 | 1 | ± | 0.14 | -0.34 | ± | 0.10 | -0.18 | ± | 0.00 | 0.23 | ± | 0.20 |
| Msi2 | 1 | ± | 0.00 | 0.47 | ± | 0.04 | 0.62 | ± | 0.05 | 0.12 | ± | 0.02 |
| Mxra8 | 1 | ± | 0.12 | 0.45 | ± | 0.00 | 0.80 | ± | 0.01 | 0.50 | ± | 0.07 |
| Myl12a | 1 | ± | 0.16 | 1.39 | ± | 0.16 | 1.96 | ± | 0.02 | 1.20 | ± | 0.17 |
| Nagpa | 1 | ± | 0.07 | -0.30 | ± | 0.02 | -0.64 | ± | 0.21 | -0.26 | ± | 0.07 |
| Nceh1 | 1 | ± | 0.05 | 0.61 | ± | 0.07 | 0.85 | ± | 0.16 | 0.46 | ± | 0.10 |

| | Values Normalized to Controls (Differences are Log(2), so +1 = 2x change) | | | | | | | | | | | |
|---|---|---|---|---|---|---|---|---|---|---|---|---|
| Gene Symbol | Control | | | Control+SB | | | R899X | | | R899X+SB | | |
| Oaz1 | 1 | ± | 0.09 | 0.42 | ± | 0.09 | 0.56 | ± | 0.00 | -0.06 | ± | 0.45 |
| Ovca2 | 1 | ± | 0.72 | 0.46 | ± | 0.21 | -0.10 | ± | 0.02 | -0.44 | ± | 0.08 |
| Ppan | 1 | ± | 0.11 | 0.32 | ± | 0.15 | 0.62 | ± | 0.09 | 0.24 | ± | 0.05 |
| Prkaca | 1 | ± | 0.20 | 0.40 | ± | 0.02 | 0.82 | ± | 0.08 | 0.25 | ± | 0.30 |
| Ptma | 1 | ± | 0.01 | -0.43 | ± | 0.11 | -0.72 | ± | 0.18 | -0.39 | ± | 0.14 |
| Rhoa | 1 | ± | 0.05 | 0.81 | ± | 0.06 | 1.28 | ± | 0.07 | 0.82 | ± | 0.10 |
| Rny3 | 1 | ± | 0.04 | 0.77 | ± | 0.06 | 1.53 | ± | 0.07 | 0.50 | ± | 0.38 |
| Rpl3 | 1 | ± | 0.12 | -0.39 | ± | 0.06 | -0.96 | ± | 0.00 | -0.30 | ± | 0.30 |
| Rpl4 | 1 | ± | 0.33 | 0.71 | ± | 0.30 | 1.27 | ± | 0.20 | 0.57 | ± | 0.12 |
| Rpph1 | 1 | ± | 0.24 | 0.36 | ± | 0.07 | 0.77 | ± | 0.39 | 0.10 | ± | 0.01 |
| Rps13 | 1 | ± | 0.18 | 0.58 | ± | 0.03 | 0.83 | ± | 0.07 | 0.36 | ± | 0.30 |
| Rps8 | 1 | ± | 0.05 | 0.31 | ± | 0.03 | 0.62 | ± | 0.11 | 0.00 | ± | 0.24 |
| Scamp2 | 1 | ± | 0.08 | -0.33 | ± | 0.01 | -0.55 | ± | 0.02 | -0.25 | ± | 0.14 |
| Scarna2 | 1 | ± | 0.12 | 0.41 | ± | 0.07 | 0.75 | ± | 0.06 | 0.38 | ± | 0.04 |
| Sec14l4 | 1 | ± | 0.02 | -0.33 | ± | 0.06 | -0.52 | ± | 0.02 | -0.13 | ± | 0.00 |
| Sfrp1 | 1 | ± | 0.11 | -0.40 | ± | 0.04 | -0.80 | ± | 0.12 | -0.33 | ± | 0.21 |
| Sike1 | 1 | ± | 0.16 | -0.52 | ± | 0.08 | -0.99 | ± | 0.12 | -0.45 | ± | 0.06 |
| Slain2 | 1 | ± | 0.18 | 0.72 | ± | 0.04 | 1.12 | ± | 0.01 | 0.60 | ± | 0.17 |
| Slc48a1 | 1 | ± | 0.02 | -0.30 | ± | 0.08 | -0.50 | ± | 0.01 | -0.17 | ± | 0.10 |
| Smok4a | 1 | ± | 0.14 | 0.91 | ± | 0.07 | 1.19 | ± | 0.01 | 0.42 | ± | 0.19 |
| Snord116 | 1 | ± | 0.15 | 0.78 | ± | 0.06 | 0.90 | ± | 0.00 | 0.03 | ± | 0.04 |
| Snord15b | 1 | ± | 0.06 | 0.42 | ± | 0.18 | 1.05 | ± | 0.18 | 0.26 | ± | 0.05 |
| Snord49b | 1 | ± | 0.00 | 0.40 | ± | 0.12 | 0.47 | ± | 0.09 | 0.07 | ± | 0.18 |
| Snord57 | 1 | ± | 0.05 | 0.35 | ± | 0.03 | 0.91 | ± | 0.10 | 0.29 | ± | 0.26 |
| Speer7-ps1 | 1 | ± | 0.09 | 0.34 | ± | 0.09 | 0.39 | ± | 0.04 | -0.10 | ± | 0.31 |
| Taf1d | 1 | ± | 0.07 | 0.45 | ± | 0.01 | 0.54 | ± | 0.10 | 0.17 | ± | 0.13 |
| Taf1d | 1 | ± | 0.07 | 0.50 | ± | 0.01 | 0.52 | ± | 0.08 | 0.13 | ± | 0.16 |
| Taf1d | 1 | ± | 0.07 | 0.45 | ± | 0.01 | 0.54 | ± | 0.10 | 0.17 | ± | 0.13 |
| Tlcd1 | 1 | ± | 0.05 | 0.36 | ± | 0.12 | 0.66 | ± | 0.18 | 0.23 | ± | 0.29 |
| Tmem202 | 1 | ± | 0.04 | 0.35 | ± | 0.02 | 0.92 | ± | 0.23 | 0.26 | ± | 0.00 |
| Trp53i11 | 1 | ± | 0.04 | -0.37 | ± | 0.08 | -0.50 | ± | 0.07 | -0.04 | ± | 0.29 |
| Tuba1b | 1 | ± | 0.31 | 1.23 | ± | 0.19 | 1.57 | ± | 0.19 | 1.01 | ± | 0.08 |
| Ube2d2a | 1 | ± | 0.00 | 0.51 | ± | 0.16 | 0.55 | ± | 0.26 | 0.11 | ± | 0.17 |
| Ube2l3 | 1 | ± | 0.09 | 0.42 | ± | 0.02 | 0.71 | ± | 0.01 | 0.37 | ± | 0.02 |
| Vmn1r127 | 1 | ± | 0.12 | 0.62 | ± | 0.08 | 0.86 | ± | 0.21 | 0.29 | ± | 0.23 |
| Vmn1r2 | 1 | ± | 0.43 | 0.65 | ± | 0.27 | 0.94 | ± | 0.01 | 0.54 | ± | 0.11 |
| Vmp1 | 1 | ± | 0.22 | 0.88 | ± | 0.12 | 0.90 | ± | 0.00 | 0.37 | ± | 0.16 |
| Wisp2 | 1 | ± | 0.02 | -0.40 | ± | 0.05 | -0.50 | ± | 0.09 | -0.20 | ± | 0.12 |
| Ywhaz | 1 | ± | 0.14 | 0.73 | ± | 0.00 | 1.00 | ± | 0.03 | 0.55 | ± | 0.15 |
| Zfp187 | 1 | ± | 0.16 | 0.85 | ± | 0.25 | 1.05 | ± | 0.07 | 0.54 | ± | 0.12 |
| Zfp36l1 | 1 | ± | 0.12 | 0.94 | ± | 0.05 | 1.29 | ± | 0.05 | 0.68 | ± | 0.35 |
| Zfp526 | 1 | ± | 0.17 | 0.48 | ± | 0.05 | 0.66 | ± | 0.19 | 0.30 | ± | 0.00 |
| Zfp760 | 1 | ± | 0.14 | -0.35 | ± | 0.17 | -0.80 | ± | 0.13 | -0.33 | ± | 0.02 |

**Table A.1: List of genes represented in the heatmap of Figure 3.7 B**

| Gene (MGI) | Gene Description | $log_2$(FC) | p-value |
|---|---|---|---|
| 1810014B01Rik | RIKEN cDNA 1810014B01 gene [Source:MGI Symbol;Acc:MGI:1913513] | -0.36 | 7.4E-03 |
| 1810022K09Rik | RIKEN cDNA 1810022K09 gene [Source:MGI Symbol;Acc:MGI:1916376] | 0.46 | 2.5E-03 |
| 2810001G20Rik | RIKEN cDNA 2810001G20 gene [Source:MGI Symbol;Acc:MGI:1913706] | 0.35 | 9.8E-03 |
| 4833407H14Rik | RIKEN cDNA 4833407H14 gene [Source:MGI Symbol;Acc:MGI:1921149] | 0.47 | 1.9E-03 |
| 5930430L01Rik | RIKEN cDNA 5930430L01 gene [Source:MGI Symbol;Acc:MGI:2443110] | -0.38 | 5.0E-03 |
| Abhd5 | abhydrolase domain containing 5 [Source:MGI Symbol;Acc:MGI:1914719] | -0.38 | 5.7E-03 |
| Ace | angiotensin I converting enzyme (peptidyl-dipeptidase A) 1 [Source:MGI Symbol;Acc:MGI:87874] | -0.62 | 1.7E-03 |
| Acvrl1 | activin A receptor, type II-like 1 [Source:MGI Symbol;Acc:MGI:1338946] | -0.49 | 2.2E-03 |
| Adgre1 | adhesion G protein-coupled receptor E1 [Source:MGI Symbol;Acc:MGI:106912] | -0.49 | 2.5E-03 |
| Afap1l1 | actin filament associated protein 1-like 1 [Source:MGI Symbol;Acc:MGI:2147199] | 0.33 | 9.4E-03 |
| Alkbh6 | alkB homolog 6 [Source:MGI Symbol;Acc:MGI:2142037] | 0.37 | 8.4E-03 |
| Angptl2 | angiopoietin-like 2 [Source:MGI Symbol;Acc:MGI:1347002] | -0.48 | 3.3E-03 |
| Arhgef37 | Rho guanine nucleotide exchange factor (GEF) 37 [Source:MGI Symbol;Acc:MGI:3045339] | -0.66 | 5.6E-04 |
| Atp11a | ATPase, class VI, type 11A [Source:MGI Symbol;Acc:MGI:1354735] | -0.49 | 3.8E-03 |
| B3gnt7 | UDP-GlcNAc:betaGal beta-1,3-N-acetylglucosaminyltransferase 7 [Source:MGI Symbol;Acc:MGI:2384394] | -0.45 | 3.4E-03 |
| Bmx | BMX non-receptor tyrosine kinase [Source:MGI Symbol;Acc:MGI:1101778] | -0.55 | 2.1E-03 |
| C130050O18Rik | RIKEN cDNA C130050O18 gene [Source:MGI Symbol;Acc:MGI:2442694] | -0.48 | 5.7E-03 |
| C1galt1c1 | C1GALT1-specific chaperone 1 [Source:MGI Symbol;Acc:MGI:1913493] | -0.36 | 9.0E-03 |
| C3 | complement component 3 [Source:MGI Symbol;Acc:MGI:88227] | -0.40 | 6.2E-03 |
| Ccr2 | chemokine (C-C motif) receptor 2 [Source:MGI Symbol;Acc:MGI:106185] | -0.43 | 5.7E-03 |
| Cd177 | CD177 antigen [Source:MGI Symbol;Acc:MGI:1916141] | -0.62 | 5.7E-03 |
| Cd200 | CD200 antigen [Source:MGI Symbol;Acc:MGI:1196990] | 0.40 | 8.7E-03 |
| Cd302 | CD302 antigen [Source:MGI Symbol;Acc:MGI:1913455] | -0.59 | 1.6E-03 |
| Cd320 | CD320 antigen [Source:MGI Symbol;Acc:MGI:1860083] | 0.34 | 9.6E-03 |
| Cfh | complement component factor h [Source:MGI Symbol;Acc:MGI:88385] | -0.92 | 2.1E-04 |
| Churc1 | churchill domain containing 1 [Source:MGI Symbol;Acc:MGI:1923684] | 0.45 | 8.0E-03 |
| Clec7a | C-type lectin domain family 7, member a [Source:MGI Symbol;Acc:MGI:1861431] | -0.45 | 7.0E-03 |
| Col7a1 | collagen, type VII, alpha 1 [Source:MGI Symbol;Acc:MGI:88462] | 0.36 | 7.0E-03 |
| Crybg3 | beta-gamma crystallin domain containing 3 [Source:MGI Symbol;Acc:MGI:2676311] | -0.51 | 1.3E-03 |
| Ctla2b | cytotoxic T lymphocyte-associated protein 2 beta [Source:MGI Symbol;Acc:MGI:88555] | 0.37 | 8.4E-03 |
| Ddit4 | DNA-damage-inducible transcript 4 [Source:MGI Symbol;Acc:MGI:1921997] | 0.44 | 2.6E-03 |
| Dnajc24 | DnaJ heat shock protein family (Hsp40) member C24 [Source:MGI Symbol;Acc:MGI:1919522] | 0.39 | 5.7E-03 |
| Dnase1l1 | deoxyribonuclease 1-like 1 [Source:MGI Symbol;Acc:MGI:109628] | -0.42 | 9.5E-03 |
| Dock1 | dedicator of cytokinesis 1 [Source:MGI Symbol;Acc:MGI:2429765] | -0.43 | 4.1E-03 |
| Dock5 | dedicator of cytokinesis 5 [Source:MGI Symbol;Acc:MGI:2652871] | -0.38 | 9.3E-03 |
| Dyrk3 | dual-specificity tyrosine-(Y)-phosphorylation regulated kinase 3 [Source:MGI Symbol;Acc:MGI:1330300] | 0.37 | 5.9E-03 |
| E230001N04Rik | RIKEN cDNA E230001N04 gene [Source:MGI Symbol;Acc:MGI:2443549] | 0.62 | 1.2E-03 |
| Egr3 | early growth response 3 [Source:MGI Symbol;Acc:MGI:1306780] | -0.36 | 6.7E-03 |
| Erdr1 | erythroid differentiation regulator 1 [Source:MGI Symbol;Acc:MGI:2384747] | -0.53 | 5.7E-03 |
| F13a1 | coagulation factor XIII, A1 subunit [Source:MGI Symbol;Acc:MGI:1921395] | -0.41 | 4.1E-03 |
| Fam126b | family with sequence similarity 126, member B [Source:MGI Symbol;Acc:MGI:1098784] | -0.38 | 5.2E-03 |
| Fbxo10 | F-box protein 10 [Source:MGI Symbol;Acc:MGI:2686937] | -0.40 | 3.9E-03 |
| Fcnb | ficolin B [Source:MGI Symbol;Acc:MGI:1341158] | -0.63 | 5.3E-04 |
| Fgd4 | FYVE, RhoGEF and PH domain containing 4 [Source:MGI Symbol;Acc:MGI:2183747] | -0.46 | 2.2E-03 |
| Fn1 | fibronectin 1 [Source:MGI Symbol;Acc:MGI:95566] | -0.52 | 1.1E-03 |
| Fosl2 | fos-like antigen 2 [Source:MGI Symbol;Acc:MGI:102858] | -0.45 | 6.7E-03 |
| Galnt9 | UDP-N-acetyl-alpha-D-galactosamine:polypeptide N-acetylgalactosaminyltransferase 9 [Source:MGI Symbol;Acc:MGI:2677965] | -0.65 | 6.8E-04 |
| Gda | guanine deaminase [Source:MGI Symbol;Acc:MGI:95678] | -0.46 | 2.8E-03 |
| Gdap10 | ganglioside-induced differentiation-associated-protein 10 [Source:MGI Symbol;Acc:MGI:1338008] | -0.42 | 7.1E-03 |
| Gm11131 | predicted gene 11131 [Source:MGI Symbol;Acc:MGI:3779386] | 0.40 | 5.4E-03 |
| Gm14548 | predicted gene 14548 [Source:MGI Symbol;Acc:MGI:3709645] | -0.63 | 5.0E-04 |
| Gm15448 | predicted gene 15448 [Source:MGI Symbol;Acc:MGI:3705216] | -0.53 | 1.7E-03 |
| Gm15879 | predicted gene 15879 [Source:MGI Symbol;Acc:MGI:3802012] | 0.40 | 6.2E-03 |
| Gm15922 | predicted gene 15922 [Source:MGI Symbol;Acc:MGI:3802148] | -0.62 | 1.3E-03 |
| Gm1966 | predicted gene 1966 [Source:MGI Symbol;Acc:MGI:3584360] | -0.43 | 3.2E-03 |
| Gm21887 | predicted gene, 21887 [Source:MGI Symbol;Acc:MGI:5434051] | -2.11 | 2.9E-06 |
| Gm26947 | predicted gene, 26947 [Source:MGI Symbol;Acc:MGI:5504062] | 0.40 | 5.2E-03 |
| Gm28187 | predicted gene 28187 [Source:MGI Symbol;Acc:MGI:5578893] | -0.53 | 5.5E-03 |
| Gm340 | predicted gene 340 [Source:MGI Symbol;Acc:MGI:2685186] | -0.55 | 2.7E-03 |
| Gm35147 | predicted gene, 35147 [Source:MGI Symbol;Acc:MGI:5594306] | -0.52 | 1.2E-03 |
| Gm37403 | predicted gene, 37403 [Source:MGI Symbol;Acc:MGI:5610631] | -0.58 | 7.3E-03 |
| Gm44423 | predicted gene, 44423 [Source:MGI Symbol;Acc:MGI:5690815] | -0.39 | 4.5E-03 |
| Gm45884 | predicted gene 45884 [Source:MGI Symbol;Acc:MGI:5804999] | -0.47 | 5.5E-03 |
| Gm9938 | predicted gene 9938 [Source:MGI Symbol;Acc:MGI:3641836] | -0.34 | 9.6E-03 |
| Gramd3 | GRAM domain containing 3 [Source:MGI Symbol;Acc:MGI:1914815] | 0.34 | 9.5E-03 |
| Grcc10 | gene rich cluster, C10 gene [Source:MGI Symbol;Acc:MGI:1315201] | 0.33 | 9.2E-03 |
| Hip1 | huntingtin interacting protein 1 [Source:MGI Symbol;Acc:MGI:1099804] | -0.41 | 3.5E-03 |
| Hmgcll1 | 3-hydroxymethyl-3-methylglutaryl-Coenzyme A lyase-like 1 [Source:MGI Symbol;Acc:MGI:2446108] | -0.33 | 9.8E-03 |
| Hmgcs1 | 3-hydroxy-3-methylglutaryl-Coenzyme A synthase 1 [Source:MGI Symbol;Acc:MGI:107592] | -0.36 | 8.5E-03 |
| Ifi211 | interferon activated gene 211 [Source:MGI Symbol;Acc:MGI:3041120] | -0.49 | 2.4E-03 |

| | | | |
|---|---|---|---|
| Ighv1-12 | immunoglobulin heavy variable V1-12 [Source:MGI Symbol;Acc:MGI:3646284] | -0.82 | 7.3E-03 |
| Ighv1-26 | immunoglobulin heavy variable 1-26 [Source:MGI Symbol;Acc:MGI:4439641] | -0.55 | 1.9E-03 |
| Ighv1-50 | immunoglobulin heavy variable 1-50 [Source:MGI Symbol;Acc:MGI:4439753] | -1.25 | 4.3E-03 |
| Ighv1-77 | immunoglobulin heavy variable 1-77 [Source:MGI Symbol;Acc:MGI:4439670] | -1.19 | 1.4E-04 |
| Ighv3-8 | immunoglobulin heavy variable V3-8 [Source:MGI Symbol;Acc:MGI:3645298] | 0.88 | 1.0E-04 |
| Ighv4-1 | immunoglobulin heavy variable 4-1 [Source:MGI Symbol;Acc:MGI:4439536] | 0.42 | 7.6E-03 |
| Igip | IgA inducing protein [Source:MGI Symbol;Acc:MGI:1924271] | 0.37 | 6.8E-03 |
| Igkv13-84 | immunoglobulin kappa chain variable 13-84 [Source:MGI Symbol;Acc:MGI:96514] | -0.46 | 2.1E-03 |
| Igkv14-111 | immunoglobulin kappa variable 14-111 [Source:MGI Symbol;Acc:MGI:4439863] | 0.47 | 2.9E-03 |
| Igkv16-104 | immunoglobulin kappa variable 16-104 [Source:MGI Symbol;Acc:MGI:2685913] | -0.56 | 4.8E-03 |
| Igkv3-10 | immunoglobulin kappa variable 3-10 [Source:MGI Symbol;Acc:MGI:1330821] | -0.65 | 5.0E-04 |
| Igkv4-70 | immunoglobulin kappa chain variable 4-70 [Source:MGI Symbol;Acc:MGI:2686348] | -2.89 | 1.6E-03 |
| Igkv4-86 | immunoglobulin kappa variable 4-86 [Source:MGI Symbol;Acc:MGI:2685305] | 0.48 | 2.5E-03 |
| Igkv5-39 | immunoglobulin kappa variable 5-39 [Source:MGI Symbol;Acc:MGI:2686255] | -0.53 | 7.3E-03 |
| Igkv6-32 | immunoglobulin kappa variable 6-32 [Source:MGI Symbol;Acc:MGI:3641634] | 0.49 | 1.5E-03 |
| Igkv9-124 | immunoglobulin kappa chain variable 9-124 [Source:MGI Symbol;Acc:MGI:3646892] | -0.78 | 1.5E-04 |
| Il17rb | interleukin 17 receptor B [Source:MGI Symbol;Acc:MGI:1355292] | 0.39 | 5.5E-03 |
| Il6st | interleukin 6 signal transducer [Source:MGI Symbol;Acc:MGI:96560] | -0.35 | 7.4E-03 |
| Il9r | interleukin 9 receptor [Source:MGI Symbol;Acc:MGI:96564] | 0.47 | 2.2E-03 |
| Irs1 | insulin receptor substrate 1 [Source:MGI Symbol;Acc:MGI:99454] | 0.48 | 1.8E-03 |
| Itga1 | integrin alpha 1 [Source:MGI Symbol;Acc:MGI:96599] | -0.53 | 3.6E-03 |
| Itpripl2 | inositol 1,4,5-triphosphate receptor interacting protein-like 2 [Source:MGI Symbol;Acc:MGI:2442416] | -0.34 | 9.3E-03 |
| Kcnk5 | potassium channel, subfamily K, member 5 [Source:MGI Symbol;Acc:MGI:1336175] | 0.35 | 8.8E-03 |
| Kctd12b | potassium channel tetramerisation domain containing 12b [Source:MGI Symbol;Acc:MGI:2444667] | -0.45 | 3.9E-03 |
| Klf11 | Kruppel-like factor 11 [Source:MGI Symbol;Acc:MGI:2653368] | 0.38 | 7.9E-03 |
| Klf9 | Kruppel-like factor 9 [Source:MGI Symbol;Acc:MGI:1333856] | 0.63 | 1.0E-03 |
| Krt80 | keratin 80 [Source:MGI Symbol;Acc:MGI:1921377] | -0.51 | 1.3E-03 |
| Ldlr | low density lipoprotein receptor [Source:MGI Symbol;Acc:MGI:96765] | -0.66 | 2.6E-03 |
| Lilra6 | leukocyte immunoglobulin-like receptor, subfamily A (with TM domain), member 6 [Source:MGI Symbol;Acc:MGI:1195969] | -0.44 | 3.0E-03 |
| Lmntd2 | lamin tail domain containing 2 [Source:MGI Symbol;Acc:MGI:1919250] | 0.50 | 1.9E-03 |
| Lnpep | leucyl/cystinyl aminopeptidase [Source:MGI Symbol;Acc:MGI:2387123] | -0.39 | 4.7E-03 |
| Lrp1 | low density lipoprotein receptor-related protein 1 [Source:MGI Symbol;Acc:MGI:96828] | -0.57 | 5.3E-03 |
| Ly6a | lymphocyte antigen 6 complex, locus A [Source:MGI Symbol;Acc:MGI:107527] | 0.43 | 3.5E-03 |
| Megf9 | multiple EGF-like-domains 9 [Source:MGI Symbol;Acc:MGI:1918264] | -0.43 | 2.8E-03 |
| Met | met proto-oncogene [Source:MGI Symbol;Acc:MGI:96969] | -0.39 | 6.0E-03 |
| Mitf | microphthalmia-associated transcription factor [Source:MGI Symbol;Acc:MGI:104554] | -0.43 | 7.9E-03 |
| Mlkl | mixed lineage kinase domain-like [Source:MGI Symbol;Acc:MGI:1921818] | -0.39 | 6.1E-03 |
| Ms4a6d | membrane-spanning 4-domains, subfamily A, member 6D [Source:MGI Symbol;Acc:MGI:1916024] | -0.44 | 5.5E-03 |
| Msr1 | macrophage scavenger receptor 1 [Source:MGI Symbol;Acc:MGI:98257] | -0.67 | 4.2E-03 |
| mt-Nd1 | mitochondrially encoded NADH dehydrogenase 1 [Source:MGI Symbol;Acc:MGI:101787] | 0.42 | 4.9E-03 |
| mt-Nd2 | mitochondrially encoded NADH dehydrogenase 2 [Source:MGI Symbol;Acc:MGI:102500] | 0.44 | 8.2E-03 |
| Myzap | myocardial zonula adherens protein [Source:MGI Symbol;Acc:MGI:2142908] | 0.38 | 6.6E-03 |
| Nlrp1a | NLR family, pyrin domain containing 1A [Source:MGI Symbol;Acc:MGI:2684861] | -0.49 | 2.4E-03 |
| Nrg1 | neuregulin 1 [Source:MGI Symbol;Acc:MGI:96083] | -0.59 | 3.7E-03 |
| Nrp1 | neuropilin 1 [Source:MGI Symbol;Acc:MGI:106206] | -0.46 | 6.4E-03 |
| Nt5e | 5' nucleotidase, ecto [Source:MGI Symbol;Acc:MGI:99782] | 0.56 | 3.1E-03 |
| Olfm1 | olfactomedin 1 [Source:MGI Symbol;Acc:MGI:1860437] | -0.61 | 5.4E-04 |
| Pdcd4 | programmed cell death 4 [Source:MGI Symbol;Acc:MGI:107490] | 0.34 | 8.1E-03 |
| Per1 | period circadian clock 1 [Source:MGI Symbol;Acc:MGI:1098283] | 0.64 | 1.2E-03 |
| Pi16 | peptidase inhibitor 16 [Source:MGI Symbol;Acc:MGI:1921366] | -0.39 | 7.6E-03 |
| Pigg | phosphatidylinositol glycan anchor biosynthesis, class G [Source:MGI Symbol;Acc:MGI:3576484] | -0.34 | 8.2E-03 |
| Pik3ip1 | phosphoinositide-3-kinase interacting protein 1 [Source:MGI Symbol;Acc:MGI:1917016] | 0.75 | 2.4E-04 |
| Pira2 | paired-Ig-like receptor A2 [Source:MGI Symbol;Acc:MGI:1195970] | -0.45 | 9.4E-03 |
| Plcb1 | phospholipase C, beta 1 [Source:MGI Symbol;Acc:MGI:97613] | -0.59 | 9.3E-03 |
| Pld1 | phospholipase D1 [Source:MGI Symbol;Acc:MGI:109585] | -0.48 | 5.4E-03 |
| Pmepa1 | prostate transmembrane protein, androgen induced 1 [Source:MGI Symbol;Acc:MGI:1929600] | 0.56 | 6.4E-03 |
| Pros1 | protein S (alpha) [Source:MGI Symbol;Acc:MGI:1095733] | -0.57 | 9.3E-04 |
| Pstpip2 | proline-serine-threonine phosphatase-interacting protein 2 [Source:MGI Symbol;Acc:MGI:1335088] | -0.45 | 6.0E-03 |
| Ptar1 | protein prenyltransferase alpha subunit repeat containing 1 [Source:MGI Symbol;Acc:MGI:1921875] | -0.45 | 2.4E-03 |
| Pygm | muscle glycogen phosphorylase [Source:MGI Symbol;Acc:MGI:97830] | -0.40 | 5.5E-03 |
| Rab3ip | RAB3A interacting protein [Source:MGI Symbol;Acc:MGI:105933] | 0.35 | 8.0E-03 |
| Rab7b | RAB7B, member RAS oncogene family [Source:MGI Symbol;Acc:MGI:2442295] | -0.44 | 7.0E-03 |
| Rap2a | RAS related protein 2a [Source:MGI Symbol;Acc:MGI:97855] | -0.34 | 9.1E-03 |
| Raph1 | Ras association (RalGDS/AF-6) and pleckstrin homology domains 1 [Source:MGI Symbol;Acc:MGI:1924550] | -0.38 | 5.2E-03 |
| Rbm4 | RNA binding motif protein 4 [Source:MGI Symbol;Acc:MGI:1100865] | -0.45 | 2.3E-03 |
| Reck | reversion-inducing-cysteine-rich protein with kazal motifs [Source:MGI Symbol;Acc:MGI:1855698] | 0.34 | 8.4E-03 |
| Rgs1 | regulator of G-protein signaling 1 [Source:MGI Symbol;Acc:MGI:1354694] | 0.47 | 2.4E-03 |
| Rhou | ras homolog family member U [Source:MGI Symbol;Acc:MGI:1916831] | -0.44 | 3.4E-03 |
| Rnf144b | ring finger protein 144B [Source:MGI Symbol;Acc:MGI:2384986] | -0.63 | 1.0E-03 |
| Rpp40 | ribonuclease P 40 subunit [Source:MGI Symbol;Acc:MGI:1346084] | 0.42 | 9.8E-03 |
| Rps3a2 | ribosomal protein S3A2 [Source:MGI Symbol;Acc:MGI:3642853] | 0.50 | 1.8E-03 |

| | | | |
|---|---|---|---|
| Rxra | retinoid X receptor alpha [Source:MGI Symbol;Acc:MGI:98214] | -0.40 | 7.1E-03 |
| S1pr2 | sphingosine-1-phosphate receptor 2 [Source:MGI Symbol;Acc:MGI:99569] | -0.42 | 3.2E-03 |
| Sept10 | septin 10 [Source:MGI Symbol;Acc:MGI:1918110] | -0.53 | 1.4E-03 |
| Serpina3g | serine (or cysteine) peptidase inhibitor, clade A, member 3G [Source:MGI Symbol;Acc:MGI:105046] | 0.39 | 6.0E-03 |
| Sesn1 | sestrin 1 [Source:MGI Symbol;Acc:MGI:2155278] | 0.41 | 3.8E-03 |
| Sgms2 | sphingomyelin synthase 2 [Source:MGI Symbol;Acc:MGI:1921692] | -0.54 | 1.1E-03 |
| Shtn1 | shootin 1 [Source:MGI Symbol;Acc:MGI:1918903] | -0.72 | 3.0E-03 |
| Slc11a1 | solute carrier family 11 (proton-coupled divalent metal ion transporters), member 1 [Source:MGI Symbol;Acc:MGI:1345275] | -0.51 | 2.4E-03 |
| Slc22a17 | solute carrier family 22 (organic cation transporter), member 17 [Source:MGI Symbol;Acc:MGI:1926225] | 0.49 | 1.6E-03 |
| Slc4a1 | solute carrier family 4 (anion exchanger), member 1 [Source:MGI Symbol;Acc:MGI:109393] | -0.91 | 7.4E-05 |
| Slc8a1 | solute carrier family 8 (sodium/calcium exchanger), member 1 [Source:MGI Symbol;Acc:MGI:107956] | -0.46 | 6.3E-03 |
| Smim8 | small integral membrane protein 8 [Source:MGI Symbol;Acc:MGI:1913541] | 0.37 | 8.5E-03 |
| Sulf2 | sulfatase 2 [Source:MGI Symbol;Acc:MGI:1919293] | -0.36 | 6.3E-03 |
| Tcp11l1 | t-complex 11 like 1 [Source:MGI Symbol;Acc:MGI:2444263] | -0.43 | 3.7E-03 |
| Tgfbi | transforming growth factor, beta induced [Source:MGI Symbol;Acc:MGI:99959] | -0.47 | 2.9E-03 |
| Tiam1 | T cell lymphoma invasion and metastasis 1 [Source:MGI Symbol;Acc:MGI:103306] | -0.39 | 6.7E-03 |
| Tlr13 | toll-like receptor 13 [Source:MGI Symbol;Acc:MGI:3045213] | -0.38 | 6.0E-03 |
| Tnfsf8 | tumor necrosis factor (ligand) superfamily, member 8 [Source:MGI Symbol;Acc:MGI:88328] | 0.39 | 7.9E-03 |
| Tsc22d3 | TSC22 domain family, member 3 [Source:MGI Symbol;Acc:MGI:1196284] | 0.34 | 9.5E-03 |
| Tstd3 | thiosulfate sulfurtransferase (rhodanese)-like domain containing 3 [Source:MGI Symbol;Acc:MGI:1924282] | -0.39 | 8.2E-03 |
| Ttyh2 | tweety family member 2 [Source:MGI Symbol;Acc:MGI:2157091] | 0.42 | 3.6E-03 |
| Tuft1 | tuftelin 1 [Source:MGI Symbol;Acc:MGI:109572] | 0.39 | 5.7E-03 |
| Ugt1a7c | UDP glucuronosyltransferase 1 family, polypeptide A7C [Source:MGI Symbol;Acc:MGI:3032636] | -0.52 | 6.9E-03 |
| Utp14b | UTP14B small subunit processome component [Source:MGI Symbol;Acc:MGI:2445092] | -0.45 | 3.9E-03 |
| Vcl | vinculin [Source:MGI Symbol;Acc:MGI:98927] | -0.37 | 5.9E-03 |
| Vps13c | vacuolar protein sorting 13C [Source:MGI Symbol;Acc:MGI:2444207] | -0.44 | 2.7E-03 |
| Wnt10a | wingless-type MMTV integration site family, member 10A [Source:MGI Symbol;Acc:MGI:108071] | 0.49 | 2.7E-03 |
| Xlr3b | X-linked lymphocyte-regulated 3B [Source:MGI Symbol;Acc:MGI:109505] | 0.89 | 7.7E-05 |
| Xlr4a | X-linked lymphocyte-regulated 4A [Source:MGI Symbol;Acc:MGI:3574098] | 0.61 | 1.4E-03 |
| Xlr4b | X-linked lymphocyte-regulated 4B [Source:MGI Symbol;Acc:MGI:1350975] | 0.47 | 3.4E-03 |
| Zcchc18 | zinc finger, CCHC domain containing 18 [Source:MGI Symbol;Acc:MGI:1914245] | 0.39 | 7.0E-03 |
| Zfp1 | zinc finger protein 1 [Source:MGI Symbol;Acc:MGI:99154] | 0.46 | 5.8E-03 |
| Zfp53 | zinc finger protein 53 [Source:MGI Symbol;Acc:MGI:99200] | 0.48 | 2.4E-03 |
| Zfp566 | zinc finger protein 566 [Source:MGI Symbol;Acc:MGI:1919806] | 0.35 | 7.9E-03 |
| Zfyve9 | zinc finger, FYVE domain containing 9 [Source:MGI Symbol;Acc:MGI:2652838] | -0.79 | 1.5E-04 |
| Zkscan16 | zinc finger with KRAB and SCAN domains 16 [Source:MGI Symbol;Acc:MGI:3510405] | -0.69 | 7.9E-04 |

**Table A.2: List of genes used in the GO analysis of BM-PACs isolated from bone marrow.**
Genes highlighted in green correspond to human homologue genes with SNPs associated with worsened clinical metrics of PAH severity.

| Gene (MGI) | Gene Description | $log_2$(F | p-valu |
|---|---|---|---|
| 1810011H11Rik | RIKEN cDNA 1810011H11 gene [Source:MGI Symbol;Acc:MGI:1916319] | 1.18 | 1.3E-03 |
| 2510009E07Rik | RIKEN cDNA 2510009E07 gene [Source:MGI Symbol;Acc:MGI:1919440] | -0.53 | 5.2E-03 |
| 2610037D02Rik | RIKEN cDNA 2610037D02 gene [Source:MGI Symbol;Acc:MGI:1917290] | -0.40 | 7.4E-03 |
| 4930417O13Rik | RIKEN cDNA 4930417O13 gene [Source:MGI Symbol;Acc:MGI:1921120] | -0.90 | 3.3E-04 |
| 4930481A15Rik | RIKEN cDNA 4930481A15 gene [Source:MGI Symbol;Acc:MGI:1922181] | -0.44 | 5.2E-03 |
| A230072C01Rik | RIKEN cDNA A230072C01 gene [Source:MGI Symbol;Acc:MGI:2444644] | 0.49 | 9.8E-03 |
| Actn1 | actinin, alpha 1 [Source:MGI Symbol;Acc:MGI:2137706] | -0.61 | 8.1E-03 |
| Acvrl1 | activin A receptor, type II-like 1 [Source:MGI Symbol;Acc:MGI:1338946] | -0.58 | 4.5E-03 |
| Adssl1 | adenylosuccinate synthetase like 1 [Source:MGI Symbol;Acc:MGI:87947] | 0.45 | 4.5E-03 |
| Afap1 | actin filament associated protein 1 [Source:MGI Symbol;Acc:MGI:1917542] | -0.42 | 6.0E-03 |
| Ampd1 | adenosine monophosphate deaminase 1 [Source:MGI Symbol;Acc:MGI:88015] | -0.67 | 2.5E-03 |
| Aplp1 | amyloid beta (A4) precursor-like protein 1 [Source:MGI Symbol;Acc:MGI:88046] | 0.73 | 2.6E-03 |
| Apobec1 | apolipoprotein B mRNA editing enzyme, catalytic polypeptide 1 [Source:MGI Symbol;Acc:MGI:103298] | 0.46 | 5.0E-03 |
| Ar | androgen receptor [Source:MGI Symbol;Acc:MGI:88064] | -0.46 | 4.7E-03 |
| Arl4d | ADP-ribosylation factor-like 4D [Source:MGI Symbol;Acc:MGI:1933155] | 0.64 | 2.5E-03 |
| Asb2 | ankyrin repeat and SOCS box-containing 2 [Source:MGI Symbol;Acc:MGI:1929743] | 0.98 | 2.3E-03 |
| Aspm | asp (abnormal spindle)-like, microcephaly associated (Drosophila) [Source:MGI Symbol;Acc:MGI:1334448] | 0.65 | 2.3E-03 |
| Atp2b4 | ATPase, Ca++ transporting, plasma membrane 4 [Source:MGI Symbol;Acc:MGI:88111] | 0.43 | 5.6E-03 |
| Atp7a | ATPase, Cu++ transporting, alpha polypeptide [Source:MGI Symbol;Acc:MGI:99400] | -0.42 | 8.0E-03 |
| B130055M24Rik | RIKEN cDNA B130055M24 gene [Source:MGI Symbol;Acc:MGI:3590645] | -0.40 | 7.0E-03 |
| BC106179 | cDNA sequence BC106179 [Source:MGI Symbol;Acc:MGI:3702726] | -0.62 | 1.6E-03 |
| Bcl11b | B cell leukemia/lymphoma 11B [Source:MGI Symbol;Acc:MGI:1929913] | -0.75 | 4.7E-03 |
| Bcl9l | B cell CLL/lymphoma 9-like [Source:MGI Symbol;Acc:MGI:1933114] | -0.40 | 7.6E-03 |
| Birc5 | baculoviral IAP repeat-containing 5 [Source:MGI Symbol;Acc:MGI:1203517] | 0.55 | 9.5E-03 |
| C030034L19Rik | RIKEN cDNA C030034L19 gene [Source:MGI Symbol;Acc:MGI:2444519] | 0.73 | 2.4E-03 |
| C1qtnf6 | C1q and tumor necrosis factor related protein 6 [Source:MGI Symbol;Acc:MGI:1919959] | 0.98 | 2.3E-03 |
| Cald1 | caldesmon 1 [Source:MGI Symbol;Acc:MGI:88250] | -0.61 | 5.8E-03 |
| Camk2b | calcium/calmodulin-dependent protein kinase II, beta [Source:MGI Symbol;Acc:MGI:88257] | 0.95 | 1.3E-03 |
| Car12 | carbonic anhydrase 12 [Source:MGI Symbol;Acc:MGI:1923709] | -0.65 | 6.7E-03 |
| Ccl5 | chemokine (C-C motif) ligand 5 [Source:MGI Symbol;Acc:MGI:98262] | 0.52 | 2.7E-03 |
| Ccna2 | cyclin A2 [Source:MGI Symbol;Acc:MGI:108069] | 0.54 | 2.9E-03 |
| Ccnb2 | cyclin B2 [Source:MGI Symbol;Acc:MGI:88311] | 0.72 | 8.6E-03 |
| Ccnd1 | cyclin D1 [Source:MGI Symbol;Acc:MGI:88313] | 0.93 | 1.2E-03 |
| Ccr2 | chemokine (C-C motif) receptor 2 [Source:MGI Symbol;Acc:MGI:106185] | 0.60 | 1.6E-03 |
| Ccr6 | chemokine (C-C motif) receptor 6 [Source:MGI Symbol;Acc:MGI:1333797] | -0.43 | 8.2E-03 |
| Cd101 | CD101 antigen [Source:MGI Symbol;Acc:MGI:2685862] | -0.47 | 4.6E-03 |
| Cd160 | CD160 antigen [Source:MGI Symbol;Acc:MGI:1860383] | 0.84 | 3.8E-04 |
| Cd68 | CD68 antigen [Source:MGI Symbol;Acc:MGI:88342] | 0.54 | 5.4E-03 |
| Cd86 | CD86 antigen [Source:MGI Symbol;Acc:MGI:101773] | 0.53 | 2.6E-03 |
| Cdca2 | cell division cycle associated 2 [Source:MGI Symbol;Acc:MGI:1919787] | 0.63 | 1.3E-03 |
| Cenpf | centromere protein F [Source:MGI Symbol;Acc:MGI:1313302] | 0.77 | 7.6E-04 |
| Chdh | choline dehydrogenase [Source:MGI Symbol;Acc:MGI:1860776] | 0.83 | 3.9E-03 |
| Cish | cytokine inducible SH2-containing protein [Source:MGI Symbol;Acc:MGI:103159] | 0.57 | 5.4E-03 |
| Ckb | creatine kinase, brain [Source:MGI Symbol;Acc:MGI:88407] | 0.65 | 2.2E-03 |
| Cks1b | CDC28 protein kinase 1b [Source:MGI Symbol;Acc:MGI:1889208] | 0.47 | 5.0E-03 |
| Clspn | claspin [Source:MGI Symbol;Acc:MGI:2445153] | 0.56 | 4.2E-03 |
| Cmah | cytidine monophospho-N-acetylneuraminic acid hydroxylase [Source:MGI Symbol;Acc:MGI:103227] | -0.37 | 9.8E-03 |
| Cmc2 | COX assembly mitochondrial protein 2 [Source:MGI Symbol;Acc:MGI:1913781] | 0.52 | 3.4E-03 |
| Cnga1 | cyclic nucleotide gated channel alpha 1 [Source:MGI Symbol;Acc:MGI:88436] | -0.59 | 6.9E-03 |
| Cpped1 | calcineurin-like phosphoesterase domain containing 1 [Source:MGI Symbol;Acc:MGI:2443300] | 0.41 | 6.5E-03 |
| Crtam | cytotoxic and regulatory T cell molecule [Source:MGI Symbol;Acc:MGI:1859822] | -0.46 | 4.5E-03 |
| Cyp4f16 | cytochrome P450, family 4, subfamily f, polypeptide 16 [Source:MGI Symbol;Acc:MGI:1917351] | 0.39 | 7.7E-03 |
| Dynlt1f | dynein light chain Tctex-type 1F [Source:MGI Symbol;Acc:MGI:3780996] | 0.40 | 9.3E-03 |
| E2f1 | E2F transcription factor 1 [Source:MGI Symbol;Acc:MGI:101941] | 0.51 | 2.9E-03 |
| Elovl7 | ELOVL family member 7, elongation of long chain fatty acids (yeast) [Source:MGI Symbol;Acc:MGI:1921809] | -0.59 | 5.3E-03 |
| Enc1 | ectodermal-neural cortex 1 [Source:MGI Symbol;Acc:MGI:109610] | -0.55 | 7.3E-03 |
| Ercc6l | excision repair cross-complementing rodent repair deficiency complementation group 6 like [Source:MGI Symbol;Acc:MGI:2654144] | 0.46 | 8.5E-03 |
| Erdr1 | erythroid differentiation regulator 1 [Source:MGI Symbol;Acc:MGI:2384747] | -0.95 | 2.5E-04 |
| Fam19a3 | family with sequence similarity 19, member A3 [Source:MGI Symbol;Acc:MGI:3046463] | 0.70 | 1.0E-03 |
| Fan1 | FANCD2/FANCI-associated nuclease 1 [Source:MGI Symbol;Acc:MGI:3045266] | -0.49 | 4.5E-03 |
| Fasl | Fas ligand (TNF superfamily, member 6) [Source:MGI Symbol;Acc:MGI:99255] | 0.61 | 2.0E-03 |
| Fbxo10 | F-box protein 10 [Source:MGI Symbol;Acc:MGI:2686937] | -0.44 | 5.7E-03 |
| Fes | feline sarcoma oncogene [Source:MGI Symbol;Acc:MGI:95514] | 0.58 | 1.8E-03 |
| Flt3 | FMS-like tyrosine kinase 3 [Source:MGI Symbol;Acc:MGI:95559] | 0.50 | 3.1E-03 |
| Foxm1 | forkhead box M1 [Source:MGI Symbol;Acc:MGI:1347487] | 0.54 | 2.5E-03 |
| Gabrr2 | gamma-aminobutyric acid (GABA) C receptor, subunit rho 2 [Source:MGI Symbol;Acc:MGI:95626] | -0.53 | 3.1E-03 |
| Galc | galactosylceramidase [Source:MGI Symbol;Acc:MGI:95636] | 0.52 | 8.8E-03 |
| Galm | galactose mutarotase [Source:MGI Symbol;Acc:MGI:2442420] | -0.61 | 8.9E-03 |
| Gm10101 | predicted gene 10101 [Source:MGI Symbol;Acc:MGI:3641713] | 0.40 | 7.4E-03 |
| Gm11695 | predicted gene 11695 [Source:MGI Symbol;Acc:MGI:3649841] | -0.88 | 4.8E-03 |
| Gm12185 | predicted gene 12185 [Source:MGI Symbol;Acc:MGI:3652173] | -0.49 | 5.0E-03 |
| Gm16602 | T cell receptor gamma, variable 1 [Source:MGI Symbol;Acc:MGI:98631] | 0.62 | 5.6E-03 |
| Gm21887 | predicted gene, 21887 [Source:MGI Symbol;Acc:MGI:5434051] | -2.69 | 1.2E-04 |
| Gm27003 | predicted gene, 27003 [Source:MGI Symbol;Acc:MGI:5504118] | 0.39 | 9.6E-03 |

| | | | |
|---|---|---|---|
| Gm340 | predicted gene 340 [Source:MGI Symbol;Acc:MGI:2685186] | -0.45 | 6.2E-03 |
| Gm37192 | predicted gene, 37192 [Source:MGI Symbol;Acc:MGI:5610420] | 0.79 | 5.3E-03 |
| Gm42664 | predicted gene 42664 [Source:MGI Symbol;Acc:MGI:5662801] | -0.55 | 7.8E-03 |
| Gm44174 | predicted gene, 44174 [Source:MGI Symbol;Acc:MGI:5690566] | -0.45 | 8.9E-03 |
| Gm44775 | predicted gene 44775 [Source:MGI Symbol;Acc:MGI:5753351] | 0.60 | 2.5E-03 |
| Gm45055 | predicted gene 45055 [Source:MGI Symbol;Acc:MGI:5753631] | -0.51 | 3.2E-03 |
| Gm45548 | predicted gene 45548 [Source:MGI Symbol;Acc:MGI:5791384] | 0.44 | 6.2E-03 |
| Gm45884 | predicted gene 45884 [Source:MGI Symbol;Acc:MGI:5804999] | -0.45 | 5.2E-03 |
| Gm4956 | predicted gene 4956 [Source:MGI Symbol;Acc:MGI:3647976] | 0.94 | 1.1E-03 |
| Gm6934 | predicted gene 6934 [Source:MGI Symbol;Acc:MGI:3648115] | -0.44 | 9.0E-03 |
| Gm9938 | predicted gene 9938 [Source:MGI Symbol;Acc:MGI:3641836] | -0.51 | 3.8E-03 |
| Gnaz | guanine nucleotide binding protein, alpha z subunit [Source:MGI Symbol;Acc:MGI:95780] | -0.64 | 1.2E-03 |
| Gpc1 | glypican 1 [Source:MGI Symbol;Acc:MGI:1194891] | 0.65 | 3.0E-03 |
| Gpr65 | G-protein coupled receptor 65 [Source:MGI Symbol;Acc:MGI:108031] | 0.52 | 3.2E-03 |
| Gprin3 | GPRIN family member 3 [Source:MGI Symbol;Acc:MGI:1924785] | -0.53 | 3.1E-03 |
| Gstp3 | glutathione S-transferase pi 3 [Source:MGI Symbol;Acc:MGI:2385078] | -0.45 | 6.3E-03 |
| Gzmb | granzyme B [Source:MGI Symbol;Acc:MGI:109267] | 1.08 | 1.9E-04 |
| Hic1 | hypermethylated in cancer 1 [Source:MGI Symbol;Acc:MGI:1338010] | 1.04 | 2.1E-04 |
| Id2 | inhibitor of DNA binding 2 [Source:MGI Symbol;Acc:MGI:96397] | 0.73 | 7.7E-04 |
| Igfbp4 | insulin-like growth factor binding protein 4 [Source:MGI Symbol;Acc:MGI:96439] | -0.84 | 2.4E-03 |
| Ighg1 | immunoglobulin heavy constant gamma 1 (G1m marker) [Source:MGI Symbol;Acc:MGI:96446] | 1.28 | 6.7E-03 |
| Ighg2b | immunoglobulin heavy constant gamma 2B [Source:MGI Symbol;Acc:MGI:96445] | 0.83 | 5.2E-03 |
| Iigp1 | interferon inducible GTPase 1 [Source:MGI Symbol;Acc:MGI:1926259] | -0.72 | 1.8E-03 |
| Il12rb1 | interleukin 12 receptor, beta 1 [Source:MGI Symbol;Acc:MGI:104579] | 0.75 | 7.8E-03 |
| Il12rb2 | interleukin 12 receptor, beta 2 [Source:MGI Symbol;Acc:MGI:1270861] | 0.87 | 1.6E-03 |
| Il17rb | interleukin 17 receptor B [Source:MGI Symbol;Acc:MGI:1355292] | 0.84 | 4.0E-04 |
| Il2ra | interleukin 2 receptor, alpha chain [Source:MGI Symbol;Acc:MGI:96549] | 0.62 | 7.8E-03 |
| Il2rb | interleukin 2 receptor, beta chain [Source:MGI Symbol;Acc:MGI:96550] | 0.67 | 2.6E-03 |
| Il3ra | interleukin 3 receptor, alpha chain [Source:MGI Symbol;Acc:MGI:96553] | 0.51 | 2.9E-03 |
| Il6st | interleukin 6 signal transducer [Source:MGI Symbol;Acc:MGI:96560] | -0.62 | 5.8E-03 |
| Itga7 | integrin alpha 7 [Source:MGI Symbol;Acc:MGI:102700] | -0.54 | 2.2E-03 |
| Itgae | integrin alpha E, epithelial-associated [Source:MGI Symbol;Acc:MGI:1298377] | -0.45 | 5.4E-03 |
| Jchain | immunoglobulin joining chain [Source:MGI Symbol;Acc:MGI:96493] | 0.86 | 3.5E-04 |
| Kcna2 | potassium voltage-gated channel, shaker-related subfamily, member 2 [Source:MGI Symbol;Acc:MGI:96659] | -0.77 | 6.9E-03 |
| Kif1b | kinesin family member 1B [Source:MGI Symbol;Acc:MGI:108426] | -0.49 | 6.5E-03 |
| Kif20a | kinesin family member 20A [Source:MGI Symbol;Acc:MGI:1201682] | 0.65 | 1.3E-03 |
| Kit | KIT proto-oncogene receptor tyrosine kinase [Source:MGI Symbol;Acc:MGI:96677] | 0.53 | 2.9E-03 |
| Klf3 | Kruppel-like factor 3 (basic) [Source:MGI Symbol;Acc:MGI:1342773] | -0.40 | 8.4E-03 |
| Klf6 | Kruppel-like factor 6 [Source:MGI Symbol;Acc:MGI:1346318] | -0.39 | 7.5E-03 |
| Klra13-ps | killer cell lectin-like receptor subfamily A, member 13, pseudogene [Source:MGI Symbol;Acc:MGI:1321090] | 0.54 | 9.5E-03 |
| Klra7 | killer cell lectin-like receptor, subfamily A, member 7 [Source:MGI Symbol;Acc:MGI:101901] | 0.67 | 1.9E-03 |
| Klrb1c | killer cell lectin-like receptor subfamily B member 1C [Source:MGI Symbol;Acc:MGI:107538] | 0.77 | 7.0E-04 |
| Klrb1f | killer cell lectin-like receptor subfamily B member 1F [Source:MGI Symbol;Acc:MGI:2442965] | 0.68 | 1.4E-03 |
| Klrc1 | killer cell lectin-like receptor subfamily C, member 1 [Source:MGI Symbol;Acc:MGI:1336161] | 0.87 | 3.3E-04 |
| Klrc2 | killer cell lectin-like receptor subfamily C, member 2 [Source:MGI Symbol;Acc:MGI:1336162] | 0.96 | 2.4E-04 |
| Klrc3 | killer cell lectin-like receptor subfamily C, member 3 [Source:MGI Symbol;Acc:MGI:1929720] | 0.70 | 9.2E-03 |
| Klre1 | killer cell lectin-like receptor family E member 1 [Source:MGI Symbol;Acc:MGI:2662547] | 0.55 | 3.1E-03 |
| Klrg1 | killer cell lectin-like receptor subfamily G, member 1 [Source:MGI Symbol;Acc:MGI:1355294] | 0.57 | 1.8E-03 |
| Klrk1 | killer cell lectin-like receptor subfamily K, member 1 [Source:MGI Symbol;Acc:MGI:1196250] | 0.77 | 7.0E-04 |
| Lifr | leukemia inhibitory factor receptor [Source:MGI Symbol;Acc:MGI:96788] | 1.14 | 2.3E-04 |
| Lin37 | lin-37 homolog (C. elegans) [Source:MGI Symbol;Acc:MGI:1922910] | 0.38 | 8.6E-03 |
| Lrp12 | low density lipoprotein-related protein 12 [Source:MGI Symbol;Acc:MGI:2443132] | -0.52 | 7.0E-03 |
| Lrrc8b | leucine rich repeat containing 8 family, member B [Source:MGI Symbol;Acc:MGI:2141353] | -0.48 | 4.0E-03 |
| Ly6g5b | lymphocyte antigen 6 complex, locus G5B [Source:MGI Symbol;Acc:MGI:2385809] | 0.61 | 1.4E-03 |
| Marcks | myristoylated alanine rich protein kinase C substrate [Source:MGI Symbol;Acc:MGI:96907] | 0.47 | 7.9E-03 |
| Mical2 | microtubule associated monooxygenase, calponin and LIM domain containing 2 [Source:MGI Symbol;Acc:MGI:2444947] | 0.81 | 5.0E-04 |
| Mki67 | antigen identified by monoclonal antibody Ki 67 [Source:MGI Symbol;Acc:MGI:106035] | 0.96 | 3.3E-03 |
| Mlh3 | mutL homolog 3 [Source:MGI Symbol;Acc:MGI:1353455] | -0.39 | 9.7E-03 |
| Mlxip | MLX interacting protein [Source:MGI Symbol;Acc:MGI:2141183] | 0.49 | 3.8E-03 |
| Mmp9 | matrix metallopeptidase 9 [Source:MGI Symbol;Acc:MGI:97011] | 0.95 | 5.8E-03 |
| Mmrn1 | multimerin 1 [Source:MGI Symbol;Acc:MGI:1918195] | -0.72 | 9.1E-04 |
| Mpeg1 | macrophage expressed gene 1 [Source:MGI Symbol;Acc:MGI:1333743] | 1.03 | 3.9E-03 |
| Mpp7 | membrane protein, palmitoylated 7 (MAGUK p55 subfamily member 7) [Source:MGI Symbol;Acc:MGI:1922989] | -0.52 | 8.3E-03 |
| Msrb2 | methionine sulfoxide reductase B2 [Source:MGI Symbol;Acc:MGI:1923717] | -0.51 | 2.9E-03 |
| Myct1 | myc target 1 [Source:MGI Symbol;Acc:MGI:1915882] | -0.60 | 1.8E-03 |
| Nav1 | neuron navigator 1 [Source:MGI Symbol;Acc:MGI:2183683] | -0.56 | 8.6E-03 |
| Ncapg | non-SMC condensin I complex, subunit G [Source:MGI Symbol;Acc:MGI:1930197] | 0.47 | 4.0E-03 |
| Neb | nebulin [Source:MGI Symbol;Acc:MGI:97292] | -0.78 | 8.6E-04 |
| Nedd4 | neural precursor cell expressed, developmentally down-regulated 4 [Source:MGI Symbol;Acc:MGI:97297] | 0.39 | 7.8E-03 |
| Ntng2 | netrin G2 [Source:MGI Symbol;Acc:MGI:2159341] | 0.37 | 9.9E-03 |
| Nusap1 | nucleolar and spindle associated protein 1 [Source:MGI Symbol;Acc:MGI:2675669] | 0.66 | 1.8E-03 |
| Obscn | obscurin, cytoskeletal calmodulin and titin-interacting RhoGEF [Source:MGI Symbol;Acc:MGI:2681862] | 1.17 | 2.3E-04 |
| Osbpl3 | oxysterol binding protein-like 3 [Source:MGI Symbol;Acc:MGI:1918970] | 0.55 | 3.5E-03 |
| Otub2 | OTU domain, ubiquitin aldehyde binding 2 [Source:MGI Symbol;Acc:MGI:1915399] | 0.50 | 4.0E-03 |
| P2rx7 | purinergic receptor P2X, ligand-gated ion channel, 7 [Source:MGI Symbol;Acc:MGI:1339957] | 0.84 | 6.6E-03 |

| | | | |
|---|---|---|---|
| Pard3b | par-3 family cell polarity regulator beta [Source:MGI Symbol;Acc:MGI:1919301] | -0.68 | 2.5E-03 |
| Pcgf2 | polycomb group ring finger 2 [Source:MGI Symbol;Acc:MGI:99161] | 0.52 | 2.8E-03 |
| Pclaf | PCNA clamp associated factor [Source:MGI Symbol;Acc:MGI:1915276] | 0.71 | 1.2E-03 |
| Pde1b | phosphodiesterase 1B, Ca2+-calmodulin dependent [Source:MGI Symbol;Acc:MGI:97523] | 0.43 | 8.6E-03 |
| Pde4c | phosphodiesterase 4C, cAMP specific [Source:MGI Symbol;Acc:MGI:99556] | 0.77 | 1.3E-03 |
| Pde4d | phosphodiesterase 4D, cAMP specific [Source:MGI Symbol;Acc:MGI:99555] | -0.51 | 4.6E-03 |
| Per3 | period circadian clock 3 [Source:MGI Symbol;Acc:MGI:1277134] | 0.39 | 8.2E-03 |
| Pfkfb1 | 6-phosphofructo-2-kinase/fructose-2,6-biphosphatase 1 [Source:MGI Symbol;Acc:MGI:107816] | 0.49 | 4.0E-03 |
| Pkig | protein kinase inhibitor, gamma [Source:MGI Symbol;Acc:MGI:1343086] | 0.47 | 4.1E-03 |
| Plcxd2 | phosphatidylinositol-specific phospholipase C, X domain containing 2 [Source:MGI Symbol;Acc:MGI:3647874] | -0.46 | 8.3E-03 |
| Pld4 | phospholipase D family, member 4 [Source:MGI Symbol;Acc:MGI:2144765] | 0.46 | 8.1E-03 |
| Plekhf1 | pleckstrin homology domain containing, family F (with FYVE domain) member 1 [Source:MGI Symbol;Acc:MGI:1919537] | 0.81 | 1.9E-03 |
| Ppfia4 | protein tyrosine phosphatase, receptor type, f polypeptide (PTPRF), interacting protein (liprin), alpha 4 [Source:MGI Symbol;Acc:MGI:1915757] | 0.69 | 9.6E-04 |
| Ppp1r21 | protein phosphatase 1, regulatory subunit 21 [Source:MGI Symbol;Acc:MGI:1921075] | 0.52 | 2.8E-03 |
| Prc1 | protein regulator of cytokinesis 1 [Source:MGI Symbol;Acc:MGI:1858961] | 0.42 | 8.5E-03 |
| Prkar2b | protein kinase, cAMP dependent regulatory, type II beta [Source:MGI Symbol;Acc:MGI:97760] | -0.59 | 7.4E-03 |
| Prkcg | protein kinase C, gamma [Source:MGI Symbol;Acc:MGI:97597] | 0.62 | 6.0E-03 |
| Prrt1 | proline-rich transmembrane protein 1 [Source:MGI Symbol;Acc:MGI:1932118] | 0.63 | 1.4E-03 |
| Ptch1 | patched 1 [Source:MGI Symbol;Acc:MGI:105373] | -0.43 | 5.7E-03 |
| Ptgfrn | prostaglandin F2 receptor negative regulator [Source:MGI Symbol;Acc:MGI:1277114] | -0.69 | 1.0E-03 |
| Ptprs | protein tyrosine phosphatase, receptor type, S [Source:MGI Symbol;Acc:MGI:97815] | 0.47 | 3.8E-03 |
| Rab20 | RAB20, member RAS oncogene family [Source:MGI Symbol;Acc:MGI:102789] | -0.44 | 6.5E-03 |
| Raver2 | ribonucleoprotein, PTB-binding 2 [Source:MGI Symbol;Acc:MGI:2443623] | -0.45 | 9.4E-03 |
| Rcbtb2 | regulator of chromosome condensation (RCC1) and BTB (POZ) domain containing protein 2 [Source:MGI Symbol;Acc:MGI:1917200] | 0.52 | 4.0E-03 |
| Rgs1 | regulator of G-protein signaling 1 [Source:MGI Symbol;Acc:MGI:1354694] | 0.63 | 1.9E-03 |
| Rhoc | ras homolog family member C [Source:MGI Symbol;Acc:MGI:106028] | 0.82 | 5.3E-04 |
| Runx2 | runt related transcription factor 2 [Source:MGI Symbol;Acc:MGI:99829] | 0.39 | 8.1E-03 |
| Samd3 | sterile alpha motif domain containing 3 [Source:MGI Symbol;Acc:MGI:2685469] | 0.47 | 3.9E-03 |
| Selenon | selenoprotein N [Source:MGI Symbol;Acc:MGI:2151208] | 0.60 | 4.7E-03 |
| Serpinb6b | serine (or cysteine) peptidase inhibitor, clade B, member 6b [Source:MGI Symbol;Acc:MGI:894688] | 0.52 | 3.9E-03 |
| Sh2b2 | SH2B adaptor protein 2 [Source:MGI Symbol;Acc:MGI:1345171] | 0.53 | 3.8E-03 |
| Siglech | sialic acid binding Ig-like lectin H [Source:MGI Symbol;Acc:MGI:2443256] | 1.40 | 6.6E-05 |
| Sla | src-like adaptor [Source:MGI Symbol;Acc:MGI:104295] | 0.46 | 4.4E-03 |
| Slc16a5 | solute carrier family 16 (monocarboxylic acid transporters), member 5 [Source:MGI Symbol;Acc:MGI:2443515] | -0.80 | 2.2E-03 |
| Slc25a53 | solute carrier family 25, member 53 [Source:MGI Symbol;Acc:MGI:1914312] | 0.54 | 2.3E-03 |
| Slc27a6 | solute carrier family 27 (fatty acid transporter), member 6 [Source:MGI Symbol;Acc:MGI:3036230] | 0.68 | 2.0E-03 |
| Slc35g1 | solute carrier family 35, member G1 [Source:MGI Symbol;Acc:MGI:2444789] | -0.59 | 7.7E-03 |
| Slco4a1 | solute carrier organic anion transporter family, member 4a1 [Source:MGI Symbol;Acc:MGI:1351866] | 0.80 | 8.9E-03 |
| Slfn3 | schlafen 3 [Source:MGI Symbol;Acc:MGI:1329005] | -0.46 | 9.7E-03 |
| Sntb1 | syntrophin, basic 1 [Source:MGI Symbol;Acc:MGI:101781] | -0.69 | 1.2E-03 |
| Soat2 | sterol O-acyltransferase 2 [Source:MGI Symbol;Acc:MGI:1332226] | 0.99 | 2.0E-04 |
| Socs2 | suppressor of cytokine signaling 2 [Source:MGI Symbol;Acc:MGI:1201787] | 1.06 | 1.5E-04 |
| Spag5 | sperm associated antigen 5 [Source:MGI Symbol;Acc:MGI:1927470] | 0.65 | 8.6E-03 |
| Spns3 | spinster homolog 3 [Source:MGI Symbol;Acc:MGI:1924827] | 0.47 | 4.0E-03 |
| Srgap3 | SLIT-ROBO Rho GTPase activating protein 3 [Source:MGI Symbol;Acc:MGI:2152938] | 0.71 | 1.4E-03 |
| St7 | suppression of tumorigenicity 7 [Source:MGI Symbol;Acc:MGI:1927450] | -0.57 | 4.1E-03 |
| St8sia1 | ST8 alpha-N-acetyl-neuraminide alpha-2,8-sialyltransferase 1 [Source:MGI Symbol;Acc:MGI:106011] | -0.65 | 5.6E-03 |
| St8sia6 | ST8 alpha-N-acetyl-neuraminide alpha-2,8-sialyltransferase 6 [Source:MGI Symbol;Acc:MGI:2386797] | -0.43 | 8.5E-03 |
| Stk32c | serine/threonine kinase 32C [Source:MGI Symbol;Acc:MGI:2385336] | 0.69 | 3.4E-03 |
| Ston2 | stonin 2 [Source:MGI Symbol;Acc:MGI:1918272] | -0.90 | 3.1E-04 |
| Styx | serine/threonine/tyrosine interaction protein [Source:MGI Symbol;Acc:MGI:1891150] | -0.56 | 2.1E-03 |
| Syk | spleen tyrosine kinase [Source:MGI Symbol;Acc:MGI:99515] | 0.38 | 9.9E-03 |
| Tacstd2 | tumor-associated calcium signal transducer 2 [Source:MGI Symbol;Acc:MGI:1861606] | 0.51 | 3.9E-03 |
| Tanc1 | tetratricopeptide repeat, ankyrin repeat and coiled-coil containing 1 [Source:MGI Symbol;Acc:MGI:1914110] | -0.62 | 7.0E-03 |
| Tanc2 | tetratricopeptide repeat, ankyrin repeat and coiled-coil containing 2 [Source:MGI Symbol;Acc:MGI:2444121] | -0.39 | 8.3E-03 |
| Tbc1d8 | TBC1 domain family, member 8 [Source:MGI Symbol;Acc:MGI:1927225] | 0.67 | 6.7E-03 |
| Tbkbp1 | TBK1 binding protein 1 [Source:MGI Symbol;Acc:MGI:1920424] | 1.03 | 1.4E-03 |
| Tbx21 | T-box 21 [Source:MGI Symbol;Acc:MGI:1888984] | 0.58 | 2.2E-03 |
| Tcrg-C1 | T cell receptor gamma, constant 1 [Source:MGI Symbol;Acc:MGI:98625] | 0.75 | 2.2E-03 |
| Tcrg-C2 | T-cell receptor gamma, constant 2 [Source:MGI Symbol;Acc:MGI:98626] | 0.70 | 4.3E-03 |
| Tcrg-C4 | T cell receptor gamma, constant 4 [Source:MGI Symbol;Acc:MGI:98628] | 0.67 | 1.7E-03 |
| Tcrg-V4 | T cell receptor gamma, variable 4 [Source:MGI Symbol;Acc:MGI:98634] | 0.58 | 8.1E-03 |
| Thbs1 | thrombospondin 1 [Source:MGI Symbol;Acc:MGI:98737] | -0.57 | 2.1E-03 |
| Tmem176a | transmembrane protein 176A [Source:MGI Symbol;Acc:MGI:1913308] | 0.46 | 9.4E-03 |
| Tmlhe | trimethyllysine hydroxylase, epsilon [Source:MGI Symbol;Acc:MGI:2180203] | -0.57 | 3.4E-03 |
| Tnfaip3 | tumor necrosis factor, alpha-induced protein 3 [Source:MGI Symbol;Acc:MGI:1196377] | -0.38 | 8.8E-03 |
| Tnfrsf14 | tumor necrosis factor receptor superfamily, member 14 (herpesvirus entry mediator) [Source:MGI Symbol;Acc:MGI:2675303] | -0.44 | 7.2E-03 |
| Tnfsf14 | tumor necrosis factor (ligand) superfamily, member 14 [Source:MGI Symbol;Acc:MGI:1355317] | 0.79 | 5.9E-04 |
| Tnfsf8 | tumor necrosis factor (ligand) superfamily, member 8 [Source:MGI Symbol;Acc:MGI:88328] | -0.46 | 9.4E-03 |
| Top2a | topoisomerase (DNA) II alpha [Source:MGI Symbol;Acc:MGI:98790] | 0.52 | 2.7E-03 |
| Trbj1-3 | T cell receptor beta joining 1-3 [Source:MGI Symbol;Acc:MGI:4439568] | -0.43 | 9.0E-03 |
| Trbj1-4 | T cell receptor beta joining 1-4 [Source:MGI Symbol;Acc:MGI:4439567] | -0.48 | 5.6E-03 |
| Trbj1-6 | T cell receptor beta joining 1-6 [Source:MGI Symbol;Acc:MGI:4439575] | -0.42 | 6.3E-03 |
| Trbv12-1 | T cell receptor beta, variable 12-1 [Source:MGI Symbol;Acc:MGI:98602] | -0.60 | 5.1E-03 |
| Trbv20 | T cell receptor beta, variable 20 [Source:MGI Symbol;Acc:MGI:98589] | -0.47 | 8.8E-03 |

| | | | |
|---|---|---|---|
| Trim30c | tripartite motif-containing 30C [Source:MGI Symbol;Acc:MGI:4821257] | -0.49 | 6.4E-03 |
| Trove2 | TROVE domain family, member 2 [Source:MGI Symbol;Acc:MGI:106652] | -0.42 | 6.1E-03 |
| Tspoap1 | TSPO associated protein 1 [Source:MGI Symbol;Acc:MGI:2450877] | 0.69 | 3.1E-03 |
| Ttc39c | tetratricopeptide repeat domain 39C [Source:MGI Symbol;Acc:MGI:1919997] | 0.46 | 4.3E-03 |
| Tubb1 | tubulin, beta 1 class VI [Source:MGI Symbol;Acc:MGI:107814] | -0.64 | 9.3E-03 |
| Ube2c | ubiquitin-conjugating enzyme E2C [Source:MGI Symbol;Acc:MGI:1915862] | 0.61 | 5.4E-03 |
| Utp14b | UTP14B small subunit processome component [Source:MGI Symbol;Acc:MGI:2445092] | -0.39 | 8.0E-03 |
| Wfs1 | Wolfram syndrome 1 homolog (human) [Source:MGI Symbol;Acc:MGI:1328355] | 0.42 | 9.7E-03 |
| Xcl1 | chemokine (C motif) ligand 1 [Source:MGI Symbol;Acc:MGI:104593] | 0.70 | 1.0E-03 |
| Xlr3b | X-linked lymphocyte-regulated 3B [Source:MGI Symbol;Acc:MGI:109505] | 1.13 | 3.5E-04 |
| Zfp52 | zinc finger protein 52 [Source:MGI Symbol;Acc:MGI:99199] | 0.39 | 7.7E-03 |
| Zfp683 | zinc finger protein 683 [Source:MGI Symbol;Acc:MGI:3650254] | 0.76 | 2.6E-03 |
| Zmat3 | zinc finger matrin type 3 [Source:MGI Symbol;Acc:MGI:1195270] | -0.37 | 9.2E-03 |

**Table A.3: List of genes used in the GO analysis of BM-PACs isolated from peripheral blood.** Genes highlighted in green correspond to human homologue genes with SNPs associated with worsened clinical metrics of PAH severity.

| GO Category | GO Category Description | Enrichment Ratio | FDR | Number of Genes |
|---|---|---|---|---|
| GO:0016310 | phosphorylation | 4.0 | 2.12E-03 | 18 |
| GO:0050790 | regulation of catalytic activity | 12.3 | 2.12E-03 | 8 |
| GO:2000026 | regulation of multicellular organismal development | 7.2 | 3.61E-03 | 10 |
| GO:0048468 | cell development | 3.7 | 4.75E-03 | 17 |
| GO:0051240 | positive regulation of multicellular organismal process | 11.2 | 4.75E-03 | 7 |
| GO:0071310 | cellular response to organic substance | 3.3 | 4.75E-03 | 20 |
| GO:0006468 | protein phosphorylation | 3.1 | 5.04E-03 | 20 |
| GO:0045595 | regulation of cell differentiation | 2.9 | 5.04E-03 | 22 |
| GO:0016477 | cell migration | 3.7 | 5.88E-03 | 16 |
| GO:0051094 | positive regulation of developmental process | 2.7 | 6.05E-03 | 24 |
| GO:0006928 | movement of cell or subcellular component | 3.9 | 6.63E-03 | 14 |
| GO:0019220 | regulation of phosphate metabolic process | 3.7 | 6.63E-03 | 15 |
| GO:0040011 | locomotion | 3.0 | 6.63E-03 | 19 |
| GO:0048870 | cell motility | 3.0 | 6.63E-03 | 20 |
| GO:0051174 | regulation of phosphorus metabolic process | 3.7 | 6.63E-03 | 15 |
| GO:0051336 | regulation of hydrolase activity | 7.8 | 6.63E-03 | 8 |
| GO:0051674 | localization of cell | 3.0 | 6.63E-03 | 20 |
| GO:0042325 | regulation of phosphorylation | 4.9 | 7.10E-03 | 11 |
| GO:0045597 | positive regulation of cell differentiation | 8.6 | 7.10E-03 | 7 |
| GO:0051247 | positive regulation of protein metabolic process | 8.6 | 7.10E-03 | 7 |
| GO:0022603 | regulation of anatomical structure morphogenesis | 3.7 | 8.94E-03 | 14 |
| GO:0032270 | positive regulation of cellular protein metabolic process | 2.6 | 8.94E-03 | 22 |
| GO:0071495 | cellular response to endogenous stimulus | 23.3 | 8.94E-03 | 4 |
| GO:0080134 | regulation of response to stress | 4.6 | 8.94E-03 | 11 |
| GO:0001932 | regulation of protein phosphorylation | 3.1 | 1.11E-02 | 17 |
| GO:0043085 | positive regulation of catalytic activity | 2.4 | 1.17E-02 | 25 |
| GO:0007167 | enzyme linked receptor protein signaling pathway | 20.6 | 1.27E-02 | 4 |
| GO:0040012 | regulation of locomotion | 3.7 | 1.32E-02 | 13 |
| GO:0051270 | regulation of cellular component movement | 3.0 | 1.33E-02 | 17 |
| GO:0000902 | cell morphogenesis | 2.3 | 1.51E-02 | 25 |
| GO:0030334 | regulation of cell migration | 5.9 | 1.64E-02 | 8 |
| GO:0032989 | cellular component morphogenesis | 2.7 | 1.64E-02 | 19 |
| GO:0000904 | cell morphogenesis involved in differentiation | 5.7 | 2.22E-02 | 8 |
| GO:0060284 | regulation of cell development | 3.3 | 2.22E-02 | 14 |
| GO:2000145 | regulation of cell motility | 2.5 | 2.22E-02 | 20 |
| GO:0023014 | signal transduction by protein phosphorylation | 4.0 | 2.23E-02 | 11 |
| GO:0051345 | positive regulation of hydrolase activity | 4.9 | 2.23E-02 | 9 |
| GO:0000165 | MAPK cascade | 3.1 | 2.26E-02 | 15 |
| GO:0022604 | regulation of cell morphogenesis | 2.6 | 2.28E-02 | 19 |
| GO:0001817 | regulation of cytokine production | 10.5 | 2.34E-02 | 5 |
| GO:0007169 | transmembrane receptor protein tyrosine kinase signaling pathway | 3.9 | 2.34E-02 | 11 |
| GO:0010720 | positive regulation of cell development | 3.4 | 2.34E-02 | 13 |
| GO:0001816 | cytokine production | 3.3 | 2.68E-02 | 13 |
| GO:0006954 | inflammatory response | 6.2 | 2.68E-02 | 7 |
| GO:0048812 | neuron projection morphogenesis | 2.5 | 2.68E-02 | 20 |
| GO:0048858 | cell projection morphogenesis | 2.6 | 2.68E-02 | 18 |
| GO:0010769 | regulation of cell morphogenesis involved in differentiation | 2.4 | 2.69E-02 | 20 |
| GO:0032990 | cell part morphogenesis | 2.3 | 2.69E-02 | 23 |
| GO:0016049 | cell growth | 4.1 | 2.70E-02 | 10 |

| | | | | |
|---|---|---|---|---|
| GO:0031347 | regulation of defense response | 2.4 | 2.93E-02 | 21 |
| GO:0009611 | response to wounding | 3.7 | 2.93E-02 | 11 |
| GO:0001819 | positive regulation of cytokine production | 5.9 | 3.15E-02 | 7 |
| GO:0010770 | positive regulation of cell morphogenesis involved in differentiation | 5.8 | 3.27E-02 | 7 |
| GO:0048588 | developmental cell growth | 13.6 | 3.28E-02 | 4 |
| GO:0040013 | negative regulation of locomotion | 9.1 | 3.36E-02 | 5 |
| GO:0051271 | negative regulation of cellular component movement | 4.0 | 3.36E-02 | 10 |
| GO:0048675 | axon extension | 3.6 | 3.44E-02 | 11 |
| GO:0006909 | phagocytosis | 3.9 | 3.45E-02 | 10 |
| GO:0030336 | negative regulation of cell migration | 2.6 | 3.49E-02 | 17 |
| GO:1990138 | neuron projection extension | 2.2 | 3.49E-02 | 23 |
| GO:2000146 | negative regulation of cell motility | 23.5 | 3.70E-02 | 3 |
| GO:0030516 | regulation of axon extension | 3.3 | 3.79E-02 | 12 |
| GO:0060560 | developmental growth involved in morphogenesis | 2.3 | 3.79E-02 | 20 |
| GO:0061387 | regulation of extent of cell growth | 3.5 | 3.86E-02 | 11 |
| GO:0043277 | apoptotic cell clearance | 72.1 | 3.86E-02 | 2 |
| GO:0045773 | positive regulation of axon extension | 2.8 | 4.00E-02 | 15 |
| GO:0072376 | protein activation cascade | 3.5 | 4.15E-02 | 11 |
| GO:0050772 | positive regulation of axonogenesis | 2.5 | 4.32E-02 | 17 |
| GO:0006929 | substrate-dependent cell migration | 3.4 | 4.34E-02 | 11 |
| GO:0060978 | angiogenesis involved in coronary vascular morphogenesis | 11.6 | 4.64E-02 | 4 |

**Table A.4: Complete list of significantly enriched gene ontology categories for BM-PACs isolated from bone marrow.**
GO terms are sorted in ascending order by adjusted p-value (or fold difference ratio, FDR).

| GO Category | GO Category Description | Enrichment Ratio | FDR | Number of Genes |
|---|---|---|---|---|
| GO:0019221 | cytokine-mediated signaling pathway | 6.89 | 2.46E-08 | 21 |
| GO:0071310 | cellular response to organic substance | 2.95 | 2.46E-08 | 47 |
| GO:0046649 | lymphocyte activation | 4.95 | 9.91E-08 | 25 |
| GO:0071345 | cellular response to cytokine stimulus | 5.11 | 9.91E-08 | 24 |
| GO:0002376 | immune system process | 2.76 | 9.91E-08 | 47 |
| GO:0045321 | leukocyte activation | 4.40 | 2.86E-07 | 26 |
| GO:0001775 | cell activation | 4.06 | 2.86E-07 | 28 |
| GO:0042110 | T cell activation | 5.55 | 5.16E-07 | 20 |
| GO:0070489 | T cell aggregation | 5.55 | 5.16E-07 | 20 |
| GO:0071593 | lymphocyte aggregation | 5.53 | 5.16E-07 | 20 |
| GO:0070486 | leukocyte aggregation | 5.44 | 6.27E-07 | 20 |
| GO:0051240 | positive regulation of multicellular organismal process | 3.03 | 1.05E-06 | 36 |
| GO:0034097 | response to cytokine | 4.26 | 1.28E-06 | 24 |
| GO:0002697 | regulation of immune effector process | 6.75 | 1.28E-06 | 16 |
| GO:0007159 | leukocyte cell-cell adhesion | 5.11 | 1.39E-06 | 20 |
| GO:0006955 | immune response | 3.22 | 6.29E-06 | 30 |
| GO:0002252 | immune effector process | 4.34 | 8.25E-06 | 21 |
| GO:0002684 | positive regulation of immune system process | 3.81 | 1.72E-05 | 23 |
| GO:0050776 | regulation of immune response | 4.26 | 2.30E-05 | 20 |
| GO:2000401 | regulation of lymphocyte migration | 19.66 | 2.40E-05 | 7 |
| GO:0007049 | cell cycle | 2.76 | 3.31E-05 | 33 |
| GO:0002520 | immune system development | 3.37 | 3.58E-05 | 25 |
| GO:0008284 | positive regulation of cell proliferation | 3.47 | 3.87E-05 | 24 |
| GO:0051301 | cell division | 4.25 | 4.14E-05 | 19 |
| GO:0042127 | regulation of cell proliferation | 2.70 | 4.37E-05 | 33 |
| GO:0048534 | hematopoietic or lymphoid organ development | 3.41 | 4.72E-05 | 24 |
| GO:0002682 | regulation of immune system process | 3.09 | 4.91E-05 | 27 |
| GO:0002699 | positive regulation of immune effector process | 7.87 | 4.91E-05 | 11 |
| GO:0008283 | cell proliferation | 2.47 | 5.25E-05 | 37 |
| GO:0002521 | leukocyte differentiation | 4.34 | 5.27E-05 | 18 |
| GO:2000404 | regulation of T cell migration | 23.03 | 5.27E-05 | 6 |
| GO:0030097 | hemopoiesis | 3.45 | 5.68E-05 | 23 |
| GO:1903047 | mitotic cell cycle process | 3.71 | 6.07E-05 | 21 |
| GO:0072676 | lymphocyte migration | 12.45 | 6.21E-05 | 8 |
| GO:0098602 | single organism cell adhesion | 3.53 | 6.62E-05 | 22 |
| GO:0009607 | response to biotic stimulus | 3.39 | 6.94E-05 | 23 |
| GO:0016337 | single organismal cell-cell adhesion | 3.63 | 7.68E-05 | 21 |
| GO:0022402 | cell cycle process | 3.04 | 8.53E-05 | 26 |
| GO:0051249 | regulation of lymphocyte activation | 4.89 | 1.01E-04 | 15 |
| GO:0000278 | mitotic cell cycle | 3.41 | 1.06E-04 | 22 |
| GO:0002694 | regulation of leukocyte activation | 4.50 | 1.19E-04 | 16 |
| GO:1901623 | regulation of lymphocyte chemotaxis | 28.78 | 1.29E-04 | 5 |
| GO:0048584 | positive regulation of response to stimulus | 2.43 | 1.30E-04 | 35 |
| GO:0002443 | leukocyte mediated immunity | 5.50 | 1.45E-04 | 13 |
| GO:0002250 | adaptive immune response | 5.05 | 1.46E-04 | 14 |
| GO:0042102 | positive regulation of T cell proliferation | 10.59 | 1.62E-04 | 8 |
| GO:0001912 | positive regulation of leukocyte mediated cytotoxicity | 17.71 | 1.79E-04 | 6 |
| GO:0002703 | regulation of leukocyte mediated immunity | 7.43 | 1.80E-04 | 10 |
| GO:0050870 | positive regulation of T cell activation | 7.29 | 2.10E-04 | 10 |
| GO:0001819 | positive regulation of cytokine production | 4.84 | 2.19E-04 | 14 |
| GO:0032649 | regulation of interferon-gamma production | 10.01 | 2.20E-04 | 8 |
| GO:0072678 | T cell migration | 16.85 | 2.20E-04 | 6 |
| GO:0032729 | positive regulation of interferon-gamma production | 12.40 | 2.35E-04 | 7 |
| GO:0050865 | regulation of cell activation | 4.19 | 2.35E-04 | 16 |
| GO:0002705 | positive regulation of leukocyte mediated immunity | 9.80 | 2.45E-04 | 8 |
| GO:0007155 | cell adhesion | 2.46 | 2.45E-04 | 32 |
| GO:0010820 | positive regulation of T cell chemotaxis | 41.86 | 2.53E-04 | 4 |
| GO:0022610 | biological adhesion | 2.44 | 2.73E-04 | 32 |
| GO:1903039 | positive regulation of leukocyte cell-cell adhesion | 6.94 | 2.73E-04 | 10 |
| GO:0031343 | positive regulation of cell killing | 15.70 | 2.93E-04 | 6 |

| | | | | |
|---|---|---|---|---|
| GO:2000406 | positive regulation of T cell migration | 23.03 | 2.93E-04 | 5 |
| GO:0051094 | positive regulation of developmental process | 2.70 | 3.02E-04 | 27 |
| GO:0045597 | positive regulation of cell differentiation | 3.11 | 3.10E-04 | 22 |
| GO:0032609 | interferon-gamma production | 9.21 | 3.36E-04 | 8 |
| GO:0019220 | regulation of phosphate metabolic process | 2.43 | 4.13E-04 | 31 |
| GO:0042098 | T cell proliferation | 6.54 | 4.13E-04 | 10 |
| GO:2000026 | regulation of multicellular organismal development | 2.34 | 4.19E-04 | 33 |
| GO:0051174 | regulation of phosphorus metabolic process | 2.42 | 4.19E-04 | 31 |
| GO:0051251 | positive regulation of lymphocyte activation | 5.78 | 4.19E-04 | 11 |
| GO:0010819 | regulation of T cell chemotaxis | 35.42 | 4.39E-04 | 4 |
| GO:0006952 | defense response | 2.62 | 4.69E-04 | 27 |
| GO:0050778 | positive regulation of immune response | 4.09 | 5.01E-04 | 15 |
| GO:2000403 | positive regulation of lymphocyte migration | 19.85 | 5.18E-04 | 5 |
| GO:0030217 | T cell differentiation | 5.60 | 5.18E-04 | 11 |
| GO:0050900 | leukocyte migration | 5.08 | 5.18E-04 | 12 |
| GO:0042129 | regulation of T cell proliferation | 7.20 | 5.18E-04 | 9 |
| GO:0030098 | lymphocyte differentiation | 4.66 | 5.19E-04 | 13 |
| GO:0098609 | cell-cell adhesion | 2.71 | 5.46E-04 | 25 |
| GO:0002708 | positive regulation of lymphocyte mediated immunity | 10.20 | 5.94E-04 | 7 |
| GO:0001910 | regulation of leukocyte mediated cytotoxicity | 13.03 | 6.69E-04 | 6 |
| GO:0001909 | leukocyte mediated cytotoxicity | 9.95 | 6.85E-04 | 7 |
| GO:0051707 | response to other organism | 3.12 | 6.86E-04 | 20 |
| GO:0043207 | response to external biotic stimulus | 3.11 | 7.04E-04 | 20 |
| GO:0022409 | positive regulation of cell-cell adhesion | 6.00 | 7.04E-04 | 10 |
| GO:0006468 | protein phosphorylation | 2.29 | 7.27E-04 | 32 |
| GO:0002696 | positive regulation of leukocyte activation | 5.21 | 9.05E-04 | 11 |
| GO:0050673 | epithelial cell proliferation | 4.35 | 9.67E-04 | 13 |
| GO:0050671 | positive regulation of lymphocyte proliferation | 7.61 | 1.01E-03 | 8 |
| GO:0032946 | positive regulation of mononuclear cell proliferation | 7.55 | 1.07E-03 | 8 |
| GO:0042325 | regulation of phosphorylation | 2.45 | 1.20E-03 | 27 |
| GO:0050867 | positive regulation of cell activation | 5.03 | 1.20E-03 | 11 |
| GO:0046631 | alpha-beta T cell activation | 7.37 | 1.23E-03 | 8 |
| GO:0031341 | regulation of cell killing | 11.32 | 1.30E-03 | 6 |
| GO:0050863 | regulation of T cell activation | 4.97 | 1.30E-03 | 11 |
| GO:0070665 | positive regulation of leukocyte proliferation | 7.25 | 1.33E-03 | 8 |
| GO:0010818 | T cell chemotaxis | 25.58 | 1.33E-03 | 4 |
| GO:0016310 | phosphorylation | 2.11 | 1.39E-03 | 35 |
| GO:0031349 | positive regulation of defense response | 4.89 | 1.44E-03 | 11 |
| GO:0009719 | response to endogenous stimulus | 2.36 | 1.49E-03 | 28 |
| GO:0001906 | cell killing | 8.57 | 1.49E-03 | 7 |
| GO:0030595 | leukocyte chemotaxis | 6.09 | 1.49E-03 | 9 |
| GO:0046651 | lymphocyte proliferation | 4.82 | 1.60E-03 | 11 |
| GO:0051726 | regulation of cell cycle | 2.89 | 1.62E-03 | 20 |
| GO:0032943 | mononuclear cell proliferation | 4.80 | 1.62E-03 | 11 |
| GO:0002223 | stimulatory C-type lectin receptor signaling pathway | 49.34 | 1.71E-03 | 3 |
| GO:0035747 | natural killer cell chemotaxis | 49.34 | 1.71E-03 | 3 |
| GO:2000501 | regulation of natural killer cell chemotaxis | 49.34 | 1.71E-03 | 3 |
| GO:0048585 | negative regulation of response to stimulus | 2.43 | 1.79E-03 | 26 |
| GO:0001776 | leukocyte homeostasis | 8.22 | 1.79E-03 | 7 |
| GO:1903037 | regulation of leukocyte cell-cell adhesion | 4.71 | 1.82E-03 | 11 |
| GO:0060749 | mammary gland alveolus development | 21.93 | 2.17E-03 | 4 |
| GO:0061377 | mammary gland lobule development | 21.93 | 2.17E-03 | 4 |
| GO:0001932 | regulation of protein phosphorylation | 2.45 | 2.17E-03 | 25 |
| GO:0007346 | regulation of mitotic cell cycle | 3.92 | 2.21E-03 | 13 |
| GO:0070661 | leukocyte proliferation | 4.59 | 2.21E-03 | 11 |
| GO:0002831 | regulation of response to biotic stimulus | 7.82 | 2.32E-03 | 7 |
| GO:0001816 | cytokine production | 3.27 | 2.42E-03 | 16 |
| GO:0001817 | regulation of cytokine production | 3.41 | 2.65E-03 | 15 |
| GO:0045595 | regulation of cell differentiation | 2.20 | 3.17E-03 | 29 |
| GO:0022407 | regulation of cell-cell adhesion | 4.04 | 3.20E-03 | 12 |
| GO:0050670 | regulation of lymphocyte proliferation | 5.37 | 3.38E-03 | 9 |
| GO:0045954 | positive regulation of natural killer cell mediated cytotoxicity | 19.19 | 3.46E-03 | 4 |

| | | | | |
|---|---|---|---|---|
| GO:0032944 | regulation of mononuclear cell proliferation | 5.34 | 3.46E-03 | 9 |
| GO:0055064 | chloride ion homeostasis | 38.38 | 3.50E-03 | 3 |
| GO:0048247 | lymphocyte chemotaxis | 12.25 | 3.54E-03 | 5 |
| GO:0006873 | cellular ion homeostasis | 3.30 | 3.60E-03 | 15 |
| GO:0002717 | positive regulation of natural killer cell mediated immunity | 18.42 | 3.95E-03 | 4 |
| GO:0031399 | regulation of protein modification process | 2.20 | 4.08E-03 | 28 |
| GO:0000280 | nuclear division | 3.25 | 4.09E-03 | 15 |
| GO:0009605 | response to external stimulus | 2.03 | 4.11E-03 | 33 |
| GO:1902531 | regulation of intracellular signal transduction | 2.24 | 4.14E-03 | 27 |
| GO:0070663 | regulation of leukocyte proliferation | 5.15 | 4.24E-03 | 9 |
| GO:0002706 | regulation of lymphocyte mediated immunity | 6.95 | 4.34E-03 | 7 |
| GO:0009968 | negative regulation of signal transduction | 2.55 | 4.65E-03 | 21 |
| GO:0002449 | lymphocyte mediated immunity | 5.08 | 4.65E-03 | 9 |
| GO:0098771 | inorganic ion homeostasis | 3.03 | 4.96E-03 | 16 |
| GO:0046640 | regulation of alpha-beta T cell proliferation | 17.06 | 5.01E-03 | 4 |
| GO:0044770 | cell cycle phase transition | 4.10 | 5.10E-03 | 11 |
| GO:0002822 | regulation of adaptive immune response based on somatic recombination of immune receptors built from immunoglobulin superfamily domains | 6.72 | 5.15E-03 | 7 |
| GO:0045087 | innate immune response | 3.14 | 5.57E-03 | 15 |
| GO:0002220 | innate immune response activating cell surface receptor signaling pathway | 31.40 | 5.96E-03 | 3 |
| GO:0002366 | leukocyte activation involved in immune response | 4.86 | 6.15E-03 | 9 |
| GO:0098542 | defense response to other organism | 3.45 | 6.46E-03 | 13 |
| GO:0002263 | cell activation involved in immune response | 4.82 | 6.51E-03 | 9 |
| GO:0007169 | transmembrane receptor protein tyrosine kinase signaling pathway | 3.24 | 6.62E-03 | 14 |
| GO:1901987 | regulation of cell cycle phase transition | 4.77 | 6.88E-03 | 9 |
| GO:0045089 | positive regulation of innate immune response | 5.42 | 6.90E-03 | 8 |
| GO:0042592 | homeostatic process | 2.11 | 6.96E-03 | 28 |
| GO:0006198 | cAMP catabolic process | 28.78 | 7.42E-03 | 3 |
| GO:2000479 | regulation of cAMP-dependent protein kinase activity | 28.78 | 7.42E-03 | 3 |
| GO:0048285 | organelle fission | 3.03 | 7.65E-03 | 15 |
| GO:0030155 | regulation of cell adhesion | 3.02 | 7.90E-03 | 15 |
| GO:0030003 | cellular cation homeostasis | 3.16 | 8.17E-03 | 14 |
| GO:0046632 | alpha-beta T cell differentiation | 7.51 | 8.17E-03 | 6 |
| GO:0002819 | regulation of adaptive immune response | 6.11 | 8.38E-03 | 7 |
| GO:0060326 | cell chemotaxis | 4.61 | 8.47E-03 | 9 |
| GO:0010564 | regulation of cell cycle process | 3.32 | 8.50E-03 | 13 |
| GO:0010243 | response to organonitrogen compound | 2.74 | 8.50E-03 | 17 |
| GO:0007167 | enzyme linked receptor protein signaling pathway | 2.65 | 8.50E-03 | 18 |
| GO:0046633 | alpha-beta T cell proliferation | 14.39 | 8.50E-03 | 4 |
| GO:0009617 | response to bacterium | 3.13 | 8.63E-03 | 14 |
| GO:0002688 | regulation of leukocyte chemotaxis | 7.35 | 8.74E-03 | 6 |
| GO:0007067 | mitotic nuclear division | 3.52 | 8.76E-03 | 12 |
| GO:0007059 | chromosome segregation | 4.11 | 8.81E-03 | 10 |
| GO:0031347 | regulation of defense response | 3.28 | 9.12E-03 | 13 |
| GO:0010562 | positive regulation of phosphorus metabolic process | 2.46 | 9.35E-03 | 20 |
| GO:0045937 | positive regulation of phosphate metabolic process | 2.46 | 9.35E-03 | 20 |
| GO:0042269 | regulation of natural killer cell mediated cytotoxicity | 13.54 | 1.03E-02 | 4 |
| GO:0055080 | cation homeostasis | 2.92 | 1.03E-02 | 15 |
| GO:0071495 | cellular response to endogenous stimulus | 2.36 | 1.08E-02 | 21 |
| GO:0050801 | ion homeostasis | 2.78 | 1.08E-02 | 16 |
| GO:0044772 | mitotic cell cycle phase transition | 3.98 | 1.08E-02 | 10 |
| GO:0050715 | positive regulation of cytokine secretion | 6.98 | 1.09E-02 | 6 |
| GO:0051656 | establishment of organelle localization | 3.66 | 1.09E-02 | 11 |
| GO:0055082 | cellular chemical homeostasis | 2.77 | 1.09E-02 | 16 |
| GO:0002715 | regulation of natural killer cell mediated immunity | 13.16 | 1.10E-02 | 4 |
| GO:0002695 | negative regulation of leukocyte activation | 5.64 | 1.20E-02 | 7 |
| GO:0006874 | cellular calcium ion homeostasis | 3.60 | 1.23E-02 | 11 |
| GO:0009628 | response to abiotic stimulus | 2.39 | 1.23E-02 | 20 |
| GO:0009214 | cyclic nucleotide catabolic process | 23.03 | 1.26E-02 | 3 |
| GO:0010648 | negative regulation of cell communication | 2.32 | 1.32E-02 | 21 |
| GO:0002683 | negative regulation of immune system process | 3.56 | 1.32E-02 | 11 |
| GO:0051653 | spindle localization | 12.45 | 1.32E-02 | 4 |

| | | | | |
|---|---|---|---|---|
| GO:0051640 | organelle localization | 3.31 | 1.36E-02 | 12 |
| GO:0023057 | negative regulation of signaling | 2.31 | 1.36E-02 | 21 |
| GO:0002827 | positive regulation of T-helper 1 type immune response | 21.59 | 1.47E-02 | 3 |
| GO:0002834 | regulation of response to tumor cell | 21.59 | 1.47E-02 | 3 |
| GO:0002837 | regulation of immune response to tumor cell | 21.59 | 1.47E-02 | 3 |
| GO:0048878 | chemical homeostasis | 2.35 | 1.50E-02 | 20 |
| GO:0002685 | regulation of leukocyte migration | 5.37 | 1.50E-02 | 7 |
| GO:0002687 | positive regulation of leukocyte migration | 6.46 | 1.50E-02 | 6 |
| GO:0055074 | calcium ion homeostasis | 3.48 | 1.52E-02 | 11 |
| GO:0097190 | apoptotic signaling pathway | 2.90 | 1.57E-02 | 14 |
| GO:1901990 | regulation of mitotic cell cycle phase transition | 4.61 | 1.58E-02 | 8 |
| GO:1901701 | cellular response to oxygen-containing compound | 2.46 | 1.65E-02 | 18 |
| GO:0002418 | immune response to tumor cell | 20.32 | 1.70E-02 | 3 |
| GO:0050769 | positive regulation of neurogenesis | 3.40 | 1.78E-02 | 11 |
| GO:0045088 | regulation of innate immune response | 4.49 | 1.82E-02 | 8 |
| GO:0002260 | lymphocyte homeostasis | 7.89 | 1.82E-02 | 5 |
| GO:0072503 | cellular divalent inorganic cation homeostasis | 3.37 | 1.91E-02 | 11 |
| GO:0002690 | positive regulation of leukocyte chemotaxis | 7.78 | 1.92E-02 | 5 |
| GO:0050866 | negative regulation of cell activation | 5.10 | 1.93E-02 | 7 |
| GO:0071868 | cellular response to monoamine stimulus | 19.19 | 1.95E-02 | 3 |
| GO:0071870 | cellular response to catecholamine stimulus | 19.19 | 1.95E-02 | 3 |
| GO:0010035 | response to inorganic substance | 3.13 | 1.98E-02 | 12 |
| GO:0046058 | cAMP metabolic process | 6.01 | 2.04E-02 | 6 |
| GO:1901136 | carbohydrate derivative catabolic process | 6.01 | 2.04E-02 | 6 |
| GO:0046641 | positive regulation of alpha-beta T cell proliferation | 18.18 | 2.25E-02 | 3 |
| GO:0045785 | positive regulation of cell adhesion | 3.52 | 2.36E-02 | 10 |
| GO:0002824 | positive regulation of adaptive immune response based on somatic recombination of immune receptors built from immunoglobulin superfamily domains | 7.29 | 2.48E-02 | 5 |
| GO:0006875 | cellular metal ion homeostasis | 3.04 | 2.48E-02 | 12 |
| GO:0002460 | adaptive immune response based on somatic recombination of immune receptors built from immunoglobulin superfamily domains | 4.24 | 2.48E-02 | 8 |
| GO:0002347 | response to tumor cell | 17.27 | 2.57E-02 | 3 |
| GO:0046634 | regulation of alpha-beta T cell activation | 7.20 | 2.58E-02 | 5 |
| GO:0048872 | homeostasis of number of cells | 3.78 | 2.59E-02 | 9 |
| GO:1901700 | response to oxygen-containing compound | 2.04 | 2.59E-02 | 24 |
| GO:0043549 | regulation of kinase activity | 2.61 | 2.59E-02 | 15 |
| GO:0050790 | regulation of catalytic activity | 1.82 | 2.72E-02 | 31 |
| GO:0072507 | divalent inorganic cation homeostasis | 3.19 | 2.72E-02 | 11 |
| GO:0051250 | negative regulation of lymphocyte activation | 5.62 | 2.72E-02 | 6 |
| GO:0033993 | response to lipid | 2.41 | 2.72E-02 | 17 |
| GO:0001922 | B-1 B cell homeostasis | 46.05 | 2.72E-02 | 2 |
| GO:0035701 | hematopoietic stem cell migration | 46.05 | 2.72E-02 | 2 |
| GO:0070120 | ciliary neurotrophic factor-mediated signaling pathway | 46.05 | 2.72E-02 | 2 |
| GO:1901660 | calcium ion export | 46.05 | 2.72E-02 | 2 |
| GO:2000503 | positive regulation of natural killer cell chemotaxis | 46.05 | 2.72E-02 | 2 |
| GO:1901698 | response to nitrogen compound | 2.40 | 2.76E-02 | 17 |
| GO:0042113 | B cell activation | 4.09 | 2.92E-02 | 8 |
| GO:0050678 | regulation of epithelial cell proliferation | 3.67 | 2.99E-02 | 9 |
| GO:0002821 | positive regulation of adaptive immune response | 6.77 | 3.13E-02 | 5 |
| GO:0045859 | regulation of protein kinase activity | 2.65 | 3.13E-02 | 14 |
| GO:0055083 | monovalent inorganic anion homeostasis | 15.70 | 3.13E-02 | 3 |
| GO:0071867 | response to monoamine | 15.70 | 3.13E-02 | 3 |
| GO:0071869 | response to catecholamine | 15.70 | 3.13E-02 | 3 |
| GO:0042327 | positive regulation of phosphorylation | 2.36 | 3.21E-02 | 17 |
| GO:0032663 | regulation of interleukin-2 production | 9.21 | 3.26E-02 | 4 |
| GO:0042267 | natural killer cell mediated cytotoxicity | 9.21 | 3.26E-02 | 4 |
| GO:0000086 | G2/M transition of mitotic cell cycle | 6.62 | 3.39E-02 | 5 |
| GO:0019725 | cellular homeostasis | 2.42 | 3.41E-02 | 16 |
| GO:0002825 | regulation of T-helper 1 type immune response | 15.02 | 3.48E-02 | 3 |
| GO:0002228 | natural killer cell mediated immunity | 8.86 | 3.71E-02 | 4 |
| GO:0006578 | amino-acid betaine biosynthetic process | 38.38 | 3.74E-02 | 2 |
| GO:0031536 | positive regulation of exit from mitosis | 38.38 | 3.74E-02 | 2 |

| | | | | |
|---|---|---|---|---|
| GO:0072679 | thymocyte migration | 38.38 | 3.74E-02 | 2 |
| GO:2000480 | negative regulation of cAMP-dependent protein kinase activity | 38.38 | 3.74E-02 | 2 |
| GO:0009615 | response to virus | 3.89 | 3.78E-02 | 8 |
| GO:0008277 | regulation of G-protein coupled receptor protein signaling pathway | 6.40 | 3.80E-02 | 5 |
| GO:1901135 | carbohydrate derivative metabolic process | 2.19 | 3.80E-02 | 19 |
| GO:0002507 | tolerance induction | 14.39 | 3.80E-02 | 3 |
| GO:0042104 | positive regulation of activated T cell proliferation | 14.39 | 3.80E-02 | 3 |
| GO:0042330 | taxis | 2.83 | 3.96E-02 | 12 |
| GO:0007010 | cytoskeleton organization | 2.11 | 4.13E-02 | 20 |
| GO:0032496 | response to lipopolysaccharide | 3.45 | 4.17E-02 | 9 |
| GO:0040011 | locomotion | 1.95 | 4.17E-02 | 24 |
| GO:0042742 | defense response to bacterium | 3.81 | 4.17E-02 | 8 |
| GO:1902589 | single-organism organelle organization | 1.88 | 4.20E-02 | 26 |
| GO:0044839 | cell cycle G2/M phase transition | 6.19 | 4.24E-02 | 5 |
| GO:0010720 | positive regulation of cell development | 2.96 | 4.27E-02 | 11 |
| GO:0032623 | interleukin-2 production | 8.37 | 4.27E-02 | 4 |
| GO:0046425 | regulation of JAK-STAT cascade | 4.97 | 4.34E-02 | 6 |
| GO:1904892 | regulation of STAT cascade | 4.97 | 4.34E-02 | 6 |
| GO:0002698 | negative regulation of immune effector process | 6.12 | 4.34E-02 | 5 |
| GO:0042752 | regulation of circadian rhythm | 6.12 | 4.34E-02 | 5 |
| GO:0009154 | purine ribonucleotide catabolic process | 13.28 | 4.56E-02 | 3 |
| GO:0018108 | peptidyl-tyrosine phosphorylation | 3.39 | 4.57E-02 | 9 |
| GO:0001934 | positive regulation of protein phosphorylation | 2.33 | 4.63E-02 | 16 |
| GO:1902105 | regulation of leukocyte differentiation | 3.71 | 4.65E-02 | 8 |
| GO:0018212 | peptidyl-tyrosine modification | 3.36 | 4.72E-02 | 9 |
| GO:0070669 | response to interleukin-2 | 32.89 | 4.74E-02 | 2 |
| GO:0044092 | negative regulation of molecular function | 2.18 | 4.83E-02 | 18 |
| GO:0002832 | negative regulation of response to biotic stimulus | 12.79 | 4.93E-02 | 3 |
| GO:0009261 | ribonucleotide catabolic process | 12.79 | 4.93E-02 | 3 |
| GO:0036230 | granulocyte activation | 12.79 | 4.93E-02 | 3 |

**Table A.5: Complete list of significantly enriched gene ontology categories for BM-PACs isolated from peripheral blood.**
GO terms are sorted in ascending order by adjusted p-value (or fold difference ratio, FDR).

| Gene Ontology Categories | | Peripheral Blood | | | Bone Marrow | | |
|---|---|---|---|---|---|---|---|
| GO Category | GO Category Description | Enrichment Ratio | FDR | Number of Genes | Enrichment Ratio | FDR | Number of Genes |
| GO:0045597 | positive regulation of cell differentiation | 3.11 | 3.10E-04 | 22 | 3.98 | 2.12E-03 | 18 |
| GO:0051240 | positive regulation of multicellular organismal process | 3.03 | 1.05E-06 | 36 | 2.90 | 5.04E-03 | 22 |
| GO:0051094 | positive regulation of developmental process | 2.70 | 3.02E-04 | 27 | 3.13 | 5.04E-03 | 20 |
| GO:2000026 | regulation of multicellular organismal development | 2.34 | 4.19E-04 | 33 | 2.66 | 6.05E-03 | 24 |
| GO:0045595 | regulation of cell differentiation | 2.20 | 3.17E-03 | 29 | 2.61 | 8.94E-03 | 22 |
| GO:0007167 | enzyme linked receptor protein signaling pathway | 2.65 | 8.50E-03 | 18 | 3.68 | 5.88E-03 | 16 |
| GO:0016310 | phosphorylation | 2.11 | 1.39E-03 | 35 | 2.35 | 1.17E-02 | 25 |
| GO:0042325 | regulation of phosphorylation | 2.45 | 1.20E-03 | 27 | 2.70 | 1.64E-02 | 19 |
| GO:0071495 | cellular response to endogenous stimulus | 2.36 | 1.08E-02 | 21 | 2.99 | 1.33E-02 | 17 |
| GO:0001819 | positive regulation of cytokine production | 4.84 | 2.19E-04 | 14 | 4.87 | 2.23E-02 | 9 |
| GO:0007169 | transmembrane receptor protein tyrosine kinase signaling pathway | 3.24 | 6.62E-03 | 14 | 3.99 | 2.23E-02 | 11 |
| GO:0001817 | regulation of cytokine production | 3.41 | 2.65E-03 | 15 | 3.91 | 2.34E-02 | 11 |
| GO:0019220 | regulation of phosphate metabolic process | 2.43 | 4.13E-04 | 31 | 2.45 | 2.68E-02 | 20 |
| GO:0071310 | cellular response to organic substance | 2.95 | 2.46E-08 | 47 | 2.26 | 2.69E-02 | 23 |
| GO:0051174 | regulation of phosphorus metabolic process | 2.42 | 4.19E-04 | 31 | 2.45 | 2.69E-02 | 20 |
| GO:0006468 | protein phosphorylation | 2.29 | 7.27E-04 | 32 | 2.35 | 2.93E-02 | 21 |
| GO:0050790 | regulation of catalytic activity | 1.82 | 2.72E-02 | 31 | 2.30 | 1.51E-02 | 25 |
| GO:0031347 | regulation of defense response | 3.28 | 9.12E-03 | 13 | 3.95 | 3.36E-02 | 10 |
| GO:0001932 | regulation of protein phosphorylation | 2.45 | 2.17E-03 | 25 | 2.61 | 3.49E-02 | 17 |
| GO:0001816 | cytokine production | 3.27 | 2.42E-03 | 16 | 3.52 | 3.86E-02 | 11 |
| GO:0010720 | positive regulation of cell development | 2.96 | 4.27E-02 | 11 | 4.63 | 8.94E-03 | 11 |
| GO:0040011 | locomotion | 1.95 | 4.17E-02 | 24 | 2.54 | 2.22E-02 | 20 |

| |
|---|
| Development and Differentiation |
| Cytokine Production and Signaling |
| Phosphorylation and Metabolism |
| Cytoskeletal Regulation |

**Table A.6: List of significantly enriched GO categories shared by BM-PACs isolated from both peripheral blood and bone marrow**